

Cleared: March 29th, 1972
Clearing Authority: Air Force Materials Laboratory

MAGNETOABSORPTION TECHNIQUES FOR MEASURING MATERIAL PROPERTIES

*WILLIAM L. ROLLWITZ
JOHN P. CLAASSEN*

SOUTHWEST RESEARCH INSTITUTE

*** Export controls have been removed ***

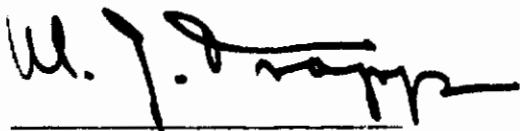
This document is subject to special export controls and each transmittal to foreign governments or foreign nationals may be made only with prior approval of the Metals and Ceramics Division (MAMD), Air Force Materials Laboratory, Wright-Patterson Air Force Base, Ohio.

FOREWORD

This report was prepared by Southwest Research Institute under USAF Contract No. AF 33(657)-10326. The work was administered under the direction of the AF Materials Laboratory Research and Technology Division, Project No. 7360, "The Chemistry and Physics of Materials," Task No. 736002, "Nondestructive Methods," with J. A. Holloway, MAMD, acting as project engineer.

This report covers work conducted from January 1965 to January 1966. The project leader at Southwest Research Institute was William L. Rollwitz, Manager of the Electronic Instrumentation Section. The project engineer was John P. Claassen, Research Engineer. The manuscript of this report was released by the authors December 1965 for publication as an RTD Technical Report.

This technical report has been reviewed and is approved.



W. J. TRAPP
Chief, Strength and Dynamics Branch
Metals and Ceramics Division
Air Force Materials Laboratory

ABSTRACT

Research under Contract AF 33(657)-10326 was continued to determine the feasibility of using magnetoabsorption for the nondestructive evaluation of material properties. Previous efforts, reported in ML-TDR-64-123 and AFML TR-65-17, have shown that magnetoabsorption signals are derived from variations of the reversible permeability of ferromagnetic specimens with magnetic environment. Further, it had been shown that magnetoabsorption signals are readily affected by changes in reversible permeability as caused by stress, heat treatment, composition, impurity, and temperature. The effort of this period has been devoted to a refinement of the magnetoabsorption measuring equipment to detect low amplitude magnetoabsorption signals from specimens offering a small effective filling factor to a sample coil or probe. These refinements are primarily discussed in the Appendices. With this improved sensitivity, variations in harmonic content of magnetoabsorption signals arising from variations in the surface properties of a plate of maraging steel were related experimentally. Magnetoabsorption waveforms were also measured from and related to a weldment of maraging steel, stressed and stress-relieved specimens of HY-80 steel, and a bulge plate of 1020 steel. Magnetoabsorption signal changes and its harmonic amplitude variations from nickel-plated aluminum rods and other ferromagnetic wires were related experimentally to applied compressive and tensile loads.

Contracts

TABLE OF CONTENTS

	<u>Page</u>
I. INTRODUCTION	1
A. Previous Effort	1
B. Simplified Model of Magnetoabsorption	4
C. Summary of Efforts for 1965	6
II. MAGNETOABSORPTION SIGNALS FROM MARAGING STEEL PLATES	8
A. General	8
B. Measurement Techniques	8
C. Magnetoabsorption Measurements from a Weldment of Maraging Steel	11
D. Experimental Results for the Slotted Plate	15
III. MAGNETOABSORPTION MEASUREMENTS ON HY-80 STEEL.	21
A. Introduction	21
B. Measurement System	21
C. First Series of Measurements	25
D. Second Series of Measurements	30
E. Conclusions	32
IV. VARIATIONS IN MAGNETOABSORPTION SIGNALS FROM NICKEL-PLATED ALUMINUM RODS UNDER INCREMENTAL LOADS	34
A. Introduction	34
B. Experimental Procedure	35
C. Experimental Results	37
D. Additional Effort	45
V. HARMONIC AMPLITUDE VARIATIONS OF MAGNETO- ABSORPTION SIGNALS FROM WIRES UNDER STRESS	49
A. General	49
B. Negative Magnetostrictive Specimens	49
C. Positive Magnetostrictive Specimens	54

Contrails

TABLE OF CONTENTS (Cont'd)

	<u>Page</u>
VI. RECOMMENDATIONS FOR ADDITIONAL EFFORT.	58
REFERENCES	59
APPENDICES	
I. Small Probes and Their Coupling Circuits	61
II. Detailed Results from a Slotted Maraging Steel Plate	68
III. Magnetoabsorption Waveform Data	74
IV. Magnetoabsorption Measurements from an Explosively Formed Sheet of 1020 Steel.	78
V. Magnetoabsorption from Nickel Films on Aluminum	80
VI. Magnetoabsorption Harmonic Amplitudes Measurements from Rods	86
VII. General Design Considerations for Marginal Oscillators.	90

LIST OF ILLUSTRATIONS

<u>Figure</u>		<u>Page</u>
1	The Variation of the Relative Reversible Permeability μ_r , as a Function of the Applied Bias Field, of a No. 26 AWG Iron Wire	2
2	The Graph of the Theoretical Calculation for the Change in the Resistance Term and the Reactance Term for a Coil with a Nickel Wire in a Varying Magnetic Bias Field	3
3	The Graph of the Measured Values of the Change in the Resistance Term and the Reactance Term for a Coil with a Nickel Wire in a Varying Magnetic Bias Field	3
4	Geometry of Sample Coil and Cylindrical Specimen	5
5	GTA Weldment of Maraging Steel	9
6	Close-Up View of Maraging Steel Plate	10
7	Laboratory Setup to Measure Magnetoabsorption Harmonic Variations Across a Plate	12
8	Block Diagram of Surface Imperfection Detection System	13
9a	Magnetoabsorption Signal Waveforms and Amplitudes at Indicated Positions for the Top and Sides of a Weldment of Maraging Steel Having a Longitudinal Bias Field	14
9b	Magnetoabsorption Signal Waveforms and Amplitudes at Indicated Positions for the Top of a Weldment of Maraging Steel Having a Transverse Bias Field	14
10a	Magnetoabsorption Signal Waveforms and Amplitudes at Indicated Positions for the Bottom of a Weldment of Maraging Steel Having a Longitudinal Bias Field	16
10b	Magnetoabsorption Signal Waveforms and Amplitudes at Indicated Positions for the Bottom of a Weldment of Maraging Steel Having a Transverse Bias Field	16
11a	Variations in the Amplitude of the Harmonics (Indicated at Left) in the Magnetoabsorption Signal Measured Along Line 10 of Specimen	17

Contrails

LIST OF ILLUSTRATIONS (Cont'd)

<u>Figure</u>		<u>Page</u>
11b	Variations in the Amplitude of the Harmonics (Indicated at Left) in the Magnetoabsorption Signal Measured Along Line 10 of Specimen.	19
12	Magnetoabsorption as a Function of Reversible Permeability.	22
13a	Superposition of the B/H Loop and the Relative Reversible Permeability Curves for Iron Thermocouple Wire	23
13b	Superposition of the B/H Loop and the Relative Reversible Permeability Curves for Unannealed Nickel Wire.	23
13c	Superposition of the B/H Loop and the Relative Reversible Permeability Curves for Annealed Nickel Wire.	23
14	Magnetoabsorption Mechanism for Providing Measurements on Only One Face of a Charpy Impact Specimen	24
15	Magnetoabsorption Detection Head for Measurements on Flat Sheets	26
16	Complete Measuring System for First Series of Measurements	27
17	Magnetoabsorption Signals, HY-80 Steel (Unstressed)	28
18	Magnetoabsorption Signals for Stressed Bend Specimens of HY-80 Steel	29
19	Probe-Specimen Geometry for Magnetoabsorption	31
20	Typical Magnetoabsorption Signals from the Top and Bottom of Specimens S-1, S-3, and S-6.	33
21	Simple Loading Device and Magnetoabsorption System	36
22	Variations of Magnetoabsorption Amplitude and Strain with Stress for Nickel-Plated Aluminum Rod of 1/8-Inch Diameter	38
23	Variation in the Peak Separation of the Magnetoabsorption Signal with Stress for 1/8-Inch Diameter Nickel-Plated Aluminum Rod	40

LIST OF ILLUSTRATIONS (Cont'd)

<u>Figure</u>		<u>Page</u>
24	Superposition of the B/H Loop and the Relative Reversible Permeability Curves for Unannealed Nickel Wire	41
25	Superposition of the B/H Loop and Relative Reversible Permeability Curves for Annealed Nickel Wire	41
26	Variations of Magnetoabsorption and Strain with Stress for an Annealed Nickel-Plated Aluminum Rod of 1/8-Inch Diameter	43
27	Variation of Magnetoabsorption Amplitude and Strain with Stress for Unannealed Nickel-Plated Aluminum Rod of 1/16-Inch Diameter	44
28	Variations of Peak Separation with Stress for Nickel-Plated Aluminum Rod of 1/16-Inch Diameter	46
29	Variation of Magnetoabsorption Amplitude and Strain with Stress for Annealed Nickel-Plated Aluminum Rod of 1/16-Inch Diameter	47
30	Magnetoabsorption Waveforms from Partially Annealed Nickel Film on an Aluminum Plate	48
31	Variations of Magnetoabsorption Amplitude, Harmonic Amplitude, and Peak Separation with Stress for Industrially Annealed Nickel Wire	50
32	Variation of Magnetoabsorption Amplitude, Harmonic Amplitude, and Peak Separation with Stress for Cold Rolled Nickel Wire	52
33	Variations of Magnetoabsorption Amplitude, Harmonic Amplitude, and Peak Separation with Stress for Nickel-Plated Aluminum Rod	53
34	Variations of Magnetoabsorption Amplitude, Harmonic Amplitude, and Peak Separation with Stress for Annealed Iron Thermocouple Wire	55
35	Variations of Magnetoabsorption Amplitude, Harmonic Amplitude, and Peak Separation with Stress for Solution Annealed 18% Maraging Steel Wire	56

Contrails

LIST OF ILLUSTRATIONS (Cont'd)

<u>Figure</u>		<u>Page</u>
36	Probe Configurations	62
37	Series Resonant Circuit Method for Coupling a Small Coil to a Marginal Oscillator	63
38	The Tuned Secondary Transformer Method of Coupling a Small Coil to a Marginal Oscillator	63
39	Ferrite Transformer and a Double-D Probe	65
40a	A Selection of Double-D Probes	67
40b	The Tips for the Probes Shown in Figure 9a	67
41a	Variations in the Amplitude of 120-cps Component of the Magnetoabsorption Signal Along the Indicated Scans for Maraging Steel Specimen Having Nine EDM Slots	69
41b	Variations in the Amplitude of 240-cps Component for the Magnetoabsorption Signal Along the Indicated Scans for Maraging Steel Specimen Having Nine EDM Slots	70
41c	Variations in the Amplitude of 360-cps Component of the Magnetoabsorption Signal Along the Indicated Scans for Maraging Steel Specimen Having Nine EDM Slots	71
41d	Variations in the Amplitude of 480-cps Component of the Magnetoabsorption Signal Along the Indicated Scans for Maraging Steel Specimen Having Nine EDM Slots	72
41e	Variations in the Amplitude of 600-cps Component of the Magnetoabsorption Signal Along the Indicated Scans for Maraging Steel Specimen Having Nine EDM Slots	73
42	Magnetoabsorption Signals - Specimen No. S-1, HY-80 Steel	75
43	Magnetoabsorption Signals - Specimen No. S-5, HY-80 Steel	76
44	Magnetoabsorption Signals - Specimen No. S-6, HY-80 Steel	77
45	Magnetoabsorption Signals from an Explosively-Formed--Dome Shaped Piece of 1020 Steel	79

Contrails

LIST OF ILLUSTRATIONS (Cont'd)

<u>Figure</u>		<u>Page</u>
46	Sample within Chucks, Sample Coil, and Bias Coils	81
47	Magnetoabsorption Waveforms as a Function of Load for Unannealed Nickel-Plated Aluminum Rod of 1/8-Inch Diameter	82
48	Magnetoabsorption Waveforms as a Function of Load for an Annealed Nickel-Plated Aluminum Rod of 1/8-Inch Diameter	83
49	Magnetoabsorption Waveform Changes with Load for Unannealed Nickel-Plated Aluminum Rod of 1/16-Inch Diameter	84
50	Magnetoabsorption Waveforms as a Function of Load for Annealed Nickel-Plated Aluminum Rod of 1/16-Inch Diameter	85
51	Block Diagram of System Measuring the Harmonic Content of a Magnetoabsorption Signal for a Sample under Stress . . .	87
52	Equipment Configuration for Monitoring and Recording Magnetoabsorption as a Function of Incremental Stress . . .	87
53	The Exploded View of the Helmholtz Biasing Magnet and the Radio-Frequency Sample Coil Plus Its Shield.	88
54	Marginal Oscillatory Configuration	90
55	Variations of Transconductance with Grid Bias and DC Load Resistance	93
56	The Automatic Level Control (ALC) System Used with the Marginal Oscillator.	93
57	The Equivalent Servo Loop for the ALC System	94
58	Biasing Through Decoupling Resistors	95
59	Plate Characteristics for 7308 Triode	96
60	Biasing Directly from Regulated Supply	96

Contrails

LIST OF ILLUSTRATIONS (Cont'd)

<u>Figure</u>		<u>Page</u>
61	Marginal Oscillator with Regulated Plate Supply and Automatic Level Control	98
62	Gain of Grounded Grid Amplifier with Variation in Grid Bias for 7308 Triode	98
63	Equivalent Circuits of the Oscillator	99
64	Broad Band Amplifier	104

LIST OF TABLES

<u>Table</u>		<u>Page</u>
1	Specifications for an RF Coil	86
2	Composition of Annealed Iron Thermocouple Wire	88
3	Analyses - 18% Nickel Maraging Steels	88
4	Definition of Parameters	99
5	Amplifier Characteristics	103

SECTION I

INTRODUCTION

A. Previous Effort

Work reported previously in TDR-64-123 [1]* gave experimental curves of the relative reversible permeability of a wire sample as a function of the intensity of a magnetic bias field applied along the axis of the wire. One such curve for number 26 AWG iron thermocouple wire in a varying magnetic bias field is shown in Figure 1. Similar curves were also obtained for both annealed and unannealed nickel.

This previous effort also produced a good correlation between the theoretically and experimentally derived variations in the impedance of a radio-frequency coil with bias field intensity. The correlation is demonstrated by a comparison of Figures 2 and 3. The theory indicated that the impedance variations of the coil with bias field were related for the most part to the changes in reversible permeability rather than changes in magneto-resistance of the sample wire. As an example, this is demonstrated by the fact that a 80% change in permeability of an iron sample caused by a 100-oersted bias field results in a coil impedance variation of approximately 83%, whereas, under the same bias field condition, the magneto-resistive change is only 0.09%. Thus, the impedance change for a coil with a wire core is of the order of the permeability change.

Much of the measurement of magnetoabsorption performed at Southwest Research Institute has used a marginal oscillatory as a detector. This device has a very high sensitivity and is very simple to use. For practical applications, the marginal oscillator offers many advantages. However, it is not sufficiently stable to permit the long-term detection of the effects of DC or very low frequency AC magnetic fields (less than 0.1 cycle per second) since the automatic RF level control system excludes these slow variations. Therefore, to utilize the advantages of the marginal oscillator, the magnetic field must be varied at a rapid and repetitive rate. For most of the tests, the magnetic bias was supplied by means of a Helmholtz pair of coils fed with 60-cycle voltage. The impedance changes are identical for the same magnitudes of positive or negative magnetic bias fields. Therefore, the basic frequency of the output of the marginal oscillator with a 60-cycle magnetic bias field will be twice 60 cycles or 120 cycles.

*Arabic numerals in brackets are reference callouts. See page 59 for List of References.

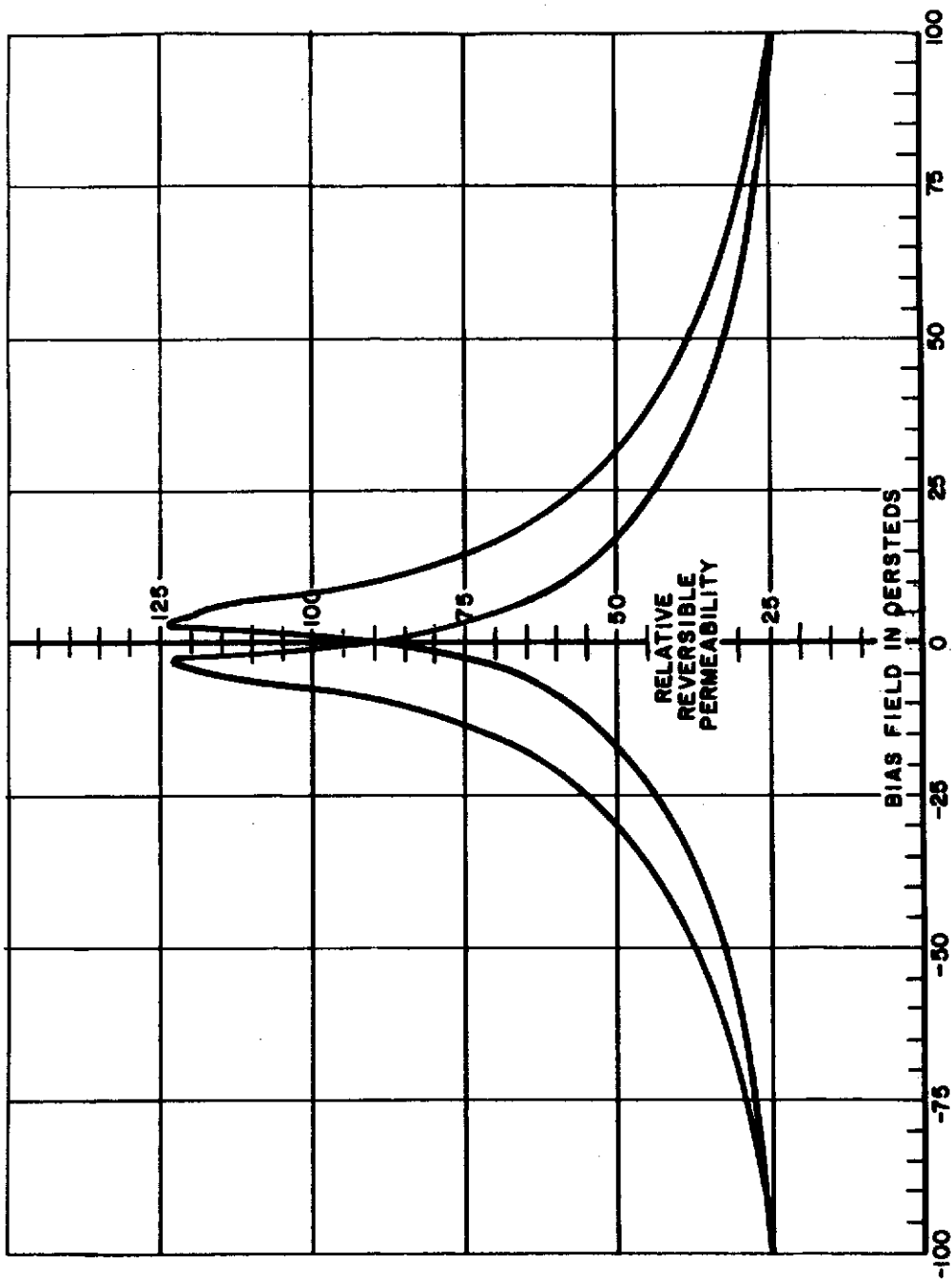


FIGURE 1. THE VARIATION OF THE RELATIVE REVERSIBLE PERMEABILITY μ_r , AS A FUNCTION OF THE APPLIED BIAS FIELD, OF A NO. 26 AWG IRON WIRE

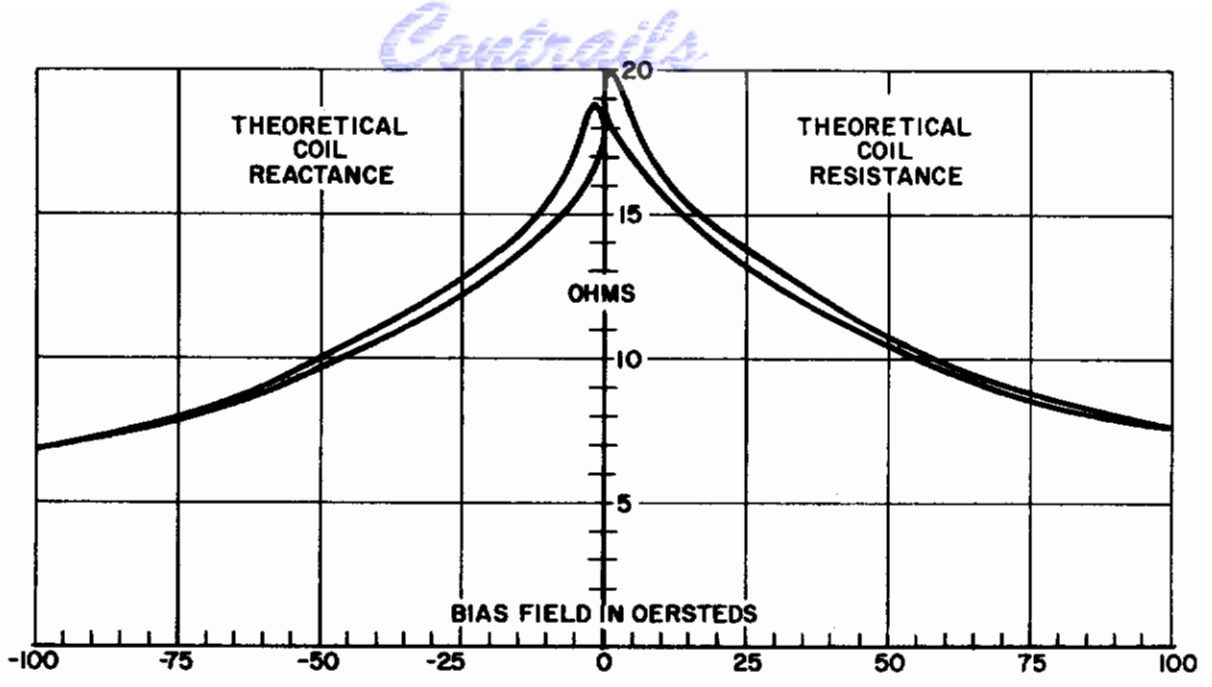


FIGURE 2. THE GRAPH OF THE THEORETICAL CALCULATION FOR THE CHANGE IN THE RESISTANCE TERM AND THE REACTANCE TERM FOR A COIL WITH A NICKEL WIRE IN A VARYING MAGNETIC BIAS FIELD

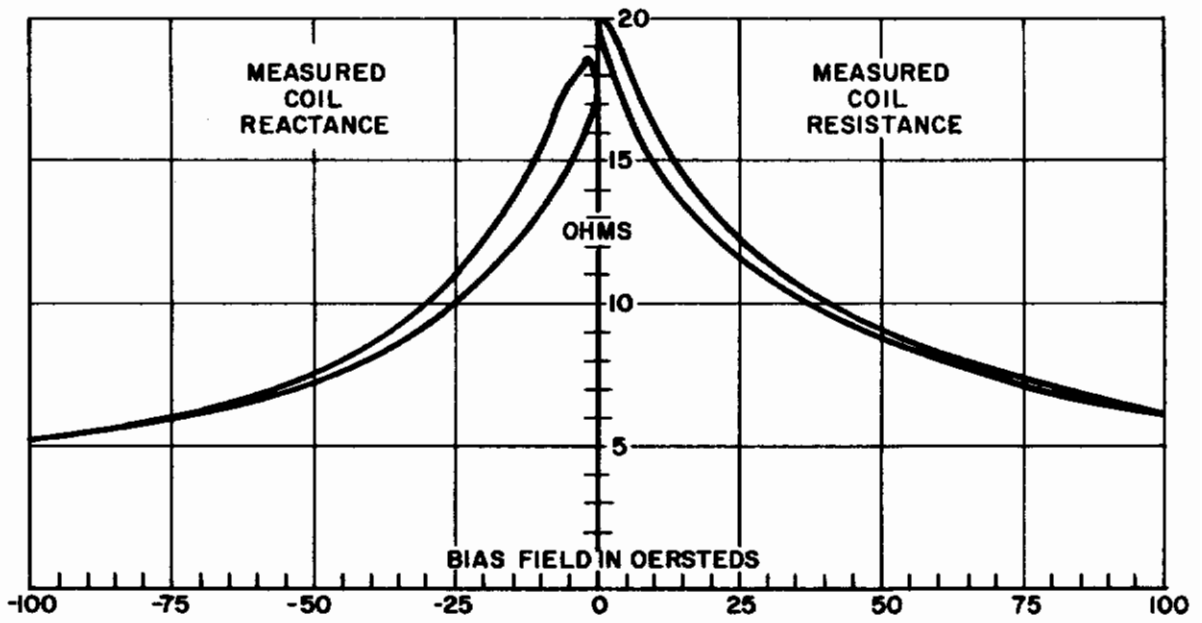


FIGURE 3. THE GRAPH OF THE MEASURED VALUES OF THE CHANGE IN THE RESISTANCE TERM AND THE REACTANCE TERM FOR A COIL WITH A NICKEL WIRE IN A VARYING MAGNETIC BIAS FIELD

The previous work [1] had shown the correlation between the theoretical curves and the experimental curves for a very slowly varying magnetic bias field. Several seconds were required to perform a complete cycle. Thus, an experimental study of the magnetoabsorption signal for nickel and iron wires with a sinusoidally varying magnetic bias field was undertaken and the results compared with the theoretically calculated curves. In addition, a study of changes in magnetoabsorption signals from several samples of cold-worked and recrystallized high purity iron in three impurity ranges was made. Finally, the variations of magnetoabsorption signals from iron and nickel were investigated as a function of dynamic and internal stresses and as a function of temperature [2].

A simplified description of the magnetoabsorption phenomena has been developed and will be presented in the following paragraphs.

B. Simplified Model of Magnetoabsorption

When a ferromagnetic specimen is inserted into a static magnetic field on which is superimposed a radio-frequency field, as shown in Figure 4, the specimen will absorb energy from the radio-frequency field. The amount of energy absorbed will depend upon the magnitude of the radio-frequency field and the electrical parameters of the specimen: permeability, μ , permittivity, ϵ , and conductivity, σ . If the magnitude of the rf field is sufficiently small, then the permeability applicable to the specimen is the reversible permeability which is defined as

$$\mu_0 \mu_r = \lim_{\Delta H_{rf} \rightarrow 0} \left(\frac{\Delta B_{rf}}{\Delta H_{rf}} \right) \quad (1)$$

for a constant value of the bias field where ΔB_{rf} is a change in induction resulting from an infinitesimal change in magnetization, ΔH_{rf} .

The configuration of Figure 4 is highly analogous to the operation of a transformer where the coil represents the primary and the cylindrical specimen the secondary. The primary coil induces circular currents in the specimen which exhibits a surface impedance that is dependent upon the electrical parameters of the specimen and its physical configuration. From electromagnetic principles, a surface impedance [3]

$$Z_s = \frac{E_s}{I_t} \quad (2)$$

can be defined for a conductor in a time varying field where E_s is the electric field at the surface, and I_t is the total current in the conductor. The exact

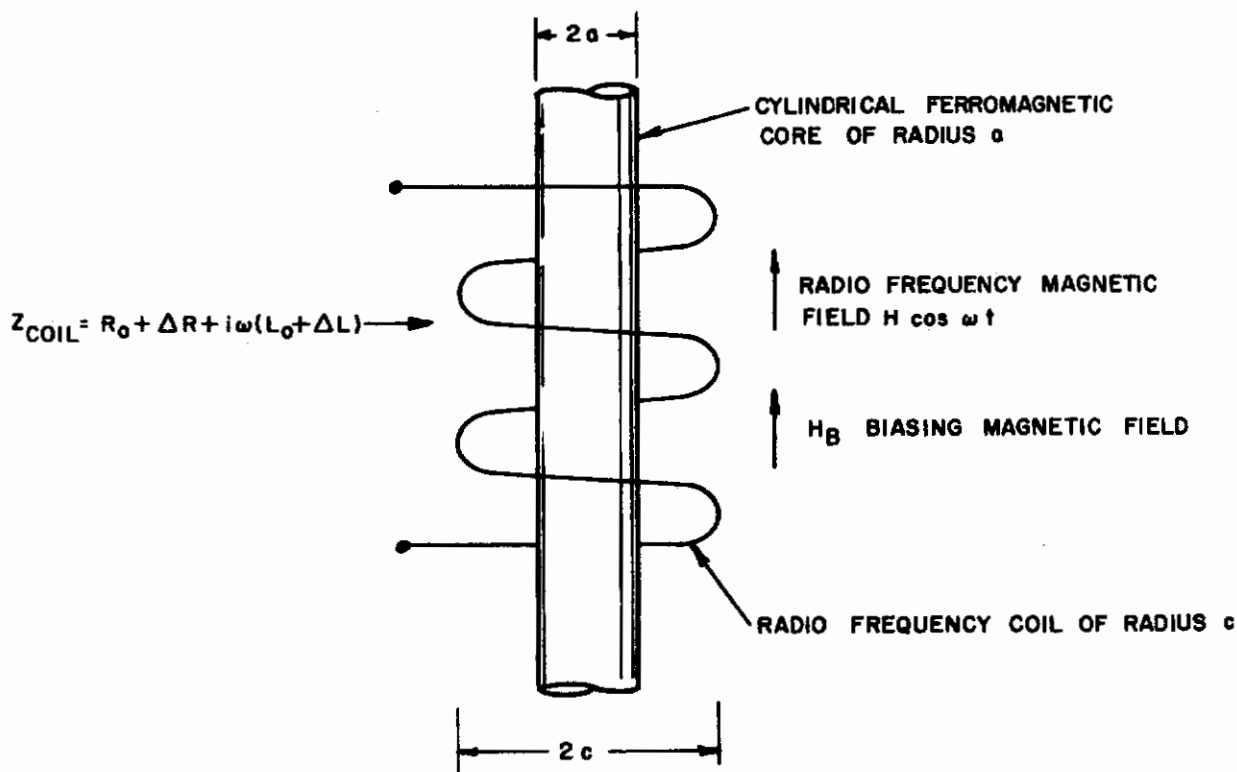


FIGURE 4. GEOMETRY OF SAMPLE COIL AND CYLINDRICAL SPECIMEN

form of the impedance reflected into the rf coil can be obtained from Equations (2) and (3) of [2]. These equations are

$$F_R = 2.23 \times 10^{-4} a \sqrt{\mu_T} - 0.18 \times 10^{-7} \tag{3}$$

$$F_L = 2.23 \times 10^{-4} a \sqrt{\mu_T} + 0.08 \times 10^{-7}$$

In this case, these express for nickel wire with radius (a) the normalized impedance reflected into the coil at a 500-kcps frequency. F_R is the dissipative part and F_L the dispersive part. The above impedance suggests that a surface impedance, derived from the definition of Equation (2)*

$$Z_s = R_s + j\omega L_s$$

$$= \sqrt{\frac{\omega \mu_0 \mu_T}{2\sigma}} (1 + j) \tag{4}$$

*The surface impedance shown is actually applicable to the case for a conducting half space. But as the skin depth becomes appreciably small compared to the diameter of the specimen, Z_s for the planar case is approached.

is involved in the impedance experienced by the coil since both Equation (3) and (4) are proportional to the square root of reversible permeability. This surface impedance at the specimen is, by the nature of the physical configuration, reflected into the rf coil. The surface impedance, when reflected, displays a dissipative term proportional to R_s and a dispersion term proportional to L_s . Thus, as the value of reversible permeability is changed by varying the static bias field, H_B , a new value of impedance is reflected into the coil. During a cyclic variation of the bias field, a magnetoabsorption signal is detected by the marginal oscillator which senses the impedance changes in the radio-frequency coil caused by the variations in the surface impedance terms R_s and ωL_s .

If a ferromagnetic test specimen is now subjected to an axial stress, the values of reversible permeability will be highly influenced. If the ferromagnetic specimen has a positive magnetostrictive characteristic, the permeability will increase for tensile stresses and decrease for compressive stresses. For a specimen having a negative magnetostrictive characteristic, the opposite is true. A more complete discussion of this effect is given in Bozorth [4] and in Reference [2]. A study of the influence of stress on the magnetoabsorption signal is the major subject of this technical report.

C. Summary of Efforts for 1965

A refinement of the magnetoabsorption measuring equipment technique was realized to detect low amplitude magnetoabsorption signals from specimens offering a small effective filling factor to a sample probe. The conditions under which the sensitivity of a marginal oscillator can be maximized and yet reproduce a magnetoabsorption signal with sufficient fidelity were derived. With these conditions serving as guidelines a vacuum tube marginal oscillator having a large sensitivity to small magnetoabsorptions was developed. Also, developed in the efforts were an assortment of probes that are effective in measuring material properties or defects at specific small areas on ferromagnetic surfaces. A transformer method by which these small probes can be coupled to a marginal oscillator and yet sustain oscillations was demonstrated.

With these equipment refinements, the variation in the magnetoabsorption signals and harmonics were measured from maraging steel plates, one of which contained a weld and the other different degrees of surface roughing. For the weldment, attempts were made to relate the magnetoabsorption signal to the direction of the stress both at the weld and at the unwelded areas. For the plate with different degrees of surface roughing, the harmonic amplitude variations were related to the observable surface conditions.

Other studies employing magnetoabsorption techniques were also performed. Samples of HY-80 that had been bent in a constant strain fixture were investigated. From these efforts, it was shown that magnetoabsorption signals can determine the direction and type of stress caused by the internal

Conclusions

or "locked-in" strains. It is also shown that magnetoabsorption signals from nickel film plated onto aluminum rods and plates can be related to the stress within the nonferromagnetic material, aluminum, when undergoing compressive and tensile loading. The method by which the nickel is plated to aluminum is described, and evidence is given to the quality of the bonding strength. It is further indicated that repetitive results (magnetoabsorption signals) can be obtained with variations in loading if the aluminum is not yielded. Finally, throughout the report, evidence is developed to indicate that harmonic analysis of the magnetoabsorption, to include both phase and amplitude information, will be a useful method by which to investigate the properties of ferromagnetic materials and nonferromagnetic materials with ferromagnetic coatings.

SECTION II

MAGNETOABSORPTION SIGNALS FROM MARAGING STEEL PLATES

A. General

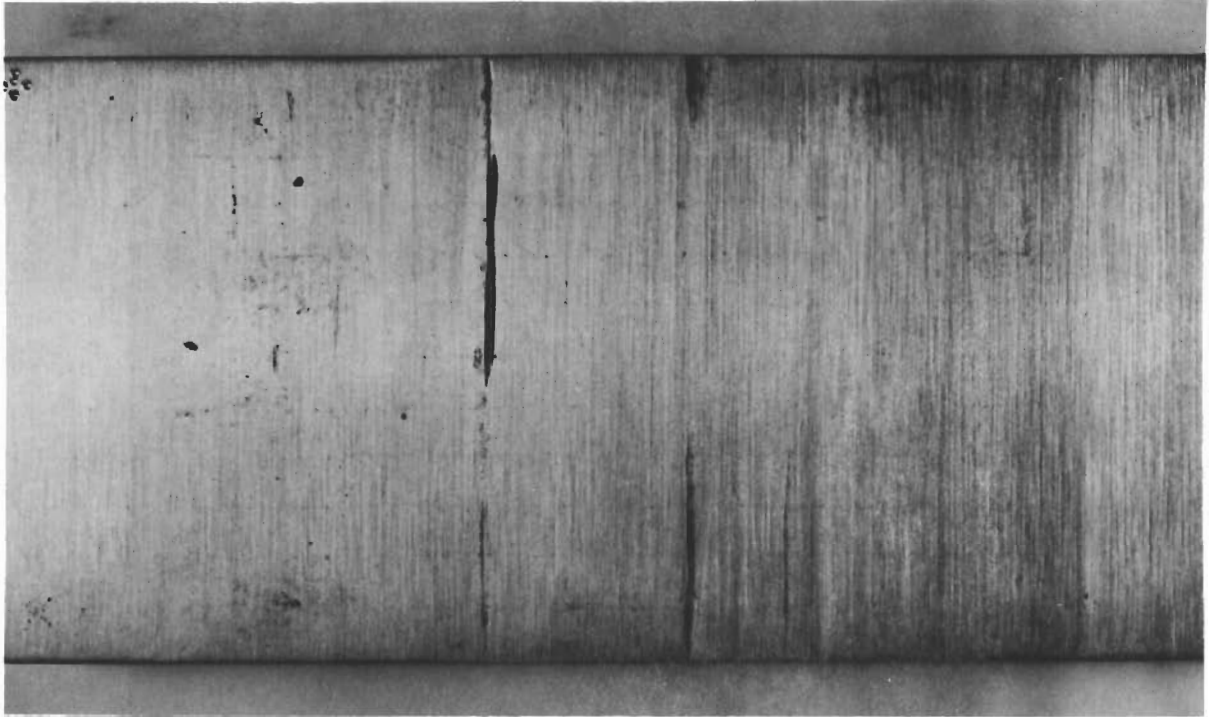
Magnetoabsorption measurements were made on a maraging steel plate containing a weld and on a ground sample of maraging steel having nine EDM slots. The surface around some slots had been scratched and roughened. The top and bottom of the welded sample, after it had been ground, are shown in Figure 5. The weld is visible as the central portion of the top of this plate.

The sample with the EDM slots is shown in Figure 6. The locations of the slots are marked with ink for ease in identification. The slots should not be confused with the numbered lines on the right and their image on the left. These numbered lines indicate the number of the scan made across the specimen. Each of the nine slots is 20 mils wide and 375 mils long. The three slots on the left side are believed to have been untouched and are approximately 30 mils deep. The three centrally located slots had been roughed to various degrees to obscure them with local surface imperfections. The degrees of roughing are visible in the photograph of Figure 6. Not visible in the photograph, however, is the evidence that the rims of the center slot of the three had been folded by grinding and honing. The right-hand slots had been ground and honed until the slots were hardly visible. The experimental observations of the influence of welds, surface conditions, and EDM slots in maraging steel plates on the magnetoabsorption signal are presented in this section. These samples were provided by the Boeing Company at the request of the Sponsor for a period of two weeks.

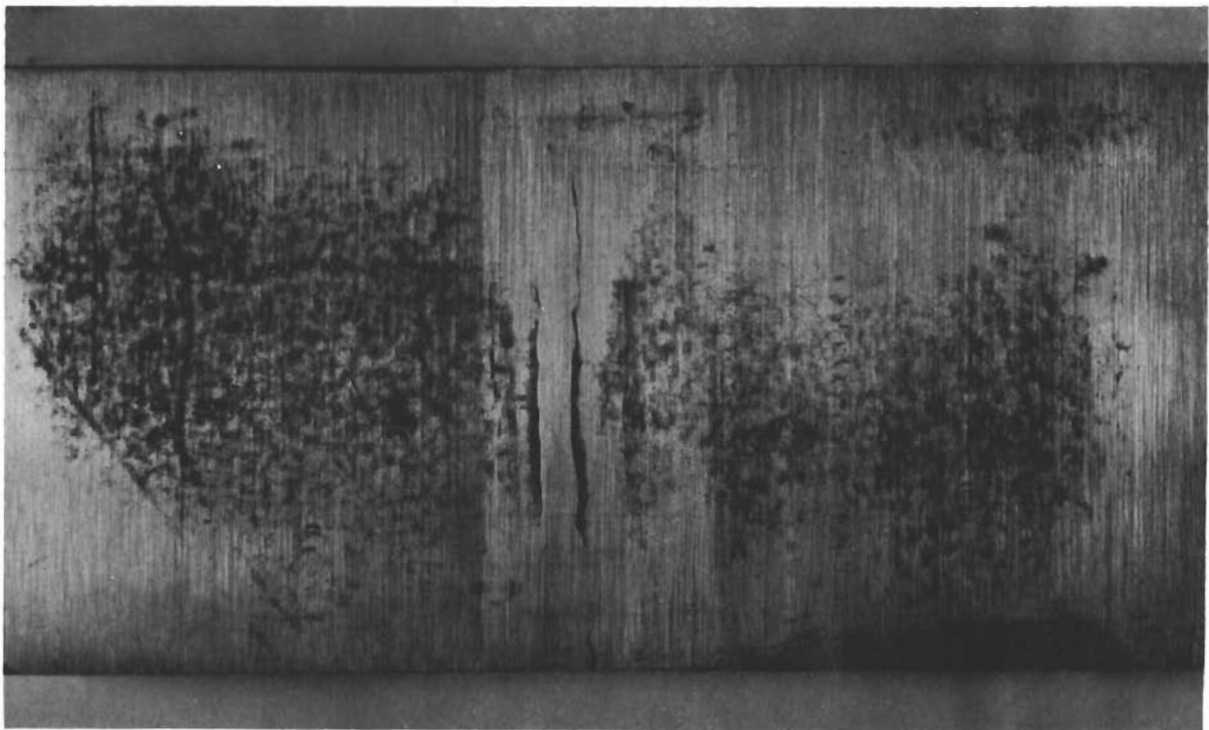
B. Measurement Techniques

Different measuring techniques were employed for the samples. For the maraging steel weldment, magnetoabsorption waveforms were photographed from an oscilloscope screen when a 1/4-inch double-D sample probe* rested at various positions on the top and bottom sides of the plate. This discrete measurement technique is suitable for a sample having well-defined regions of interest. However, for the plate with EDM slots, characteristics of the magnetoabsorption signal other than the waveform were considered. Since the material properties varied extensively over the surface, continuous measurements were appropriate. As an example, peak-to-peak amplitude of magnetoabsorption signal or harmonic amplitudes of the magnetoabsorption signal could be measured along each scan line. Phase measurements of the harmonics would also prove useful, but this type measurement could not be made without extensive equipment additions. Of the initial two measurement

*A description of probe configurations including the double-D design is presented in Appendix I.



(a)



(b)

FIGURE 5. GTA WELDMENT OF MARAGING STEEL

techniques, the harmonic amplitude analysis proved to contain information most easily related to the slots and surface conditions within the time limit allowed for the use of this sample.

The magnetic environment of the samples was varied by means of a solenoidal bias coil. The weldment was oriented with its weld both longitudinal and transverse to the direction of the bias coil, and magnetoabsorption waveforms were measured at various positions for both cases. For the specimen with EDM slots, the bias field coincided with the length of the sample. Therefore, since the slots are transverse to the length, the changes in the magnetic properties of the material will be those caused by the width and depth rather than the length of the slots. Time did not permit measurements on the EDM slotted sample with the bias field in the transverse direction.

The same double-D probe, 1/4 inch in diameter, was employed to detect the magnetoabsorption signals from the EDM specimen. The probe is supported by a long cantilever beam mounted to the carriage of a lathe. The probe, driven by the carriage, scanned the surface of the specimen. The radio-frequency field generated at the tip of the probe is primarily oriented along the direction and in the plane of the biasing magnetization. The cantilever beam, probe, bias coil configuration and other components are shown in Figure 7. The scanning probe was energized from the primary of a ferrite radio-frequency transformer whose secondary is the tank circuit of the marginal oscillator. This transformer has a very large turns ratio (150/3) so that the voltage in the primary, proportional to the absorption in the probe, is fifty times larger in the secondary. The detected amplitude change, the magnetoabsorption signal, is then harmonically analyzed so that a voltage proportional to the amplitude of a harmonic is produced. An X-Y plotter, whose X-axis is synchronized with the probe displacement rate, records the amplitude of the harmonic as a function of distance along a scan line. The block diagram of the system that measured magnetoabsorption signals is shown in Figure 8.

C. Magnetoabsorption Measurements from a Weldment of Maraging Steel

In Figure 9a are shown the magnetoabsorption signals with longitudinal bias at 21 positions on the top of the welded sample. A total of nine of these signals are in the area of the weld itself. Also included in Figure 9a are the magnetoabsorption signals from seven positions on the upper edge and seven positions on the lower edge. For all of the signals of Figure 9a, the magnetic bias field is longitudinal (parallel to the longest dimension) as shown by the arrow labeled H_B in Figure 9a. The magnetoabsorption signals show that the material in the weld is apparently under less stress than the material outside of the weld. These data may also mean that it is magnetically softer. To attempt to determine which of these two possibilities are valid, the magnetoabsorption curves with a transverse magnetic field were made, and they are displayed in Figure 9b. Experience on other samples has shown

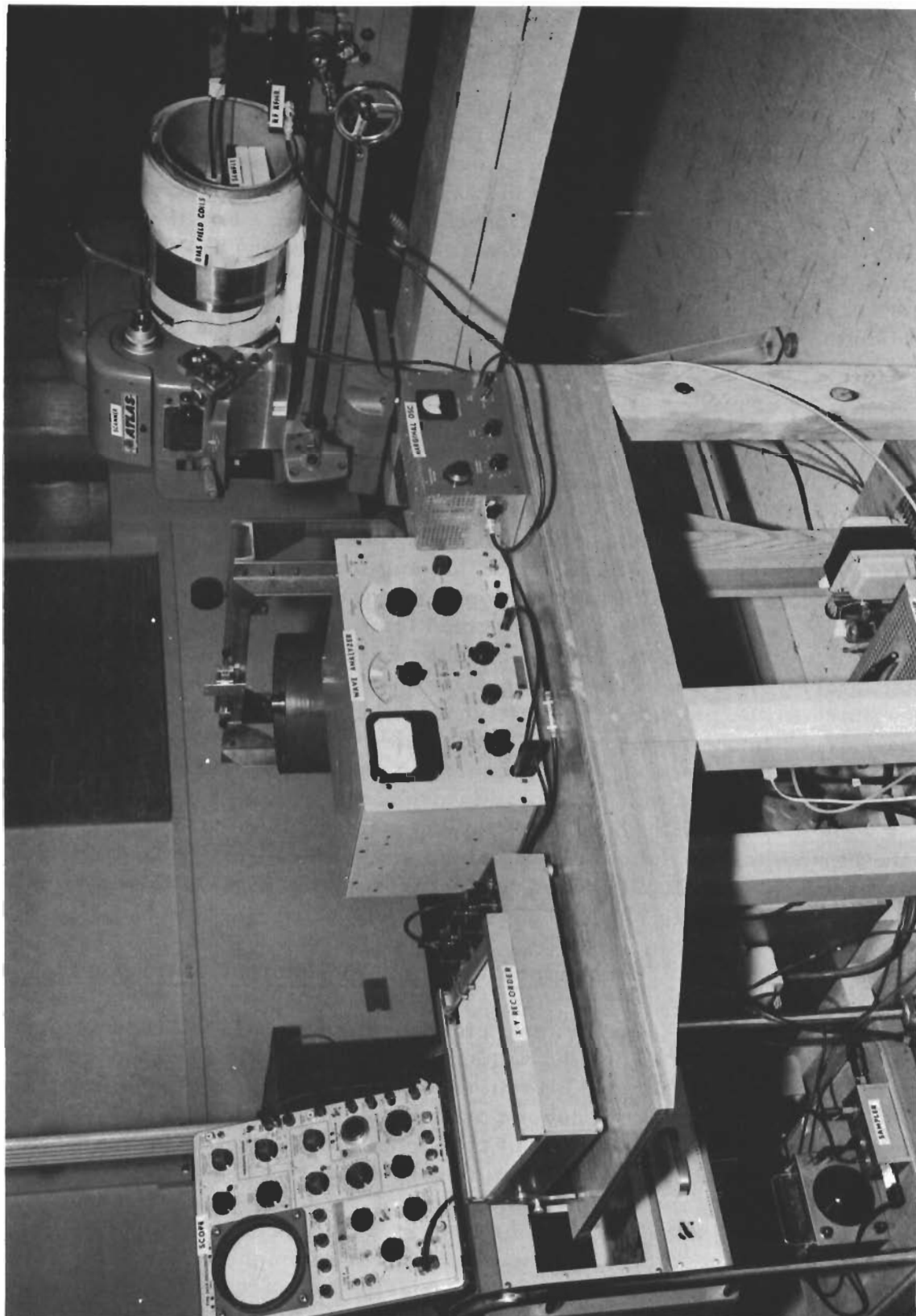


FIGURE 7. LABORATORY SETUP TO MEASURE MAGNETOABSORPTION
HARMONIC VARIATIONS ACROSS A PLATE

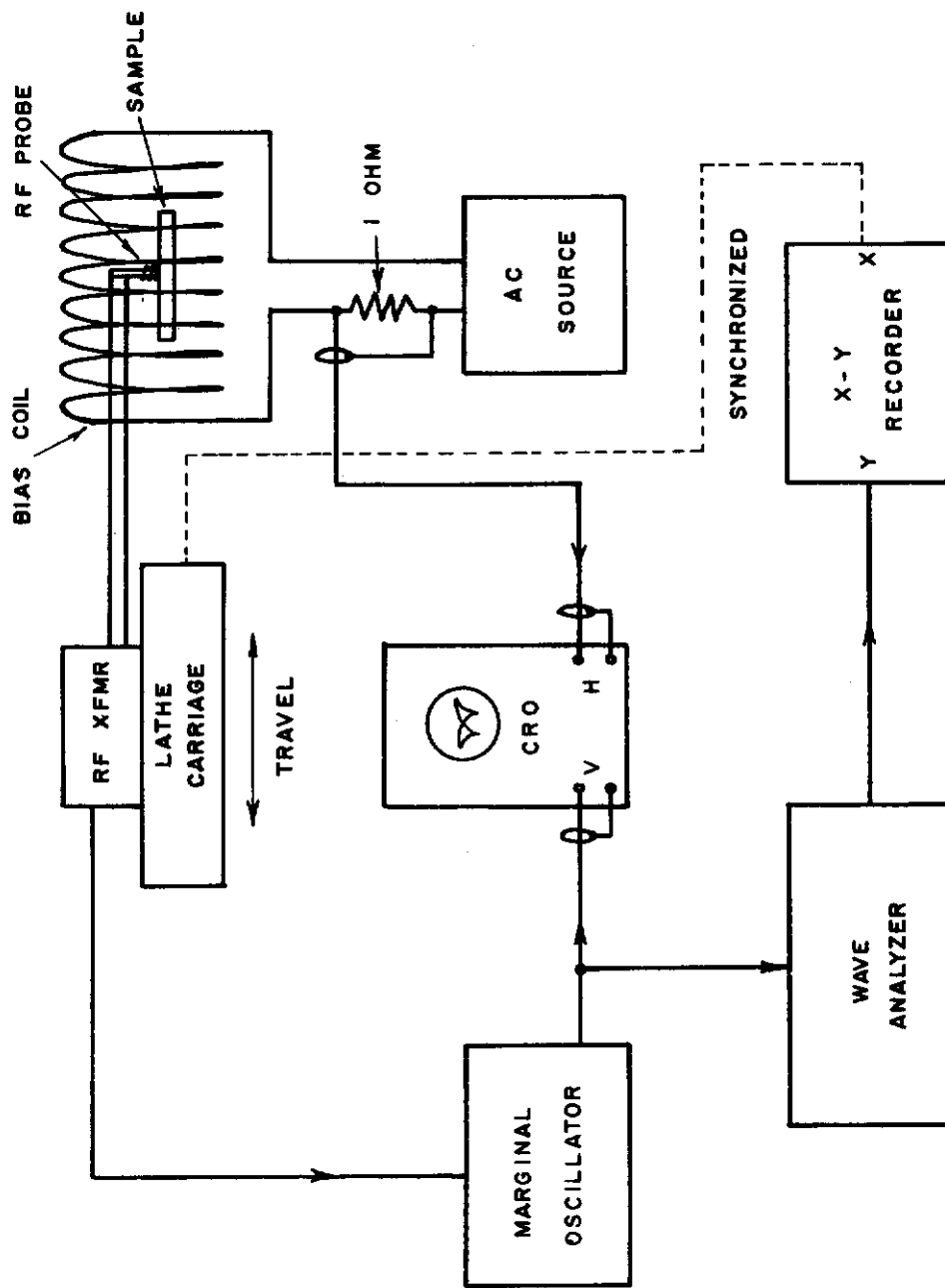


FIGURE 8. BLOCK DIAGRAM OF SURFACE IMPERFECTION DETECTION SYSTEM

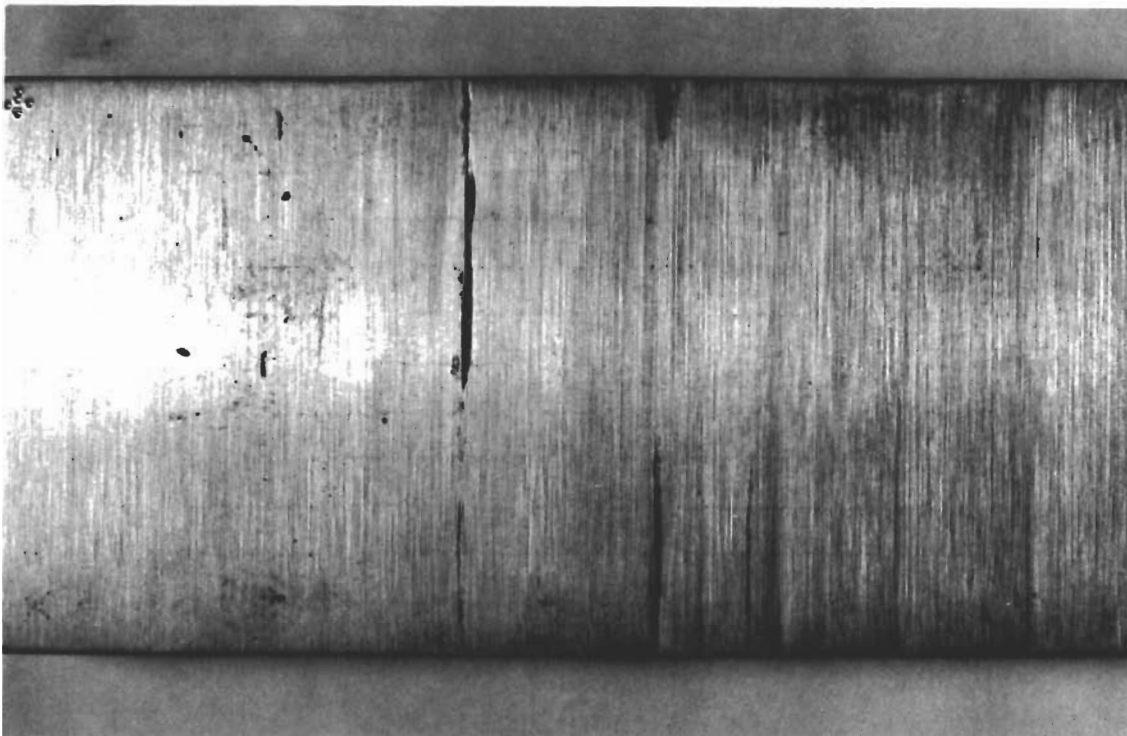


FIGURE 9a. MAGNETOABSORPTION SIGNAL WAVEFORMS AND AMPLITUDES AT INDICATED POSITIONS FOR THE TOP AND SIDES OF A WELDMENT OF MARAGING STEEL HAVING A LONGITUDINAL BIAS FIELD

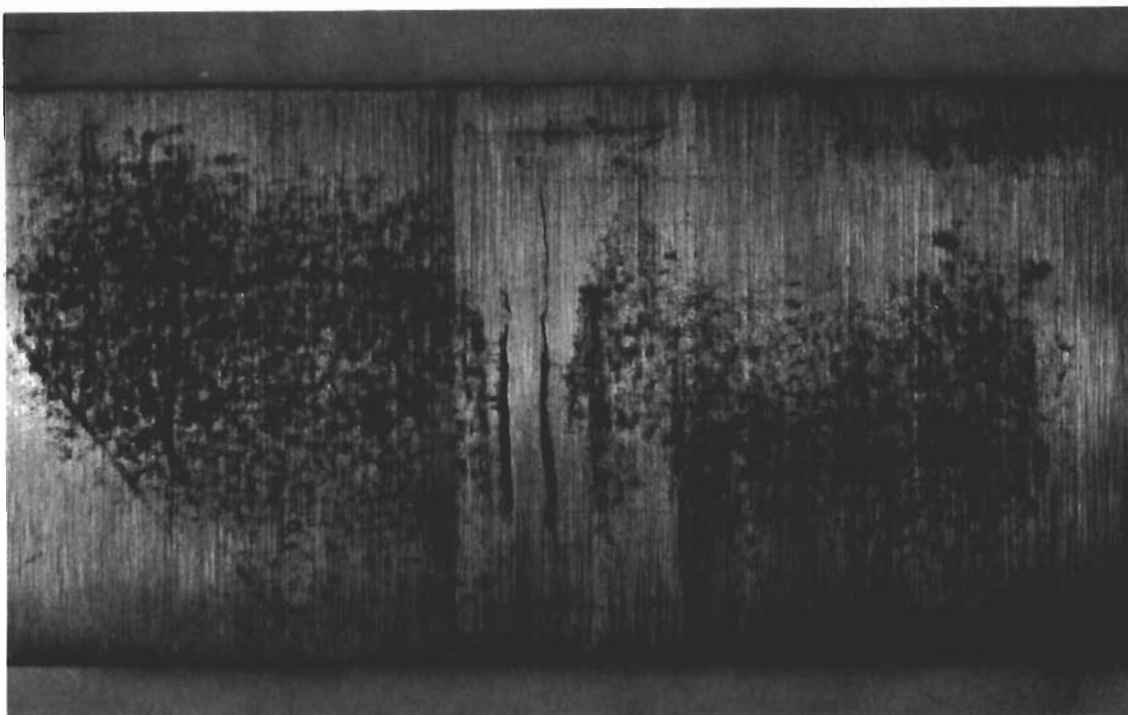


FIGURE 9b. MAGNETOABSORPTION SIGNAL WAVEFORMS AND AMPLITUDES AT INDICATED POSITIONS FOR THE TOP OF A WELDMENT OF MARAGING STEEL HAVING A TRANSVERSE BIAS FIELD

Contrails

that the magnetoabsorption signal is larger when the magnetic bias field is transverse to the direction of stress in a material. Thus, if this material obeys the same rules as previous materials, there will be a smaller magnetoabsorption signal when the bias field is parallel to the stress and a larger signal when it is transverse. A comparison of Figures 9a and 9b shows that the signals at positions 1 through 6 and 16 through 21 (outside of the weld area) are significantly larger with the transverse bias field than with the longitudinal field. In contrast, in the weld area, positions 7 through 15, the magnetoabsorption signals with the transverse field are not significantly larger than those with the longitudinal field. In fact, at some positions, they are smaller. Therefore, this evidence indicates that there is less stress in the material within the weld than outside of the weld.

The magnetoabsorption curves along the bottom of the welded sample, at the same points of Figures 9, are shown in Figure 10a for the longitudinal bias and Figure 10b for the transverse bias direction. These curves again show differences in the transverse over the longitudinal. At positions 31, 35, 32, 33, and 36 (all within the weld area), there was a significant decrease in the amplitude with the transverse direction over the longitudinal direction. In the remaining positions, there was only a slight decrease in amplitude with the transverse direction over the longitudinal direction. Therefore, it appears that the stress in the bottom of the sample, in the weld area, is quite large and is in a direction parallel to the weld direction; whereas, in the top of the sample, in the weld areas, the stress appears to be perpendicular to the weld direction and very small.

D. Experimental Results for the Slotted Plate

A comparison of the variation of the amplitudes of the fundamental (120 cps) and five of the harmonics (240, 360, 480, 600, and 720 cps) for scan line 10 is given in Figure 11a. The absolute amplitude of each harmonic is not of direct significance in this analysis, but changes in amplitude for each harmonic indicate changes in the shape of the magnetoabsorption signal. The very slight change in the amplitude at 120-cps component from end to end indicates that the amplitude of the magnetic bias is relatively constant along the length of the sample. The slight change in the 120-cps component also indicates that the first harmonic is relatively insensitive to surface irregularities such as scratches or slots. The first harmonic (120 cps) is responsive to the changes caused by the honing process used to seal the rims of the center EDM slot together as shown by the decrease in its amplitude. The subsequent higher harmonics responses are shown in the remaining frames.

The amplitude of the 240-cycle component in Figure 11a shows much more variation along the length than does the first harmonic. The greatest variations in the amplitude of this second harmonic occur in the places where an attempt was made to obscure the slots. Amplitude variations can be seen to occur at the position of the slots on line 10.

Contrails

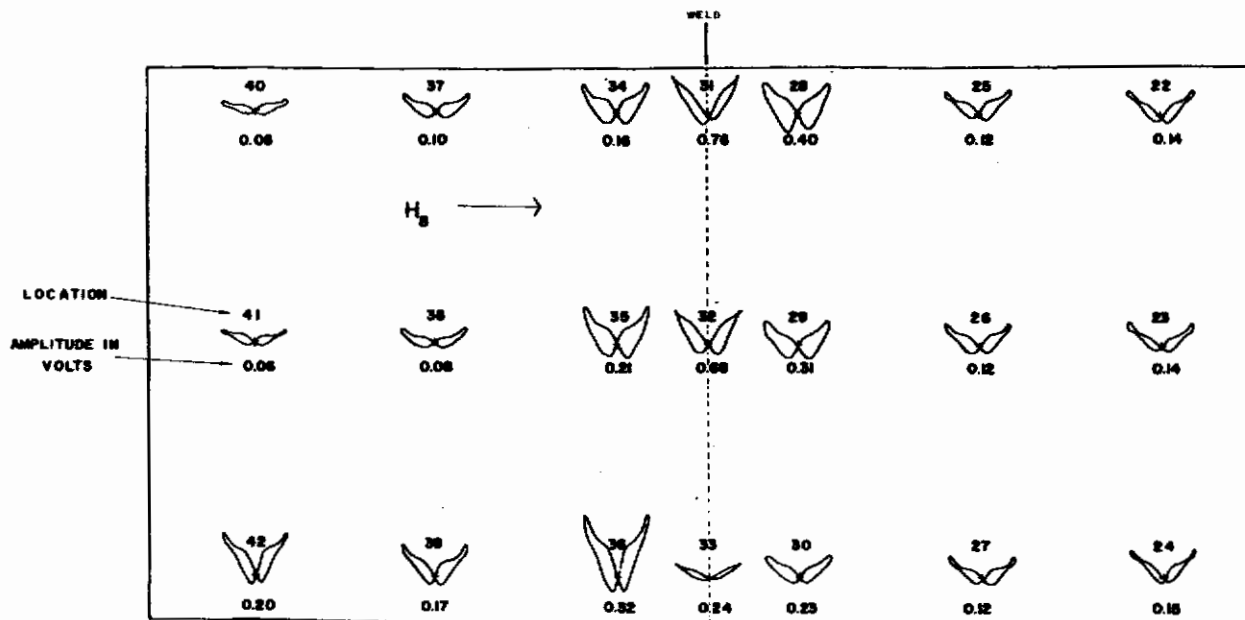


FIGURE 10a. MAGNETOABSORPTION SIGNAL WAVEFORMS AND AMPLITUDES AT INDICATED POSITIONS FOR THE BOTTOM OF A WELDMENT OF MARAGING STEEL HAVING A LONGITUDINAL BIAS FIELD

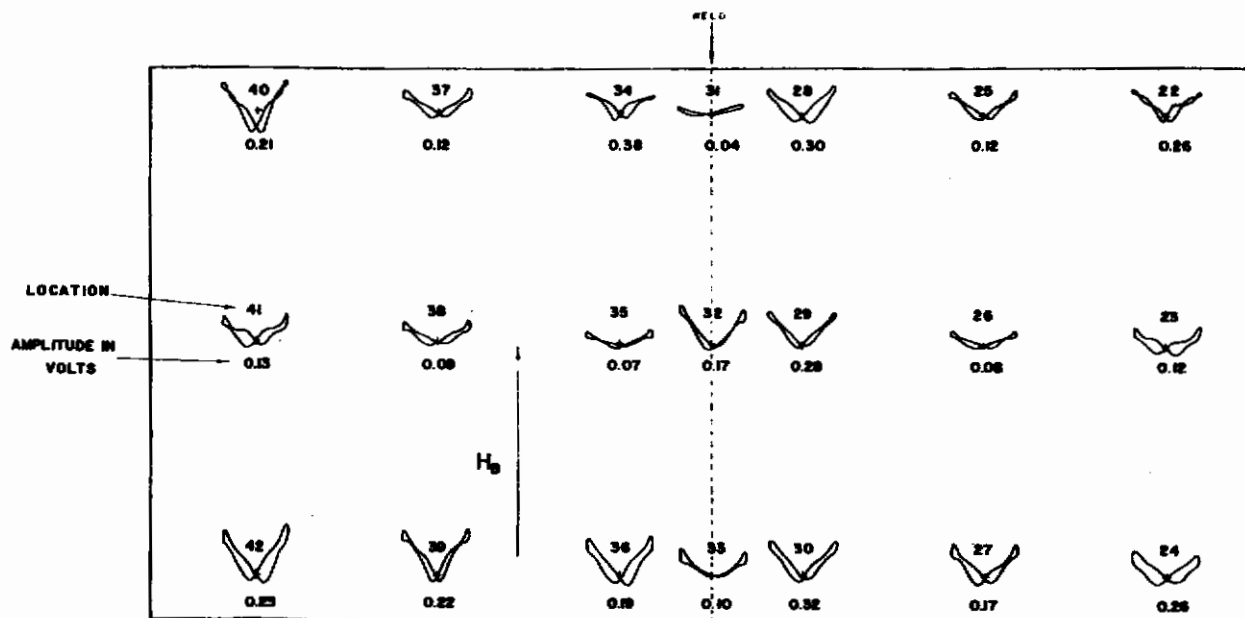


FIGURE 10b. MAGNETOABSORPTION SIGNAL WAVEFORMS AND AMPLITUDES AT INDICATED POSITIONS FOR THE BOTTOM OF A WELDMENT OF MARAGING STEEL HAVING A TRANSVERSE BIAS FIELD

Contrails

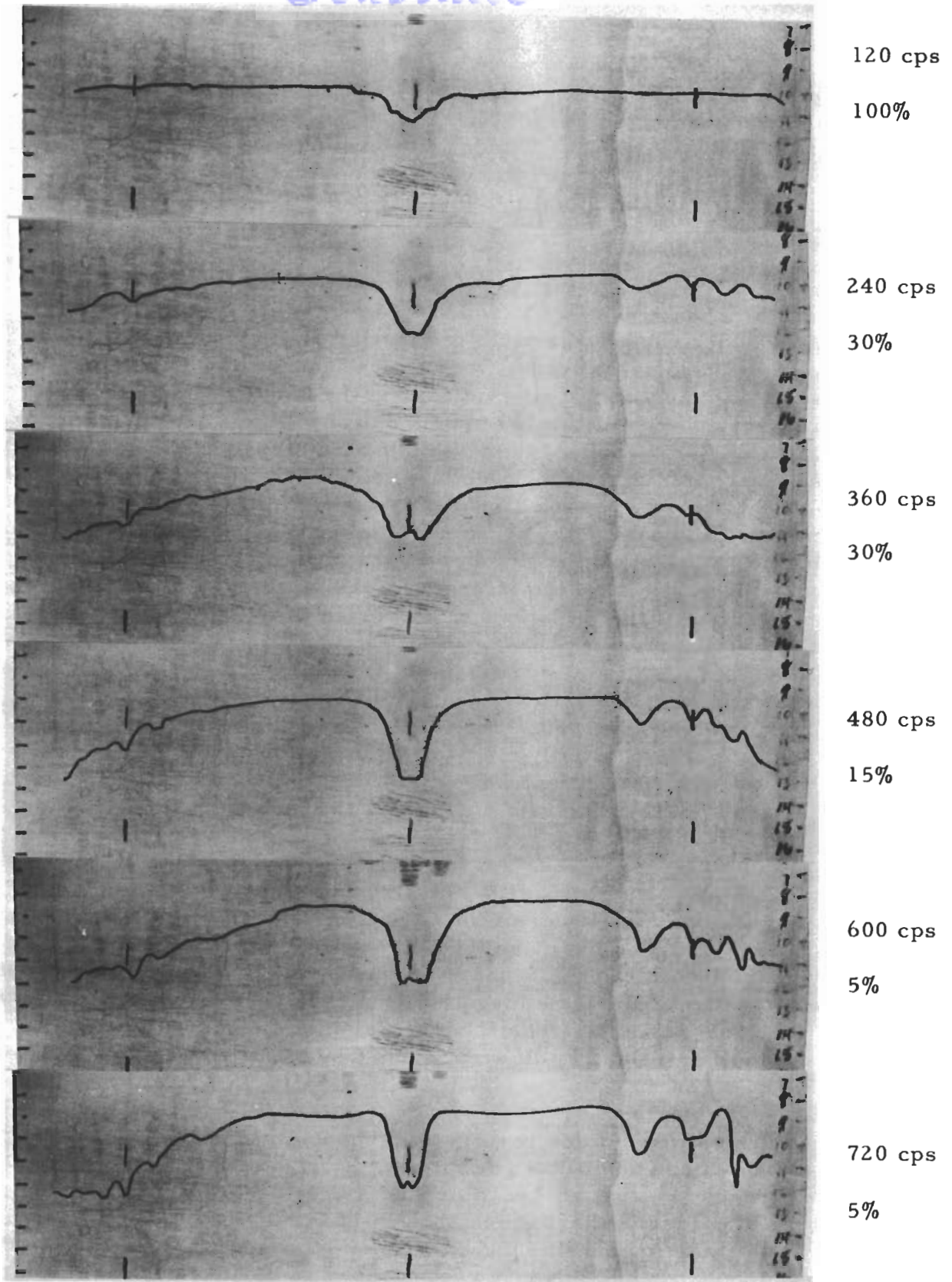


FIGURE 11a. VARIATIONS IN THE AMPLITUDE OF THE HARMONICS (INDICATED AT LEFT) IN THE MAGNETOABSORPTION SIGNAL MEASURED ALONG LINE 10 OF SPECIMEN

Contrails

The amplitudes of the 360-, 480-, 600-, and 720-cycle components of the magnetoabsorption curve each show increasing variation along the length as the frequency increases. There is a change in amplitude at each slot. There is a decrease in amplitude at the two outside slots. At the center slot, where the deep "well" in amplitude has been caused by the treatment, there is an increase in amplitude at the slot of the 360-, 600-, and 720-cycle components.

A visual inspection of the photograph of the surface of the sample of Figure 6 indicates that the areas in which the greatest preparation of the sample had been accomplished are the areas where the greatest change in the amplitudes of the harmonics occur. An as yet unmeasured variable is the exact variation in the magnetic bias field along the length. The lack of a variation in the amplitude of the 120-cycle component indicates that there is little variation in the strength of the bias field along the length. However, it may be that a variation in the magnetic bias too slight to be seen on the 120-cycle component will be a large change on the amplitudes of the higher frequency components, although the agreement between the start of the amplitude changes and the beginning of the grinding on the right side is too coincident to be caused only by variation in the strength of the magnetic bias field. The evidence to date favors the variations to be caused by sample variations rather than bias field variations.

The curves of Figure 11b are those for the variation in amplitude of the harmonics at 840, 960, 1080, 1200, and 1320 cycles. The amplitudes of these harmonics show essentially the same information as the amplitudes of the other harmonics. In addition, however, the amplitudes of the harmonics above 720 cycles appear to indicate clearly the two undisturbed regions of the sample on each side of center.

The percentage numbers with each harmonic shown on Figures 11a and 11b represent the relative amplitudes of the harmonic relative to the fundamental at 120 cps. For example, the magnitude of the variation in the amplitude of the 720-cycle component is 5% of that of the fundamental. Thus, although the variations appear to be the same magnitude for each harmonic, they are only relatively the same percentage variation in the amplitude of each harmonic, while the absolute amplitude is different according to the percentage figures shown in Figures 11a and 11b.

The harmonic amplitude responses along other scan lines were also recorded. From these additional recordings, it can be concluded from the evidence of Figures 41a through 41e in Appendix II that there are variations of the amplitude of the higher harmonics around the EDM slots. There are also variations in the amplitude of the higher harmonics caused by grinding, honing, scratching the surface, and other, as yet unknown, influences. It is further

Contrails

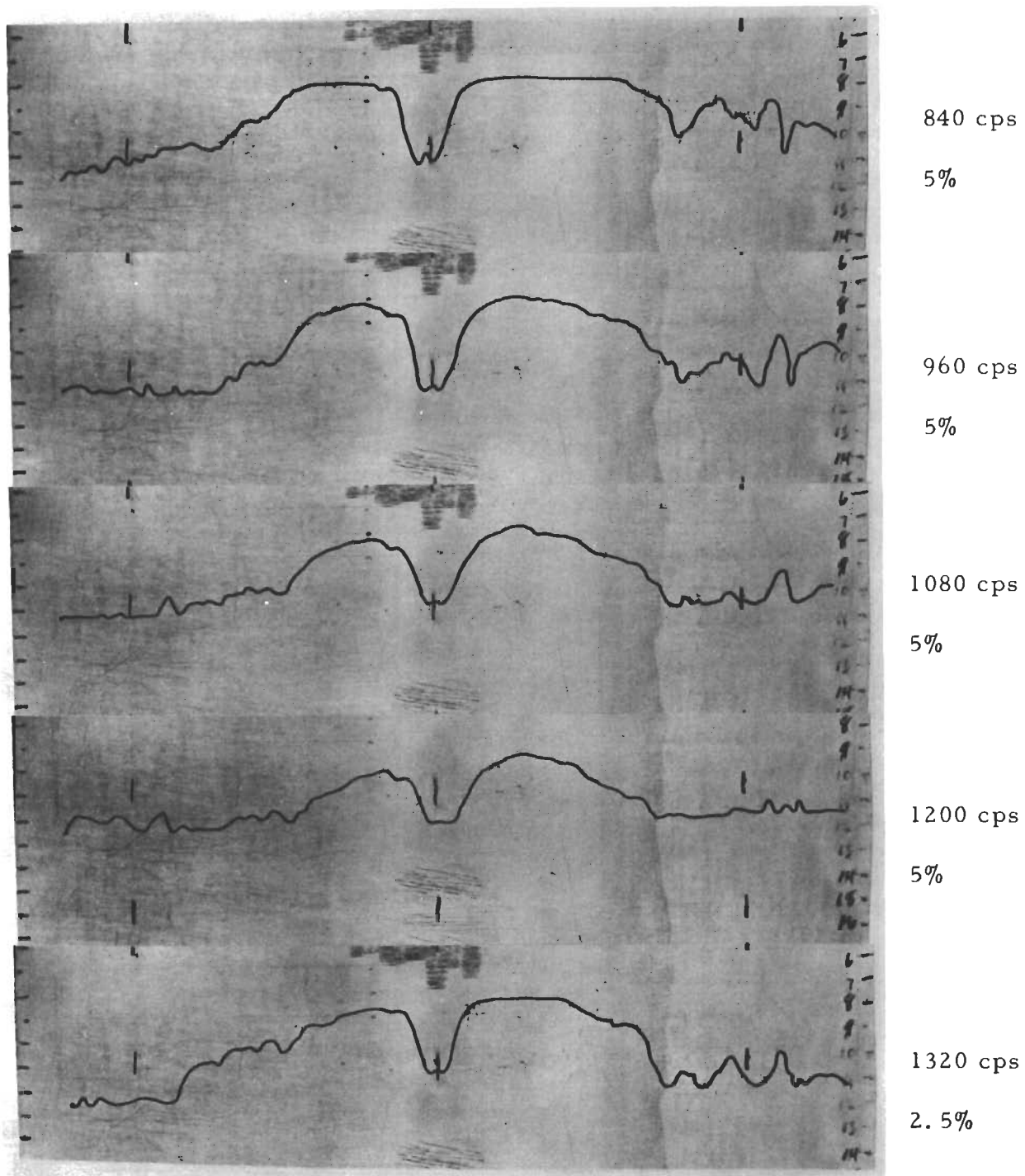


FIGURE 11b. VARIATIONS IN THE AMPLITUDE OF THE HARMONICS (INDICATED AT LEFT) IN THE MAGNETOABSORPTION SIGNAL MEASURED ALONG LINE 10 OF SPECIMEN

Contrails

concluded that the phase information for each harmonic, relative to the fundamental, must be obtained before the complete picture can be assembled of the useful information supplied by the magnetoabsorption measurements of such a sample. A detailed description of the responses from a selection of scan lines is presented in Appendix II.

SECTION III

MAGNETOABSORPTION MEASUREMENTS ON HY-80 STEEL*

A. Introduction

A limited number of magnetoabsorption measurements was performed on six specimens of HY-80 steel. Three of the specimens were unstressed. Of these three, two (S-1 and S-2) were ground to size but were given no heat treatment. The third, S-3, was stress relieved after being ground to size. The other three specimens (S-3, S-4, and S-5) were bent in a constant strain fixture with 0.45%, 0.82%, and 1.0% residual strain, respectively.

The magnetoabsorption measurements give an indication of the shape of the B/H loop for the material being investigated. That is, as the shape of the B/H loop is changed by changes in the material, the relative reversible permeability curve will also be changed. As shown in Figure 12, the magnetoabsorption curve is obtained directly from the relative reversible permeability curve. The value of the magnetoabsorption curve at any particular value of the magnetic bias is equal to a constant times the square root of the relative reversible permeability at that same magnetic bias.

Experience has shown that stress in a ferromagnetic material will cause a change in the B/H loop. In fact, sufficient stress will cause the B/H loop to become a straight line. Some of the changes in the relative reversible permeability (and therefore the magnetoabsorption signal through Fig. 12) caused by changes in the B/H loop are shown in Figures 13a, 13b, and 13c. The cold-work caused the B/H loop to become more open and of a square shape. The relative reversible permeability curve became smaller and broader. It is this kind of behavior that is to be expected with the grinding, annealing, and bending in the six samples of HY-80.

B. Measurement System

The detection head used for the first series of measurements is shown in Figure 14. With this system, the magnetic field is applied parallel to the long axis of the sample. The magnetoabsorption detection coil is at right angles to the sample and to the magnetic field. The coil is held 1/8 inch away from the material by the plastic cover (see Fig. 14). The magnetizing coils are fed with a 60-cycle voltage to provide a magnetomotive force sufficient to saturate the sample.

*For measurement of this type on a 1020 bulge plate, the reader is referred to Appendix IV.

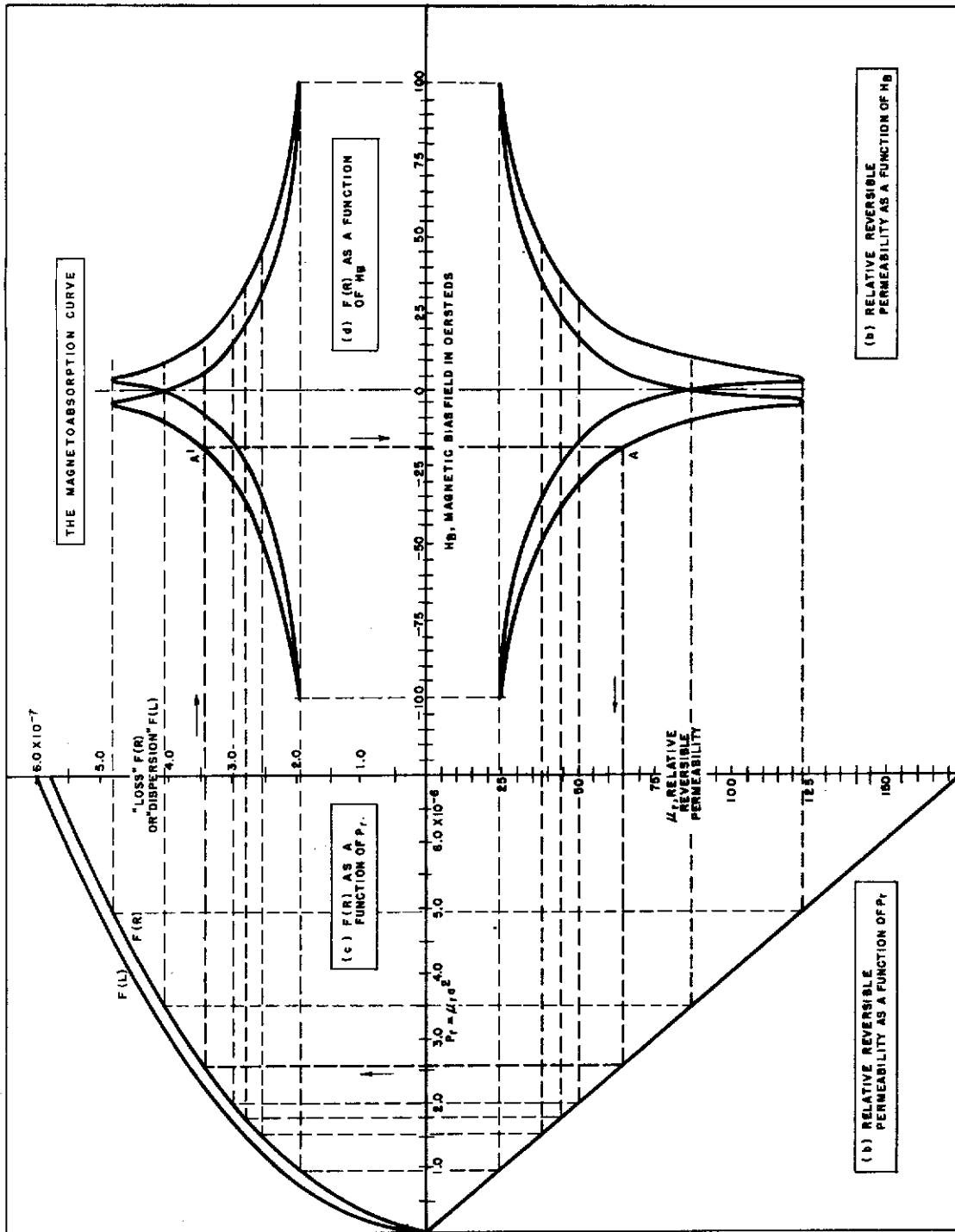


FIGURE 12. MAGNETOABSORPTION AS A FUNCTION OF REVERSIBLE PERMEABILITY

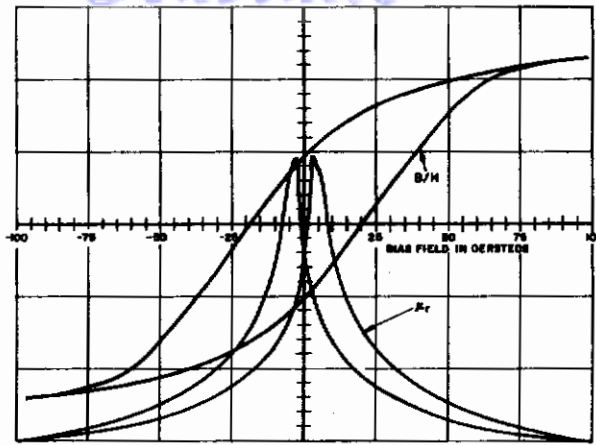


FIGURE 13a. SUPERPOSITION OF THE B/H LOOP AND THE RELATIVE REVERSIBLE PERMEABILITY CURVES FOR IRON THERMOCOUPLE WIRE

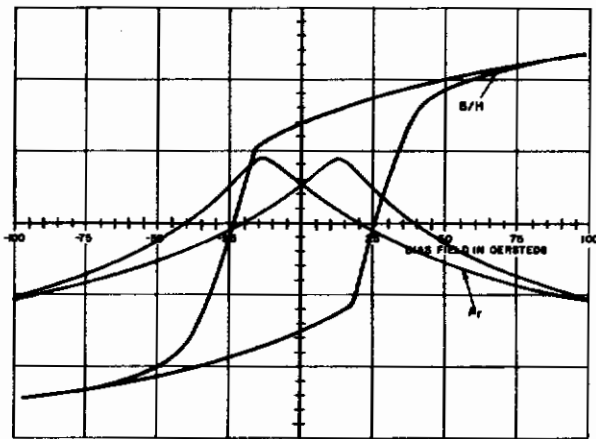


FIGURE 13b. SUPERPOSITION OF THE B/H LOOP AND THE RELATIVE REVERSIBLE PERMEABILITY CURVES FOR UNANNEALED NICKEL WIRE

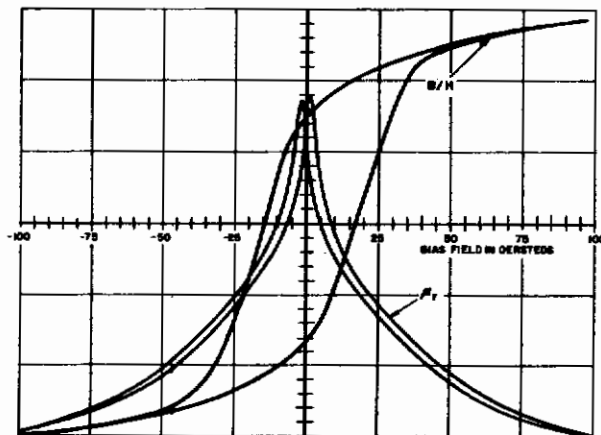


FIGURE 13c. SUPERPOSITION OF THE B/H LOOP AND THE RELATIVE REVERSIBLE PERMEABILITY CURVES FOR ANNEALED NICKEL WIRE

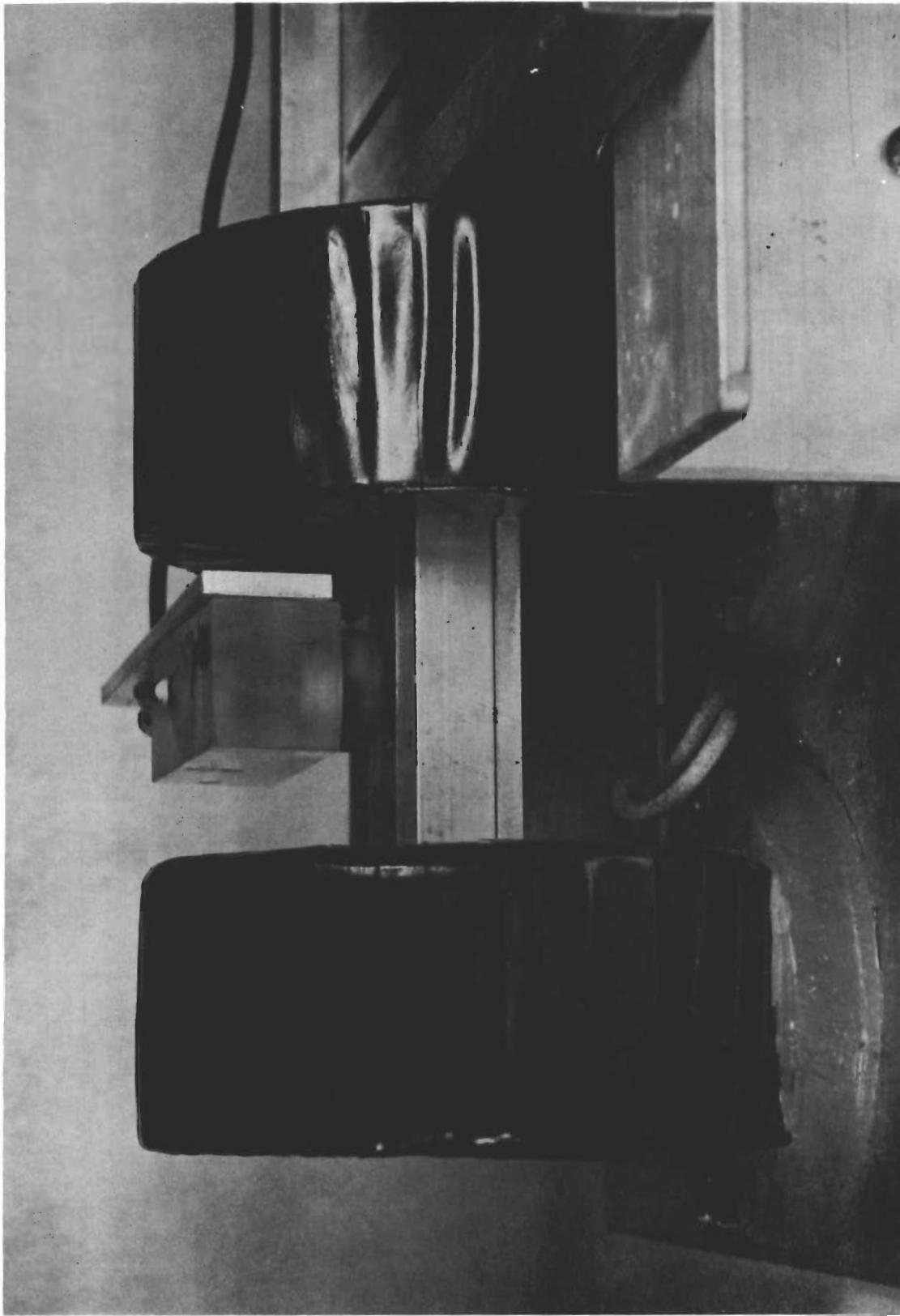


FIGURE 14. MAGNETOABSORPTION MECHANISM FOR PROVIDING MEASUREMENTS ON ONLY ONE FACE OF A CHARPY IMPACT SPECIMEN

The second series of measurements were made with the probe of Figure 15. This probe can measure the magnetoabsorption signal with the magnetizing field both perpendicular to the stress direction and parallel to the stress direction. With the system of Figure 14, the measurement could only be made with the magnetizing field parallel to the stress direction.

The photograph of Figure 16 shows the complete measuring system used for the first series of measurements. The holding mechanism for the Charpy samples has been removed to permit the samples to be pushed all of the way through the magnetizing coils.

C. First Series of Measurements

The magnetoabsorption signals from the center of the two broad faces of the first three samples (S-1, S-2, and S-3) are shown in Figure 17. The entire length was surveyed, but no signals significantly different, in either amplitude or shape, from those shown in Figure 17 were found.

The two curves from the two faces of sample S-1, Figure 17, indicate that the shaping and grinding operations have: (1) placed a residual stress in the material, and (2) induced a small magnetic field in the direction of the long axis of the sample. The curves obtained from both faces are essentially the same.

The magnetoabsorption signals from sample S-2, Figure 17, indicated the presence of a residual stress and a magnetic field. The direction of the induced magnetic field is opposite to that of sample S-1 as indicated by the opposite tilt of the magnetoabsorption signals. When the sample is reversed, the signals have the opposite tilt direction. The magnetoabsorption signal from face "A" is smaller than that from face "B" in sample S-2. This could mean a larger grinding cut on one side than another in sample S-2 and similar cuts on sample S-1.

When the sample is heat treated to relieve the stresses, the lower curves of Figure 17 are obtained for sample S-3. These curves are symmetrical and indicate a symmetrical B/H loop with no residual stress and no induced magnetic field.

The magnetoabsorption signals from the stressed samples are shown in Figure 18. For all of these specimens, the "A" face is the convex surface whereas the "B" face is the concave surface. Thus, the "A" face was in tension during the bending and is now in compression; the "B" face was in compression during the bending and is in tension afterward. On the figures, the "A" and "B" faces are labeled "Tension" and "Compression" as per their stress after bending.

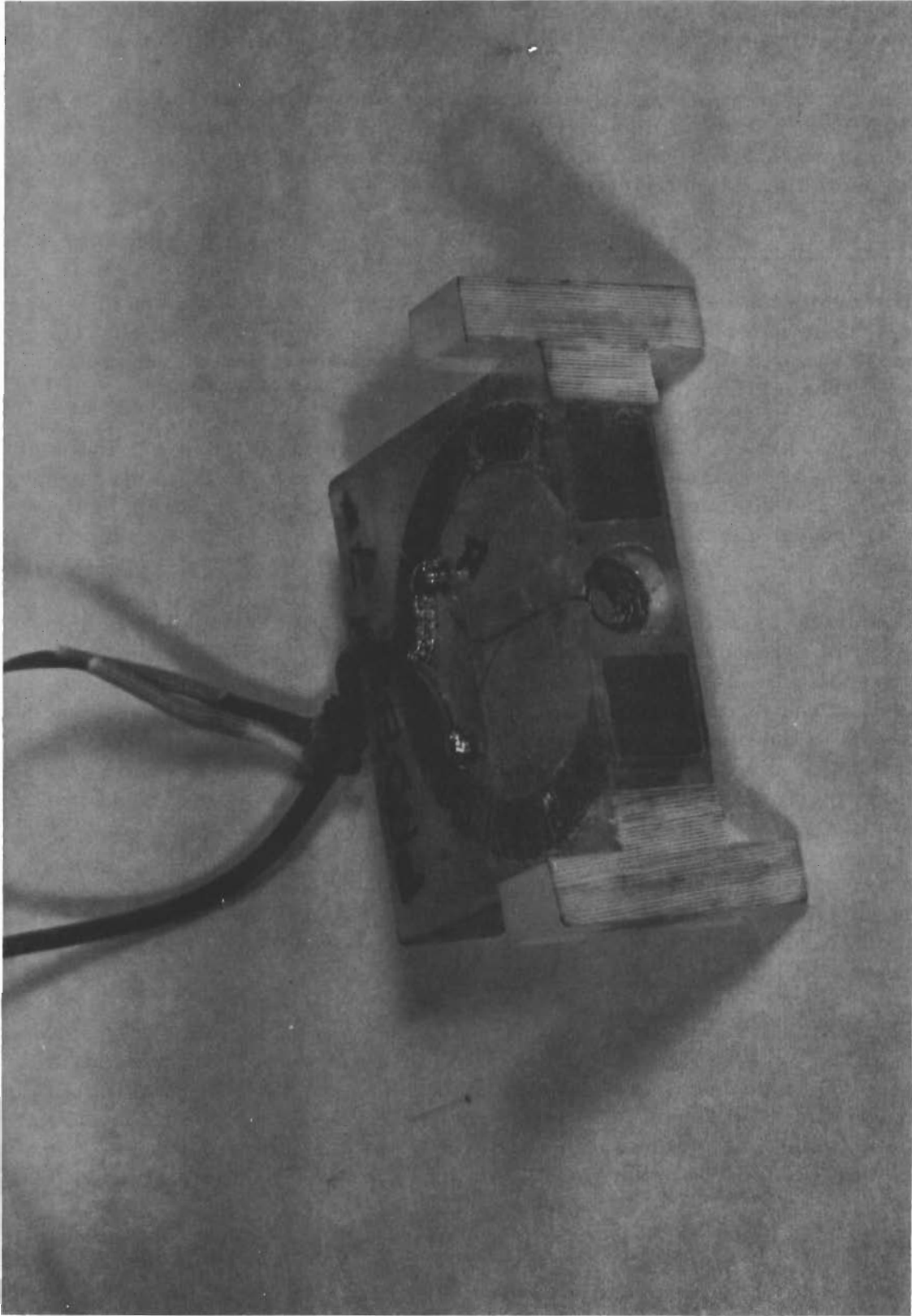


FIGURE 15. MAGNETOABSORPTION DETECTION HEAD FOR MEASUREMENTS ON FLAT SHEETS



FIGURE 16. COMPLETE MEASURING SYSTEM FOR FIRST SERIES OF MEASUREMENTS

Contrails

- Notes: ① $f_0 = 225$ Kcps
 ② Sample coil #B
 ③ EDC Detector = 0.2V
 ④ $i_{coils} = 0.2A$ (60cps AC)
 ⑤ Measured at center of $1\frac{1}{2}'' \times 12''$ faces

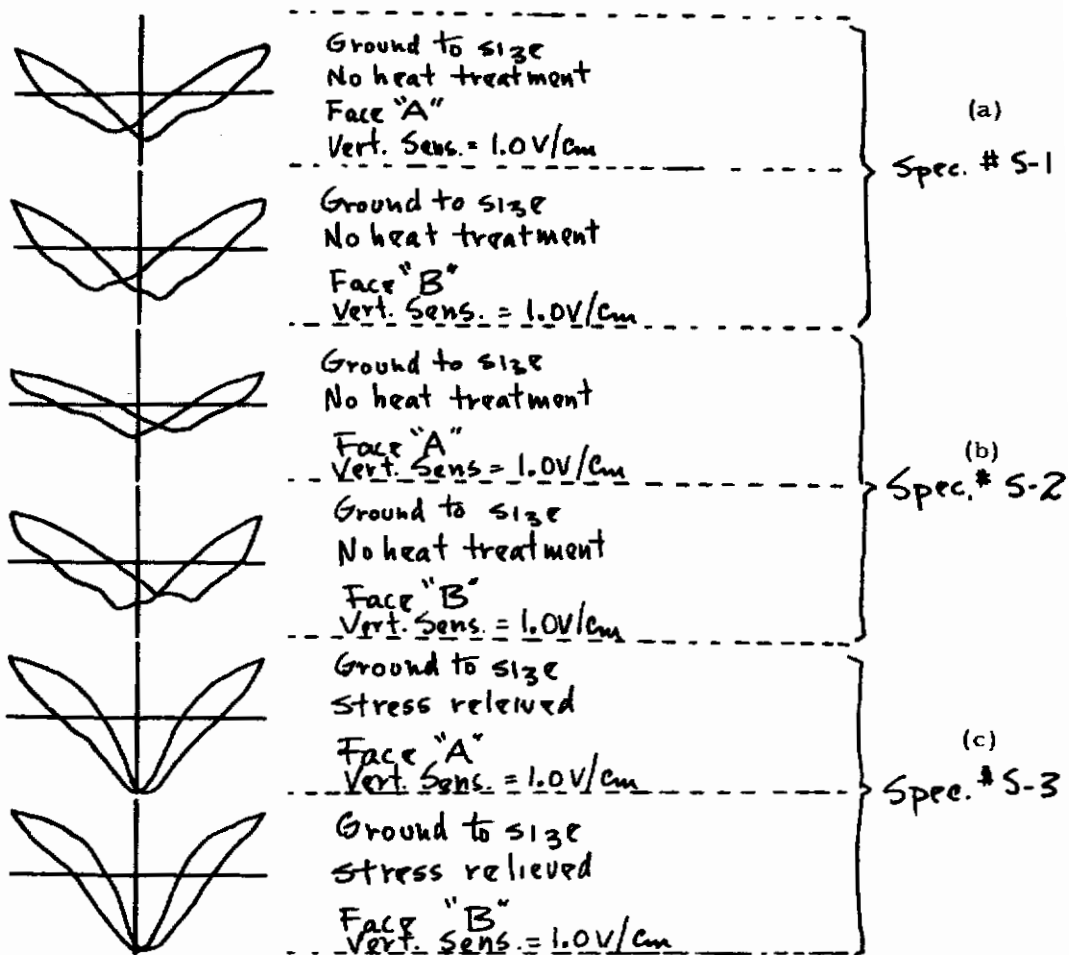


FIGURE 17. MAGNETOABSORPTION SIGNALS, HY-80 STEEL (UNSTRESSED)

Contrails

- Notes: ① $f_0 = 225$ Kcps
 ② Sample Coil #8
 ③ E_{DC} detector = 0.2V
 ④ $i_{coil} = 0.2A$ (60cps AC)
 ⑤ measured at center of $1\frac{1}{2}'' \times 12''$ faces

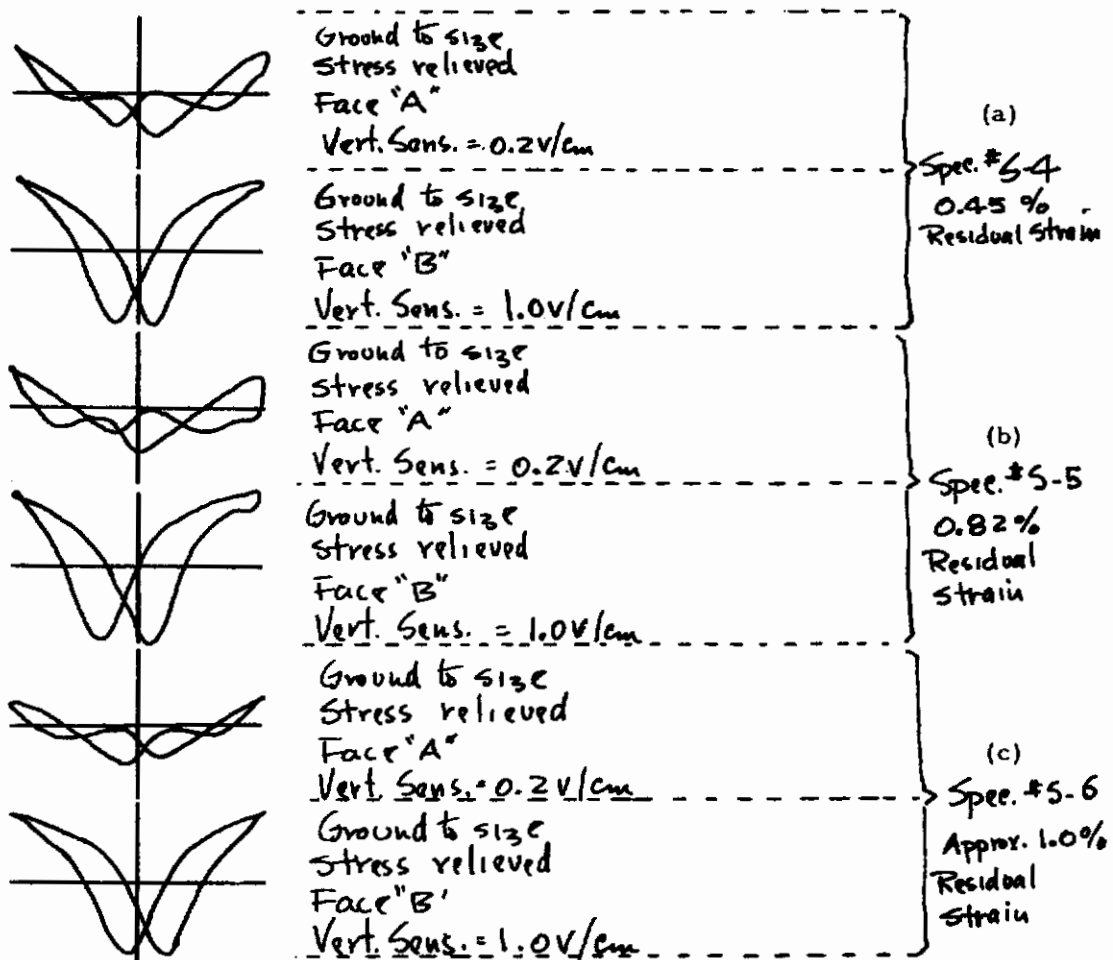


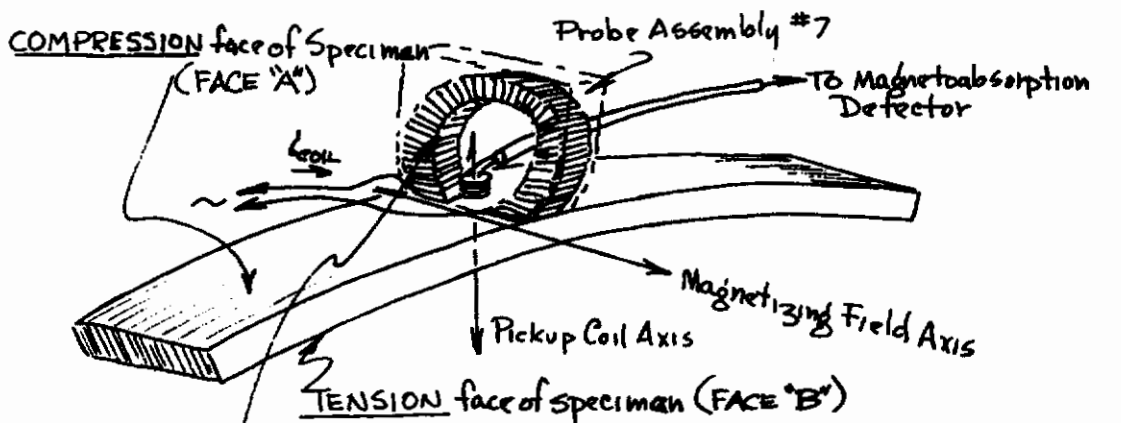
FIGURE 18. MAGNETOABSORPTION SIGNALS FOR STRESSED BEND SPECIMENS OF HY-80 STEEL

In all three of the stressed samples, the "A" face which was in tension during bending but is now in compression gave a very small magnetoabsorption signal. The signals from the "B" face are slightly larger in amplitude than the signal from the stress-relieved unstressed sample S-3. (Compare Figs. 17 and 18.) However, the shape of the magnetoabsorption signal from the "B" face of the stressed samples shows the effect of the stress in its shape. The shape of the magnetoabsorption curves from the "B" face of samples S-4, S-5, and S-6 are more open than the curves from S-3, and they show the effect of saturation. A comparison of the curves from the "B" faces of S-3 and S-6 with the curves of Figures 17 and 18 may indicate what has occurred. The flattening and opening of the B/H loop opens and flattens the magnetoabsorption curve as shown by Figures 13b and 13c. The effect of the tension in face "B" is to open the magnetoabsorption curve but not to decrease its magnitude. This is characteristic of materials such as steel with a positive magnetostriction coefficient. With the negative coefficient such as in nickel, the effect of tension is to both broaden and weaken the magnetoabsorption signal. With materials having a positive magnetostriction coefficient, a large (50% to 100% of yield) value of tension gives a 20% to 50% increase in the magnetoabsorption signal over that obtained with no stress. Therefore, since the increase is slight, if at all, the tension in the "B" face is much less than the yield value for the material.

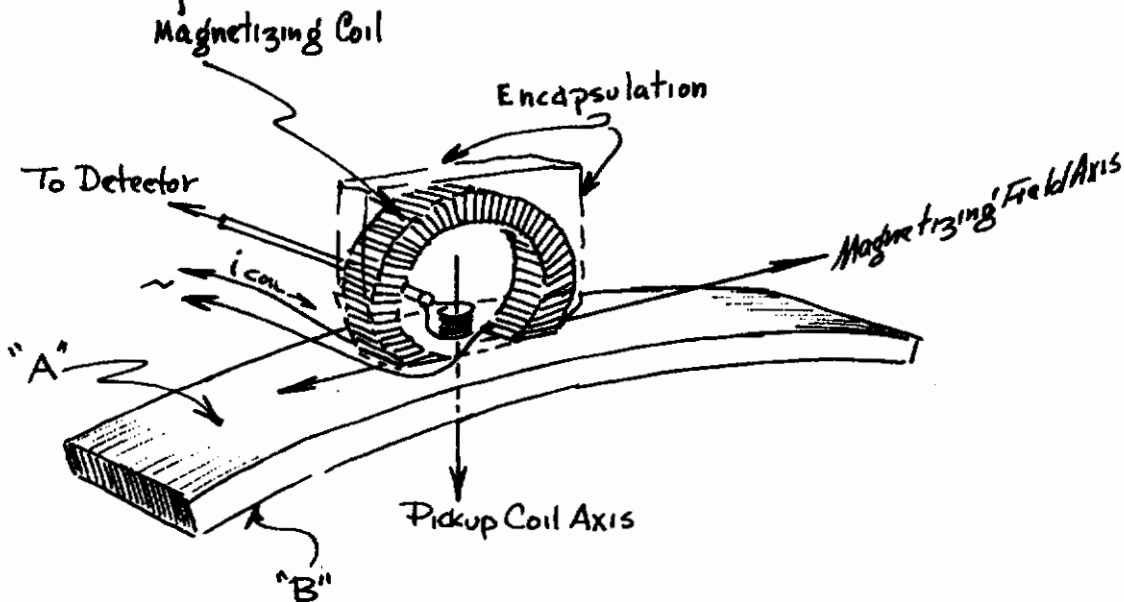
On the "A" faces of the stressed samples, however, the magnetoabsorption signal indicates that the material under compression has a complex B/H loop. The magnetoabsorption signal has a very strong 240-cycle component and a weak 120-cycle component (see Fig. 18). Since most of the previous work with magnetoabsorption has been accomplished with wire samples, no experimental evidence is available for reference for the compression condition as there is for tension. Thus, the exact shape of the B/H loop cannot be determined from experimental evidence. However, it is possible to estimate, from the shape of the magnetoabsorption curves from face "A" of Figure 18 that with compression there are two magnetic phases. One phase, represented by the inner two loops, is magnetically hardened by the compressive stress. The second phase is magnetically soft and is represented by the outer loops of Figure 18 from face "A". This second phase is obtained by the action of the magnetic forces overcoming the residual compressive forces and making the material appear unstressed or magnetically soft.

D. Second Series of Measurements

The indication of an induced magnetic field in Figures 17 and 18 along the axis of the specimen suggested the need for directional measurements. That is, the direction of the magnetic field relative to the specimen should be varied. To perform these measurements, the detection head of Figure 15 was used in the manner indicated in Figure 19. Figure 19a shows the magnetizing field perpendicular (transverse) to the long axis of the sample. Figure 19b shows the system providing the magnetic field parallel to the axis.



(a) Probe in TRANSVERSE or PERPENDICULAR position. (I)



(b) Probe in AXIAL or PARALLEL position (II)

FIGURE 19. PROBE-SPECIMEN GEOMETRY FOR MAGNETOABSORPTION

Contrails

With the detection head of Figure 15, magnetoabsorption curves were obtained with the field perpendicular and parallel from three points on each face of samples S-1, S-5, and S-6. The complete set of measurements is illustrated in Appendix III. Since the magnetoabsorption waveforms along the top or bottom for each specimen were nearly identical, only the center measurements from the top and bottom are shown in Figure 20 of the text.

With sample S-1, a larger magnetoabsorption signal was obtained with the parallel field than with the perpendicular field. Only the longitudinal signal indicated the presence of a magnetic field in the material. Thus, it can be assumed that the grinding caused a stress in the surface which made a magnetic field in the direction of the long axis. This stress caused an easy magnetic axis along the specimen length and a hard magnetic axis transverse to the length.

The bent samples S-5 and S-6 gave magnetoabsorption signals (Fig. 20) which were different from those obtained from S-1. From face "A," the hard magnetic axis is parallel to the length, as indicated by the smaller magnetoabsorption signal, and the easy magnetic axis is perpendicular to the length. Exactly the reverse is true on face "B" or the face in tension; in addition, the residual magnetic field caused by the bending is along the easy axis or perpendicular on face "A" and parallel on face "B."

E. Conclusions

From these few measurements the face in compression ("A" face) gives a larger magnetoabsorption signal when the magnetizing field is perpendicular to the stress axis and a smaller signal for the parallel case. The face in tension gives a larger magnetoabsorption signal for the parallel condition than it does for the perpendicular case. Therefore, the compression face and the tension face give opposite behavior of the magnetoabsorption signals as a function of the direction of the magnetic bias field relative to the direction of the stress. The magnetoabsorption response may be identified with the positive magnetostrictive character of HY-80, since tensile stresses in face "B" of the strained samples caused an increase in the magnetoabsorption signal, whereas compressive stresses in face "A" in the strained samples resulted in smaller magnetoabsorption signals when the bias field direction coincided with the direction of stress.

It also appears: (1) that tension broadens the magnetoabsorption curve, and (2) that compression distorts the B/H loop so that the magnetoabsorption curve displays a two-phase character.

Contrails

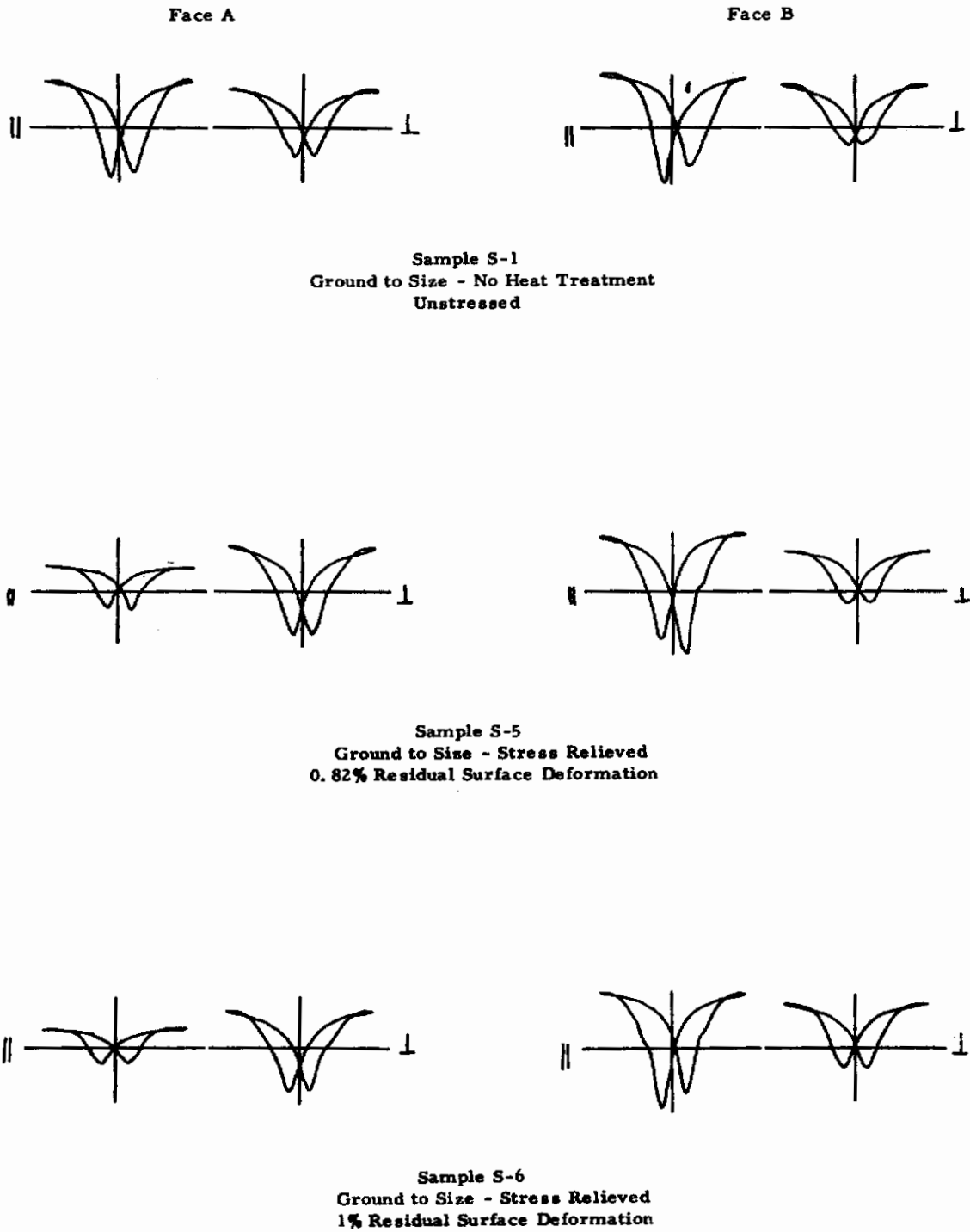


FIGURE 20. TYPICAL MAGNETOABSORPTION SIGNALS FROM THE TOP AND BOTTOM OF SPECIMENS S-1, S-5, AND S-6

SECTION IV

VARIATIONS IN MAGNETOABSORPTION SIGNALS FROM NICKEL-PLATED ALUMINUM RODS UNDER INCREMENTAL LOADS

A. Introduction

There is the possibility that the magnetoabsorption signals from the electroplated nickel coating on aluminum rods and plates can be used to measure variations in plating thickness and stress variations in aluminum. Consequently, exploratory efforts were devoted to the latter subject, i. e., stress measurement of nickel-plated aluminum rods by magnetoabsorption techniques.

As shown in Reference [2], magnetoabsorption amplitudes and shapes vary with stress in ferromagnetic materials. Since aluminum is not ferromagnetic, magnetoabsorption will not occur in this material. Consequently, stress studies in aluminum alone are not possible by magnetoabsorption methods. However, if the aluminum is plated with a thin ferromagnetic film, there exists the possibility of measuring the stress within the aluminum indirectly from the magnetoabsorption signal derived from the ferromagnetic film, particularly if the film adheres well to the base material. It has been reported in the literature [5] that the bond strength of the nickel deposit is of the order of the tensile strength of the aluminum base material when a phosphoric acid anodizing pretreatment process is employed. Recent studies of this anodizing process made for NASA by the Material Engineering Laboratory of Southwest Research Institute have shown that no blistering or separation occurred in nickel-plated aluminum samples when subjected to a 180° bend of one thickness radius. Since the film adheres well, deformation must be the same for both materials. Assuming that the strains are equal, i. e., $\lambda_1 = \lambda_2$, then the stresses τ are related by

$$\frac{\tau_1}{E_1} = \frac{\tau_2}{E_2} \quad (5)$$

within the proportional limit where τ_i = stress, and E_i = modulus of elasticity for the i^{th} material. Here, the index $i = 1$ refers to aluminum and $i = 2$ to the nickel film. Thus, if the ratio of the moduli are known and τ_2 is measured by the magnetoabsorption technique, then the stress within aluminum can be calculated. The total load P_T on the bimetallic specimen may be expressed as

$$P_T = P_1 + P_2 = \tau_1 A_1 + \tau_2 A_2 \quad (6)$$

where A_1 and A_2 are the respective cross-sectional areas. From Equations (5) and (6), it is concluded that

$$\tau_1 = \frac{P_T}{A_1 + \frac{A_2 E_2}{E_1}} \quad (7)$$

and

$$\tau_2 = \frac{P_T}{A_2 + \frac{A_1 E_1}{E_2}} \quad (8)$$

If $A_2 \frac{E_2}{E_1} \ll A_1$, then

$$\tau_1 = \frac{P_T}{A_1} \quad (9)$$

Equation (9) could have been easily derived from the fact that the film is thin, and the ratio of the moduli E_2/E_1 is not extremely large. In the experimental work described herein, τ_1 is calculated from Equation (9) and plotted as a function of the magnetoabsorption amplitude. The stress τ_2 in the nickel film was not measured quantitatively except as it provided a change in permeability and thus caused a variation in the magnetoabsorption signal.

B. Experimental Procedure

Type 4043 aluminum welding rods of two diameters (1/8 inch and 1/16 inch) were plated in cooperation with the Materials Engineering Laboratory of Southwest Research Institute. The plating process used has been reported by Bunce [5], and Spooner and Seraphim [6] and is briefly described in Appendix V. No attempts were made to measure the film thickness, but it was estimated by micrometer measurements that the thicknesses of the film are all less than one mil. After plating, a 1/8-inch diameter rod was annealed at 680°F (approximately the Curie temperature for nickel) for 30 minutes, and a 1/16-inch diameter rod was annealed at 680°F for 60 minutes. To apply compression or tension to a rod, a loading device was constructed. The device employs the principle of moment arms to apply a sizeable load without making the size of the weights cumbersome. This device is shown in Figure 21. A light source, rigidly attached to the moment arm, was employed to aid in measuring strain. The displacement of the light image on a stick was related to

the strain in the specimen. Appendix V describes the characteristics of these methods.

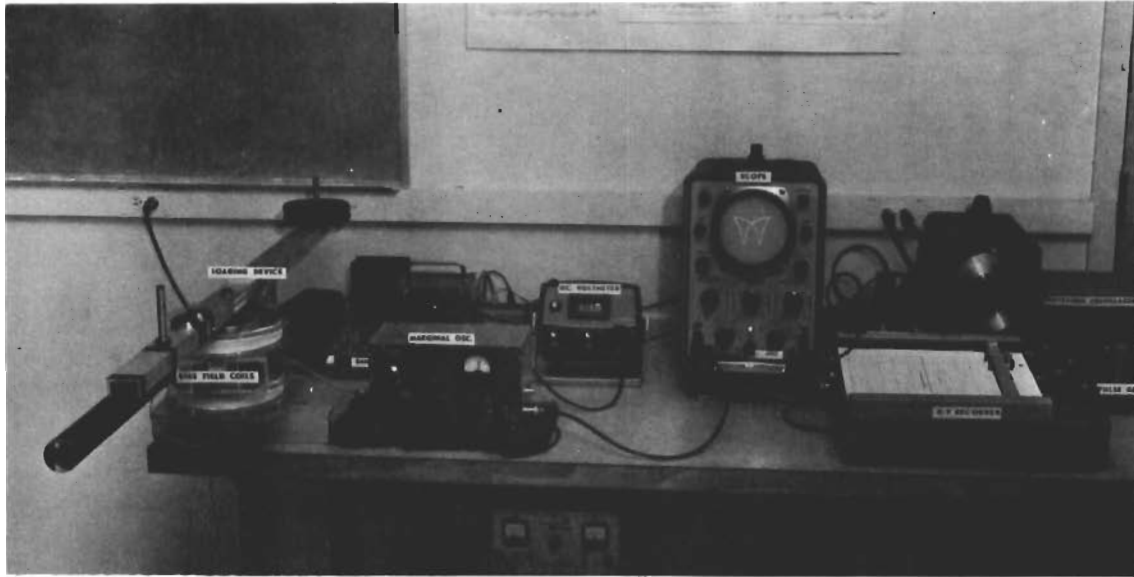


FIGURE 21. SIMPLE LOADING DEVICE AND MAGNETOABSORPTION SYSTEM

The magnetoabsorption system employed to measure the influence of stress on the plated samples is also shown in Figure 21. A small diameter, universal wound, 500 μ h sample coil was centered around the specimen. The sample coil and specimen were immersed in the center of a Helmholtz pair that varied the bias field, H_B , ± 200 oersteds at a 60-cycle rate. A marginal oscillator operating at 500 kcps detected the impedance changes occurring in the sample coil. The resistive changes were detected, and the resulting waveforms (the magnetoabsorption signal) were displayed on an oscilloscope and also plotted on an X-Y recorder through the use of a waveform translator. Both the magnetoabsorption waveform and the strain were recorded for each incremental load applied to the specimen. The rods were first loaded compressively and then were placed in tension. The compressive loads were restricted to small values to prevent buckling as predicted by Euler's formula for a column with fixed ends, i. e.,

$$\tau_b = \frac{4\pi^2 E}{\left(\frac{l}{r}\right)^2} \quad (10)$$

where

τ_b = allowable stress in psi to prevent buckling

l = length of column with fixed ends

r = radius of gyration

E = modulus of elasticity

After compression, the rods were loaded in tension until yield occurred or it was anticipated with the next weight. At no time were samples fractured in case further evaluation of the samples was necessary.

For each sample, data were reduced so that strain, peak-to-peak amplitude, and peak separation could be plotted as a function of stress. Each of these two types of magnetoabsorption response was reported in Section VII of [2]. Peak separation is a term that defines the distance in oersteds between the peaks of absorption occurring in a magnetoabsorption signal. The peak-to-peak amplitude is the total of the positive and negative maximum magnitudes.

C. Experimental Results

The 1/8-inch diameter aluminum rod in its "as plated" condition was loaded both in compression and tension. Magnetoabsorption waveforms and strain data were taken at each incremental load. Figure 47 in Appendix V shows a representative selection of magnetoabsorption signals at the effective loads indicated beneath each waveform. The negative magnetostrictive nature of nickel is observed in the decreasing amplitude of the magnetoabsorption signal, which from theory is proportional to $\sqrt{\mu_r}$, as the load changes from compression to tension. Compressive loads are preceded by a negative sign. This amplitude response as a function of stress is plotted in Figure 22. The correspondence with strain may be obtained from the same figure where strain is indicated as a function of stress. The apparent deviation of Young's modulus when the rod is subjected to compression is undoubtedly attributable to buckling since the strain increases much more rapidly than stress. It is extremely difficult to compressively load a long, small diameter rod which conceivably was slightly bent under no load conditions.

Empirical relationships can be developed to relate stress, strain, and magnetoabsorption amplitude. Examination of Figure 22 shows that magnetoabsorption amplitude A is related to stress in the tensile region by

$$A = 0.96 \exp(-\tau/1360) \quad (11)$$

The points of Equation (11) are shown on Figure 22 as triangles. Within the same region, strain and stress are linearly dependent.

It was discovered during the experimentation that consistent magnetoabsorption waveforms were obtainable within the region from the compression

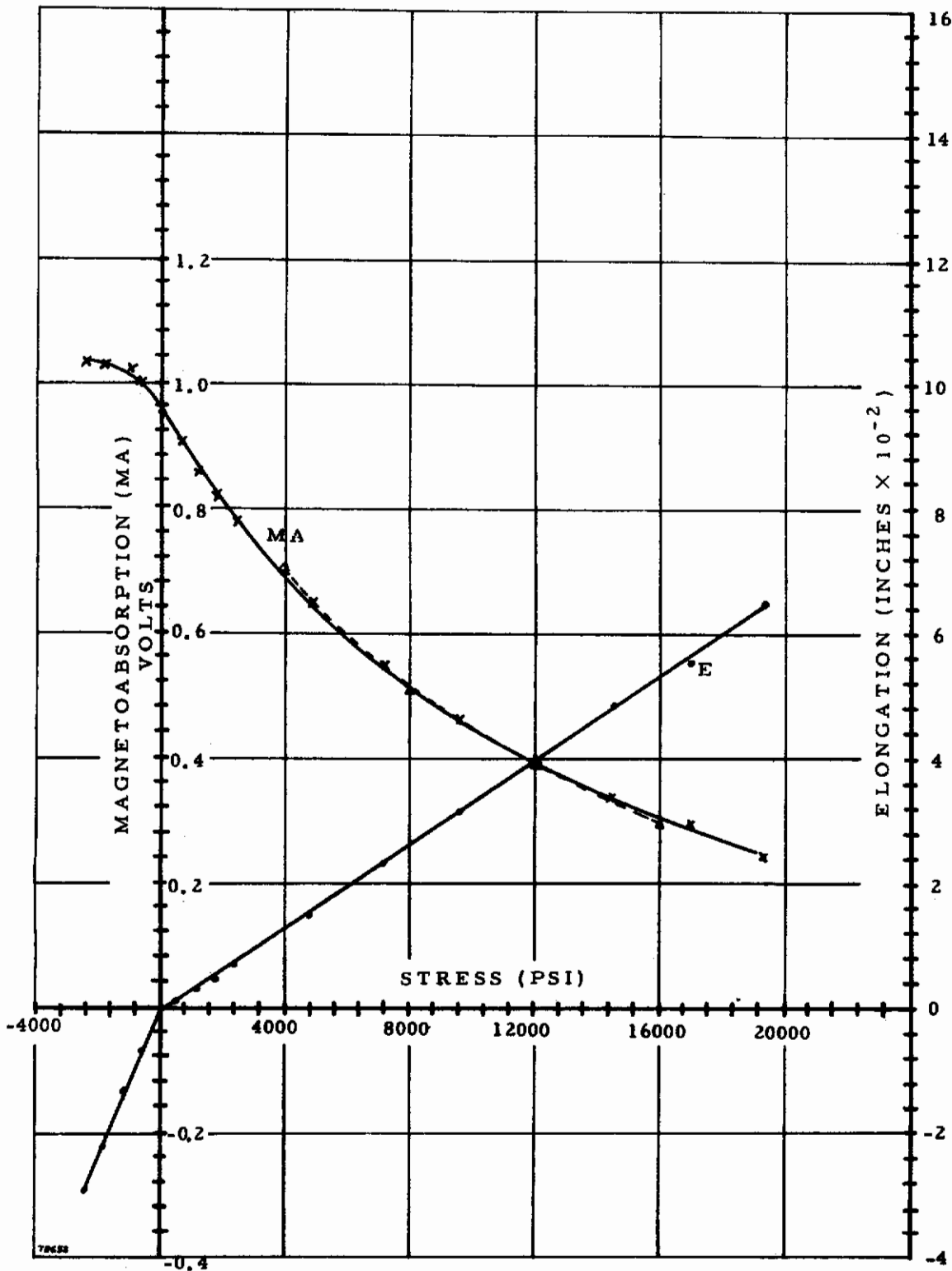


FIGURE 22. VARIATIONS OF MAGNETOABSORPTION AMPLITUDE AND STRAIN WITH STRESS FOR NICKEL-PLATED ALUMINUM ROD OF 1/8-INCH DIAMETER

data points to points near the tensile yield point. The yield point for this case is not well defined since yield was not evident from the stress-strain curves. No significant material hysteresis effects, as would destroy repeatability of the magnetoabsorption waveform, were observable for each rod investigated when loads were varied in the range noted above. Beyond the yield point for tension, repeatable magnetoabsorption waveforms were not attainable.

To show the significance of the harmonic content within the magnetoabsorption signal and to observe the influence of material hardening in the nickel film, the separation of the negative peaks of absorption were plotted as a function of stress in Figure 23 for both annealed and unannealed samples. It is important to note that this variation is indicative of the changes in the amplitude and phase of the harmonics of the magnetoabsorption signal. This type of variation is also readily observable from the waveform plots of Figure 47 in Appendix V. It is further interesting to compare Figures 18 and 19 of [2], reproduced as Figures 24 and 25, with the negative peak separation reported here. The broad or a square-loop B/H characteristics of Figure 24 shows a corresponding separation of the negative peaks of absorption for the unannealed sample of Figure 23. Whereas a narrow B/H loop for the annealed sample of Figure 25 yields a magnetoabsorption signal whose negative peaks of absorption are close together. Thus, the separation in the negative peaks is presently a qualitative indication of the stress within the nickel film which, in turn, can be further related to the stress within the aluminum.

To compare the influence that annealing has on aluminum, a plated rod of the same diameter was annealed at 680°F for 30 minutes. This annealing not only affects the mechanical properties of aluminum, but, as noted in previous reports, annealing nickel has a large influence on the strength of the magnetoabsorption signal (see Figs. 24 and 25 as an example from previous efforts). A comparison of the no-load signals for the unannealed film of Figure 22 and for the annealed film of Figure 26 shows that the annealed has a magnetoabsorption signal of approximately twice the amplitude as does the unannealed. The characteristic separation of the negative peaks of absorption is once again evident as shown by the waveforms of Figure 48 of Appendix V. As tensile stress is applied to the annealed sample, the negative peaks separate as shown in Figure 23. At a stress of 10,800 psi, the negative peak separation of the annealed sample equals that of the no-load separation of the unannealed. At a tensile stress of 14,800, the separations P_S are equal. Above 14,800 psi, the separation of the annealed sample exceeds that of the unannealed. The peaks separate linearly with stress, and the curve may be expressed by

$$\tau = 308 (P_S - 151) \quad (12)$$

for $2400 \leq \tau \leq 17,000$ psi.

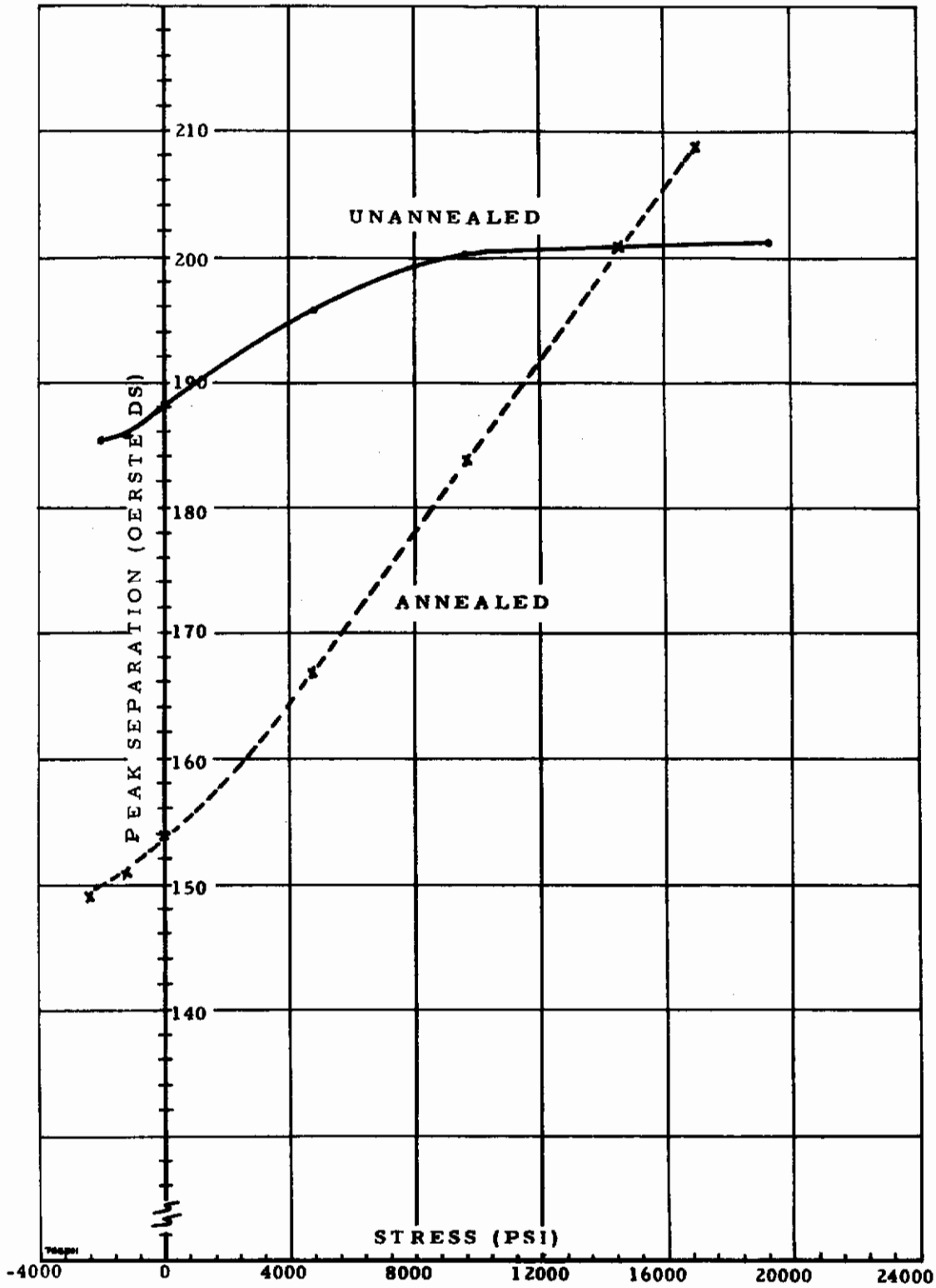


FIGURE 23. VARIATION IN THE PEAK SEPARATION OF THE MAGNETOABSORPTION SIGNAL WITH STRESS FOR 1/8-INCH DIAMETER NICKEL-PLATED ALUMINUM ROD

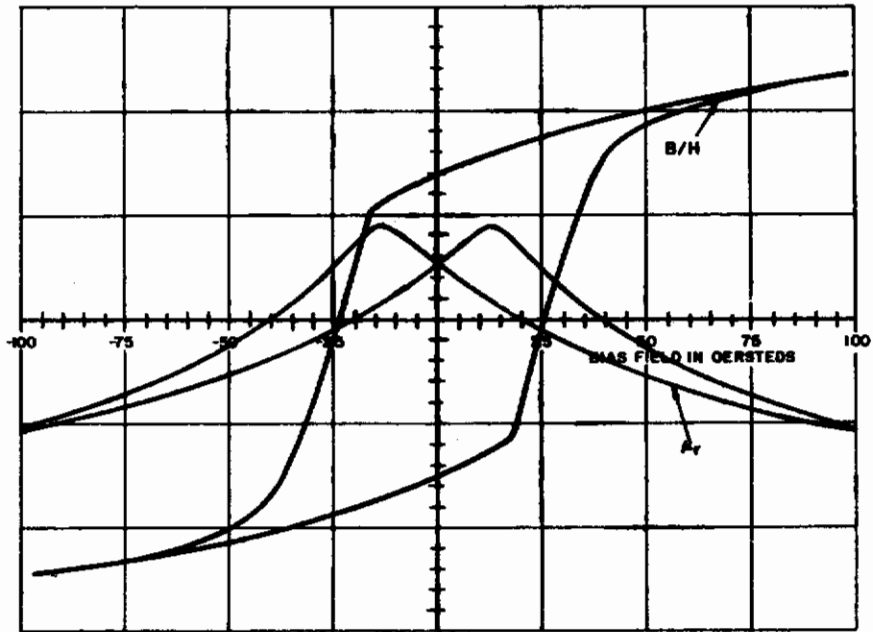


FIGURE 24. SUPERPOSITION OF THE B/H LOOP AND THE RELATIVE REVERSIBLE PERMEABILITY CURVES FOR UNANNEALED NICKEL WIRE

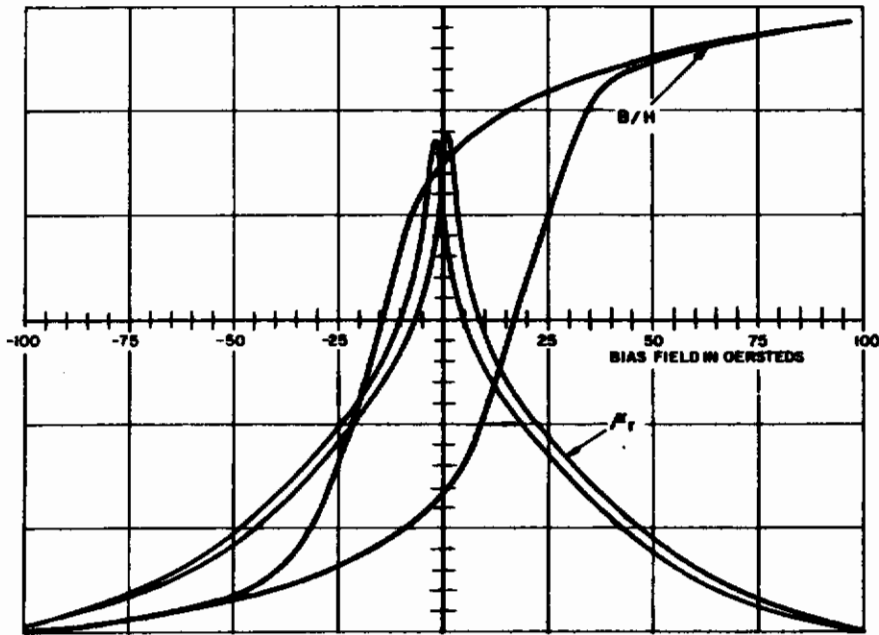


FIGURE 25. SUPERPOSITION OF THE B/H LOOP AND RELATIVE REVERSIBLE PERMEABILITY CURVES FOR ANNEALED NICKEL WIRE

Contrails

The negative magnetostrictive character of nickel is again evident since the magnetoabsorption amplitude decreases as the load varies from compression into tension. This amplitude response is shown in Figure 26 where the corresponding strain is also plotted for the same values of stress. Buckling is evident in the stress-strain response for compressive loads as was the case for the unannealed response. The magnetoabsorption amplitude is proportional to stress within the range $2400 \leq \tau \leq 10,000$ psi and may be expressed as

$$A = -1.31 \times 10^{-4} (\tau - 16,000) \quad (13)$$

In the region $10,000 \leq \tau \leq 17,000$ psi, the exponential

$$A = 3.21 \exp(-\tau/7150) \quad (14)$$

fits well. It is interesting to note from Figure 26 that stress and strain remain linearly dependent in the same region as did magnetoabsorption and stress. Further, strain λ can nearly be characterized by the same exponent as magnetoabsorption. For $\tau \geq 10,000$, the function

$$\lambda = 6.62 \times 10^{-3} \exp(\tau/7150) \quad (15)$$

is shown as a dotted curve in Figure 26. The waveforms from which these results were derived are shown in Figure 48 of Appendix V.

An unannealed nickel-plated aluminum welding rod of 1/16-inch diameter was also investigated. A selection of magnetoabsorption waveforms at various loads are shown in Figure 49 of Appendix V. The amplitudes are nearly one-half the amplitude of the 1/8-inch diameter rods as expected since the volume of ferromagnetic film is one half of that of the larger diameter rod. Again, the negative magnetostrictive properties are exhibited in the decaying amplitude of magnetoabsorption as the load increases from compression to tension. Figure 27 shows this amplitude response. The exponential

$$A = 0.405 \exp(-\tau/12,800) \quad (16)$$

may be fitted to the empirical data. The curve of Equation (16) is indicated by the triangular points of Figure 27.

The stress-strain curve is also shown in Figure 27. A linear dependence between stress and strain is exhibited to an approximate stress value of 18,000 psi. Values of strain thereafter indicated that yield had begun to occur. The value, 18,000 psi, is in good agreement with yield strength reported by aluminum manufacturers for the heat treatment given. The compressive stress-strain data indicated that the sample buckled slightly while in compression.

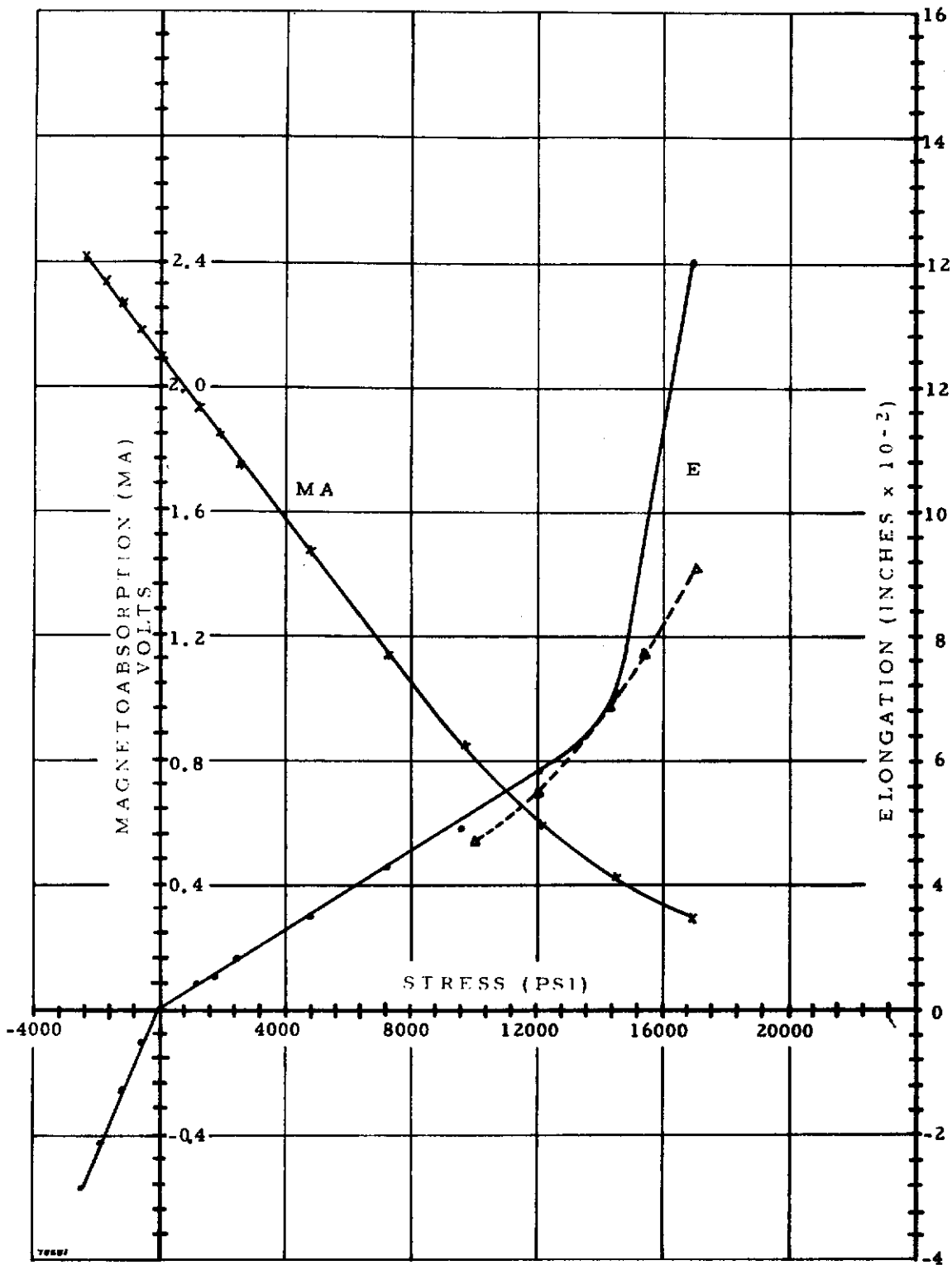


FIGURE 26. VARIATIONS OF MAGNETOABSORPTION AND STRAIN WITH STRESS FOR AN ANNEALED NICKEL-PLATED ALUMINUM ROD OF 1/8-INCH DIAMETER

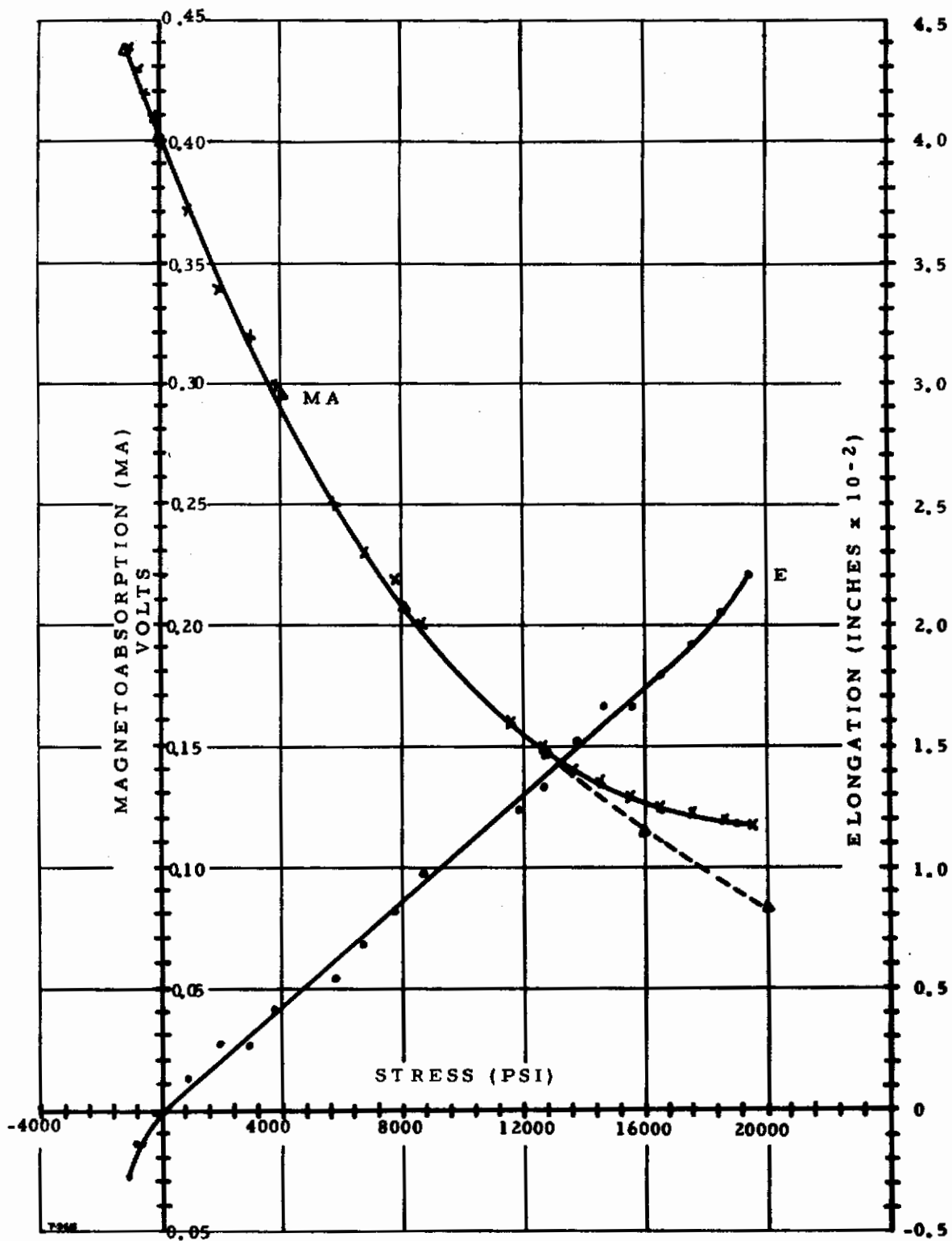


FIGURE 27. VARIATION OF MAGNETOABSORPTION AMPLITUDE AND STRAIN WITH STRESS FOR UNANNEALED NICKEL-PLATED ALUMINUM ROD OF 1/16-INCH DIAMETER

The negative peak separation as a function of stress is presented in Figure 28. No attempt was made to fit the data with a mathematical function. Increasing separation of the negative peaks of absorption with stress is seen to occur once again.

An annealed 1/16-inch aluminum welding rod of the same stock and diameter as the previous unannealed rod was also investigated as a function of stress. The selected magnetoabsorption waveform for various loads is shown in Figure 50 of Appendix V. The decreasing amplitude response with stress and the stress-strain curve are shown in Figure 29. The influence of annealing is evident in the low yield strength, approximately 6000 psi. The annealed sample had a yield strength of approximately 18,000 psi. It is interesting to compare the slopes of the stress-strain curves for the annealed and unannealed rods (Figs. 27 and 29). The strains per unit of stress are nearly equal. This is a typical response; annealing only influences the value of the yield point. The separation of the peaks of absorption with stress is shown in Figure 28. The separation generally increased to a value of 8000 psi and thereafter decreased.

D. Additional Effort

In addition to plating aluminum rods, nickel was also electrodeposited on several aluminum plates of type 1100 and 7106. Several specimens were partially-annealed at 300°F for 30 minutes. Alcoa [7] reports that heats of 300°F not exceeding 30 minutes will not change the high strength properties of 7106. Figure 30 shows that such low temperature annealing is beneficial in enhancing the amplitude of the magnetoabsorption signal without altering the material properties of 7106. These plates were to be investigated in a beam deflection device had time permitted.

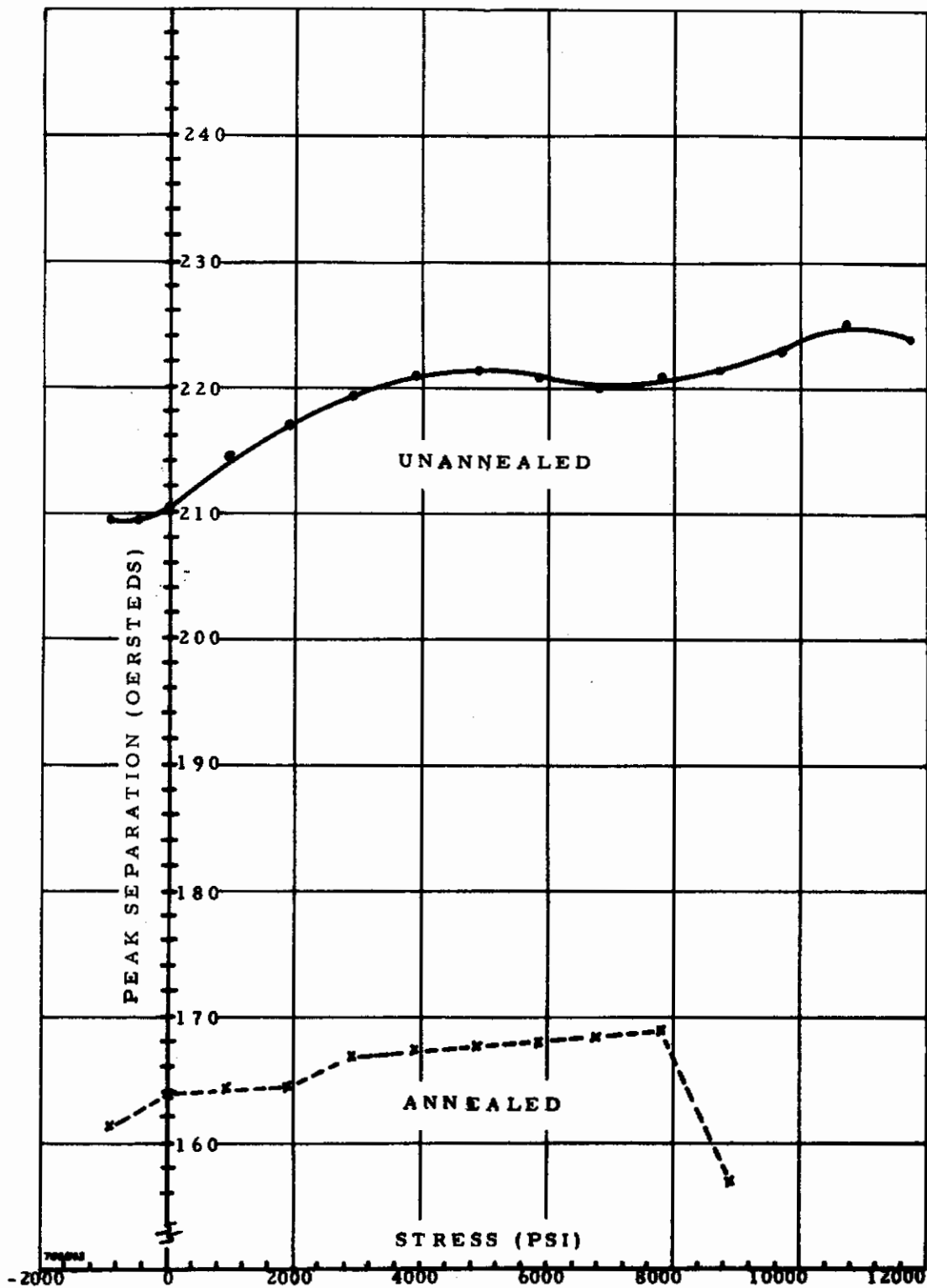


FIGURE 28. VARIATIONS OF PEAK SEPARATION WITH STRESS FOR NICKEL-PLATED ALUMINUM ROD OF 1/16-INCH DIAMETER

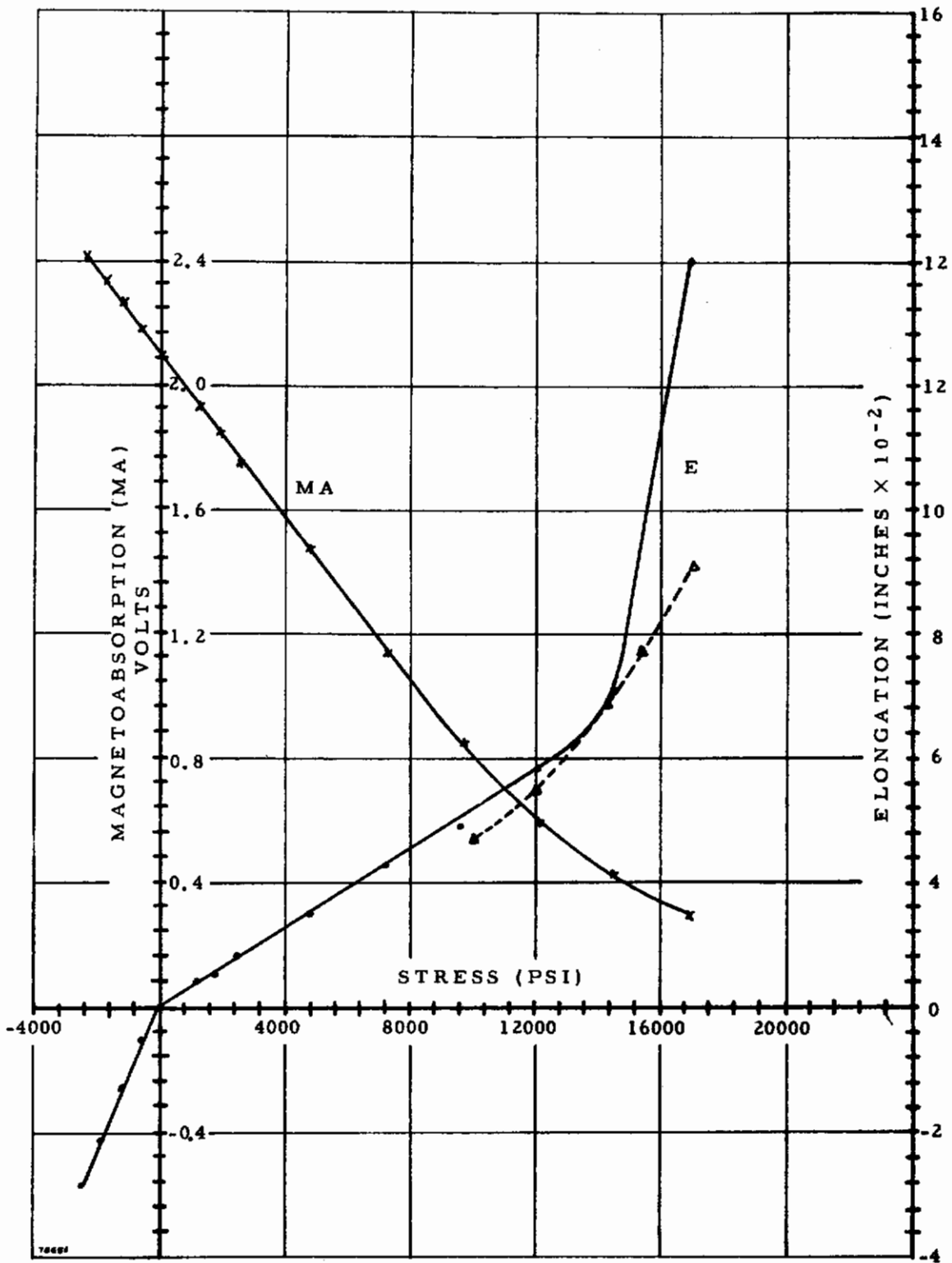
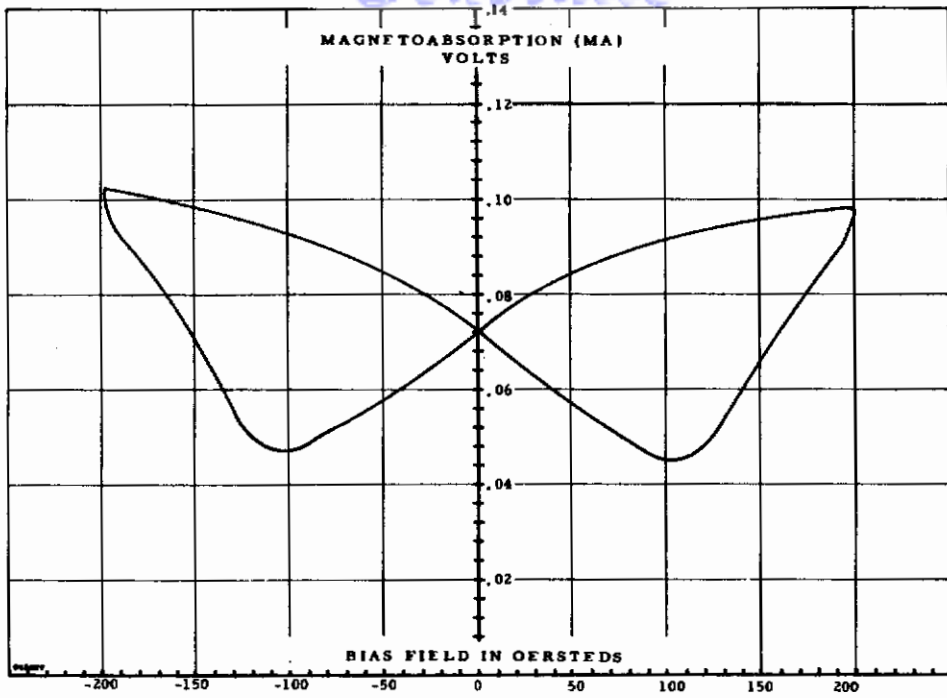
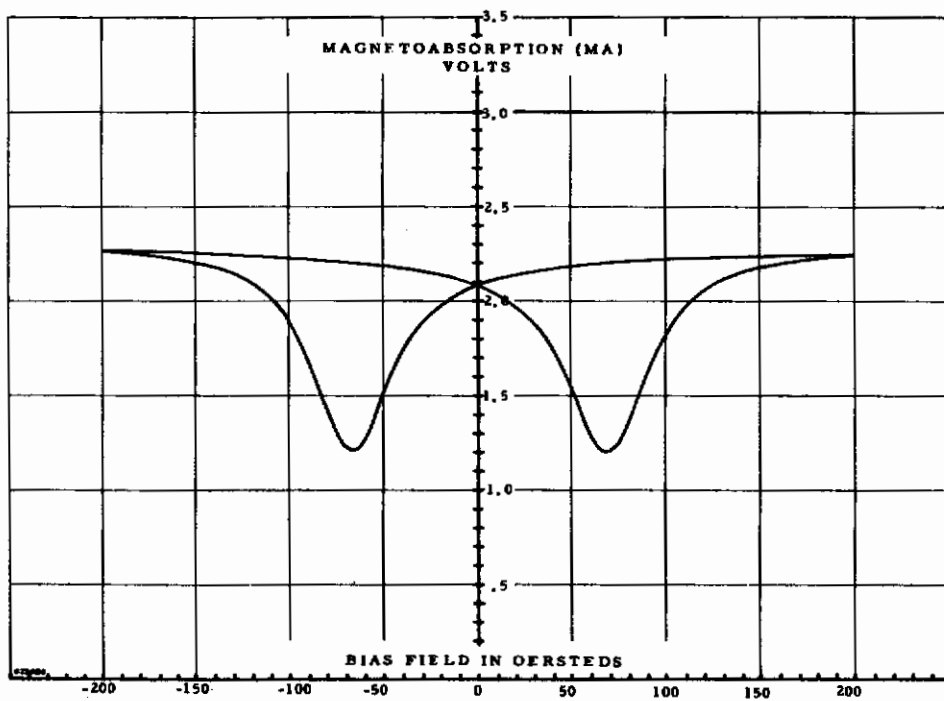


FIGURE 29. VARIATION OF MAGNETOABSORPTION AMPLITUDE AND STRAIN WITH STRESS FOR ANNEALED NICKEL-PLATED ALUMINUM ROD OF 1/16-INCH DIAMETER

Contrails



(a) As Plated with No Anneal



(b) Annealed at 300°F for 30 Min

FIGURE 30. MAGNETOABSORPTION WAVEFORMS FROM PARTIALLY ANNEALED NICKEL FILM ON AN ALUMINUM PLATE

SECTION V

HARMONIC AMPLITUDE VARIATIONS OF MAGNETOABSORPTION SIGNALS FROM WIRES UNDER STRESS

A. General

Studies of the influences of stress, applied to ferromagnetic wires or ferromagnetic-clad nonferromagnetic wires, on the magnetoabsorption signal were conducted in a manner similar to that reported in Section IV. However, in addition to measuring the stress, the magnetoabsorption waveform, the peak separation, and the amplitudes of the first five harmonics of the magnetoabsorption signal were recorded as a function of the loads applied incrementally to the wire. During this study, cold-rolled nickel, industrially annealed nickel, nickel-plated aluminum, and maraging-steel wires were examined. The experimental technique and composition of the specimens are described in Appendix VI.

B. Negative Magnetostrictive Specimens

Various wires exhibiting a negative magnetostrictive characteristic under stress had been reported previously in AFML-TR-65-17 and in Section IV. These same wires were reexamined in this study, and the amplitude response of the significant harmonics with stress are also included. Of the three specimens examined, two were furnished by Wilbur B. Driver as commercially 99% pure nickel wire, No. 14 AWG. One of these was industrially annealed with an approximated ultimate strength of 70,000 psi and the other was cold-rolled with an approximate ultimate strength of 80,000 psi. The third sample was a 1/8-inch diameter nickel-plated aluminum wire remaining from the studies reported earlier in Section IV. Nickel of the type mentioned above was actually employed in electroplating the aluminum rod.

The magnetoabsorption response of industrially annealed nickel wire is shown in Figure 31. The bold curve represents the peak-to-peak amplitude response of the magnetoabsorption signal with stress. Within the yield point, magnetoabsorption amplitude is nearly a linear function of stress and is similar to that reported in AFML-TR-65-17 for industrially annealed nickel. The rms amplitude variation of the harmonics of the magnetoabsorption signal with stress are indicated by the dashed lines of Figure 39. The frequency of the measured harmonic amplitude is denoted adjacent to each dashed curve. Only the first five harmonics were recorded in this study. In general, the changes with stress are similar to that of magnetoabsorption amplitude except for the deviation of the 120-cps and 240-cps component at 7000 psi. This discrepancy undoubtedly occurred because the experimenter had mistuned the harmonic analyzer to 180 cps, a power line harmonic located between two harmonics of the magnetoabsorption signal. It is interesting to note that the sum of the peak-to-peak amplitudes of the first five harmonics is not equal to

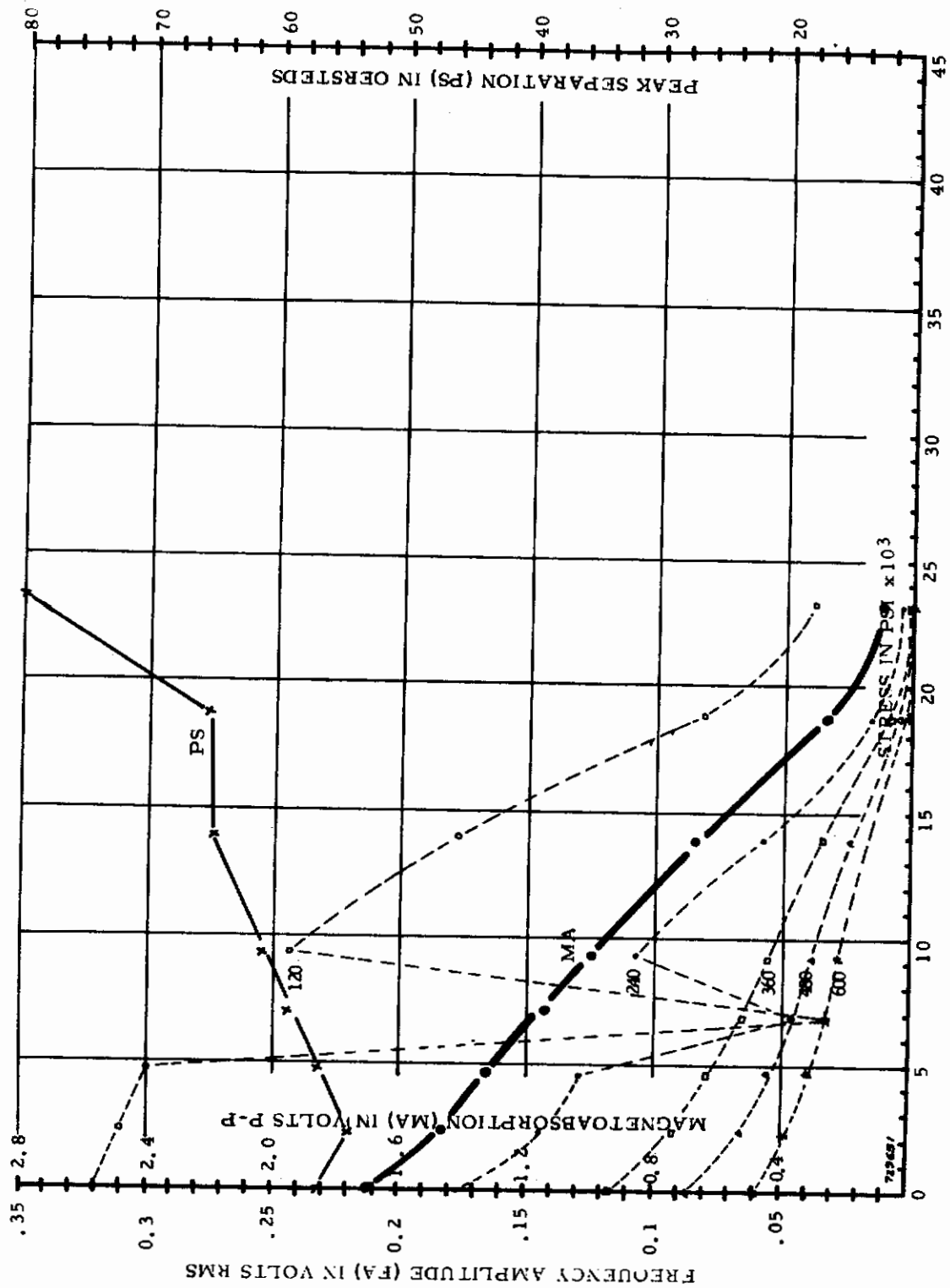


FIGURE 31. VARIATIONS OF MAGNETOABSORPTION AMPLITUDE, HARMONIC AMPLITUDE, AND PEAK SEPARATION WITH STRESS FOR INDUSTRIALLY ANNEALED NICKEL WIRE

the peak-to-peak amplitude of the magnetoabsorption signal. Further, the magnetoabsorption signal MA may be represented in Fourier form by

$$MA = \sum_{n=1}^5 A_n \cos (240\pi nt + \phi_n) \quad (17)$$

where it has been assumed that the first five harmonics are adequate in describing the magnetoabsorption signal, MA. If $\phi_n = 0$ for each harmonic, then the peak amplitude of the MA signal would be the sum of the Fourier amplitudes. However, as noted above, this is not the case in these measurements. Therefore, the phase angle cannot be considered equal to zero or a constant value. Consequently, the phase of the harmonics may also serve as a useful indication of the material state of the ferromagnetic specimen, and it may give a more sensitive indication.

Also recorded in Figure 31 is the variation of separation of the peaks of absorption with stress. Increasing peak separation together with decreasing magnetoabsorption amplitude with tensile stress have been observed previously and is a characteristic of material having a negative magnetostrictive constant.

Similar measurements were performed for cold-rolled nickel wire samples. The influence of stress on the various measured parameters is shown in Figure 32. The cold working is evidenced by (1) smaller magnetoabsorption amplitudes, (2) smaller harmonic amplitudes, (3) greater peak separations, and (4) smaller changes in amplitude per unit change in stress. It is further concluded that the yield strength of the cold-worked nickel is approximately twice that of the annealed nickel, when the results of previous observations for nickel are applied. Normally, nickel responds linearly or exponentially within the yield point; thereafter, the magnetoabsorption signal decreases less rapidly.

Similarly, studies of peak separation, harmonic content, and magnetoabsorption amplitude were conducted for the 1/8-inch diameter nickel-plated aluminum rod. These measurements are recorded in the graphs of Figure 33. Once again, magnetoabsorption and harmonic amplitudes are nearly linearly dependent upon stress. The amplitude response is very similar to that of cold-rolled nickel indicating that the nickel has a large initial internal stress. In fact, when the stress within the nickel film is estimated to be ratio of moduli of elasticities, 8/3, times that of the abscissa of Figure 33, the change of magnetoabsorption amplitude with stress in the nickel film are nearly identical with that of the cold-rolled nickel response of Figure 32.

These types of study are important in that if stress or some other material property can be easily interpreted from a harmonic of the magnetoabsorption signal, then electronic measurement of these properties can be readily simplified. As an example, if a particular harmonic is to be chosen

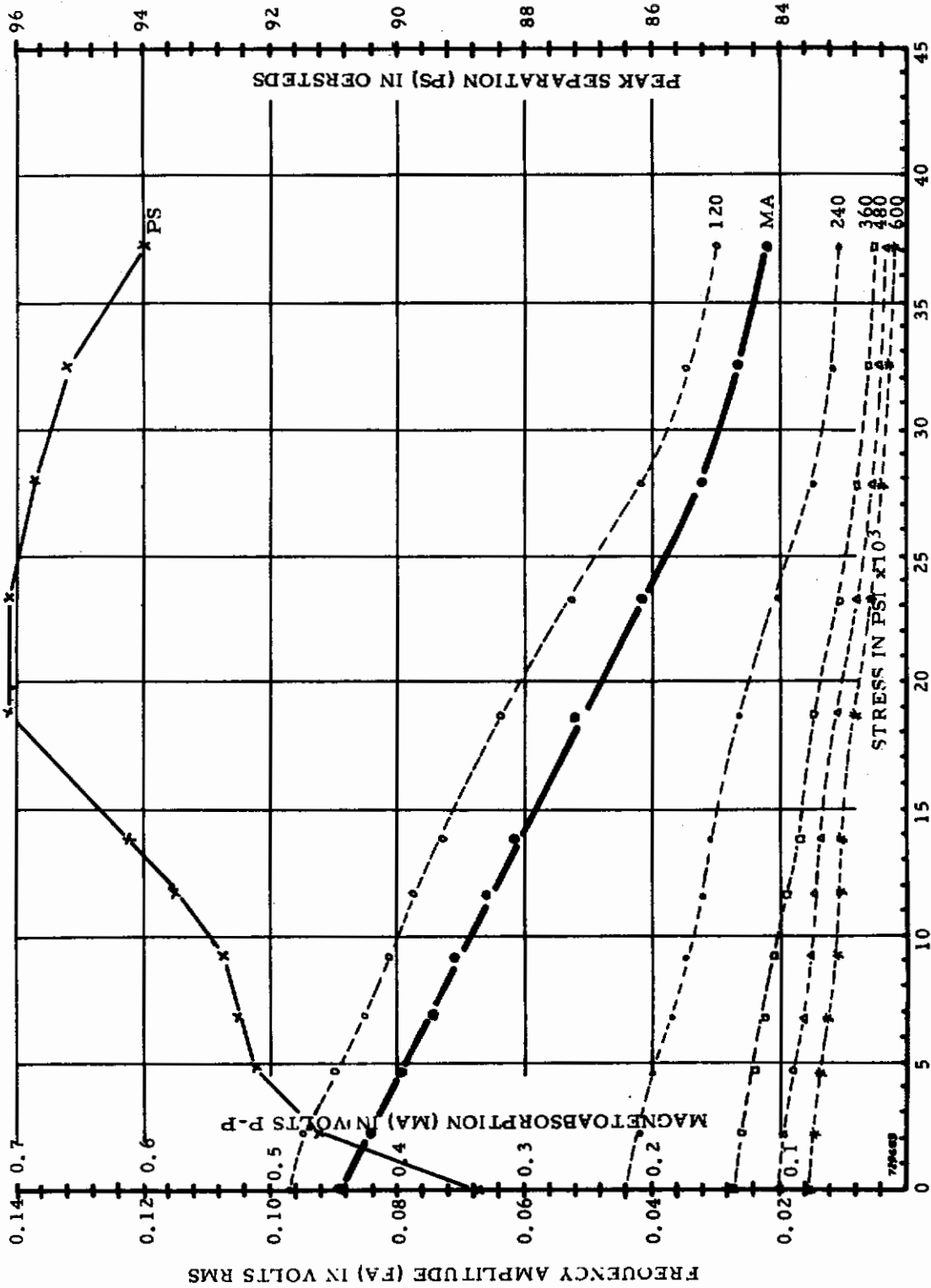


FIGURE 32. VARIATION OF MAGNETOABSORPTION AMPLITUDE, HARMONIC AMPLITUDE, AND PEAK SEPARATION WITH STRESS FOR COLD ROLLED NICKEL WIRE

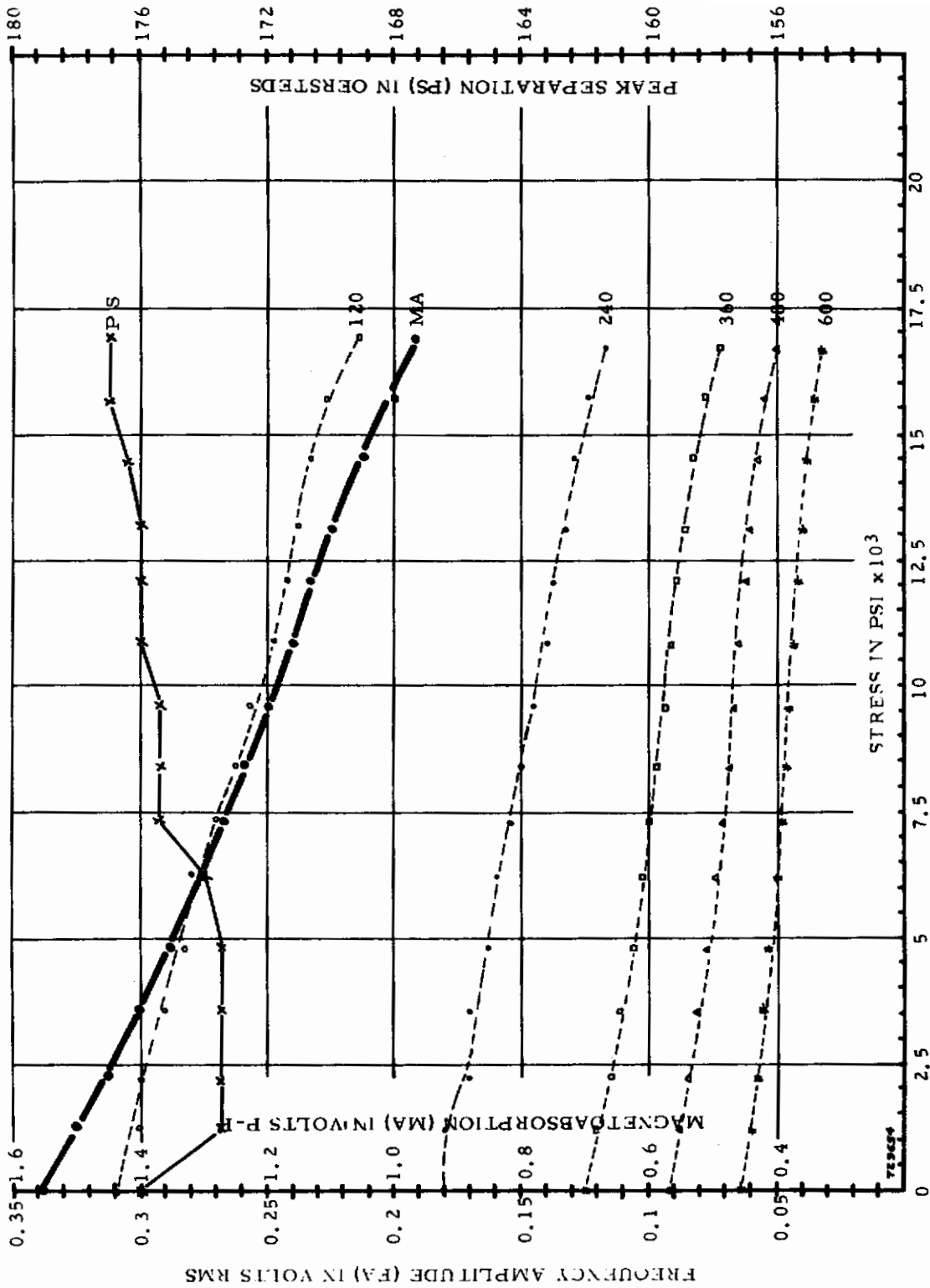


FIGURE 33. VARIATIONS OF MAGNET ABSORPTION AMPLITUDE, HARMONIC AMPLITUDE, AND PEAK SEPARATION WITH STRESS FOR NICKEL-PLATED ALUMINUM ROD

to measure stress from the curves of Figures 31, 32, and 33, it is clear that the harmonic with greatest sensitivity and the most easily predictable response to stress should be chosen.

C. Positive Magnetostrictive Specimens

Two specimens exhibiting a positive magnetostrictive characteristic over some levels of stress were examined. One material was supplied by Leeds and Northrup as annealed iron thermocouple wire. This type of ferromagnetic wire had been studied and reported in previous efforts (AFML-TR-65-17). Table 2 of Appendix VI shows the specifications for the iron billets from which this iron thermocouple wire is manufactured. From the wide specified limits, it is seen that the minimum iron content would be 99.3%.

The other material was received as samples of VascoMax 250W(CVM) from Armetco, a division of Vanadium Alloys Steel Company. VascoMax 250W is an 18% maraging steel welding filler wire. VascoMax 250W is specifically manufactured for use as filler wire in Metal Inert Gas and Tungsten Inert Gas welding of VascoMax 250, an 18% nickel ultrahigh strength maraging steel. The nominal analysis for VascoMax 250 together with a certified analysis of the welding filler wire is shown in Table 3 of Appendix VI. From these analyses, it is seen that the primary differences in the welding wire is the slightly smaller nickel and larger cobalt contents. The wire was received in the solution annealed state, and magnetoabsorption measurements were performed in the "as-received" condition. Time limitations prevented maraging this wire and performing similar measurements. Maraging would have brought the ultimate strength of this material to approximately 250 kpsi.

The influence of stress on magnetoabsorption amplitude and its harmonics for iron thermocouple wire is shown in Figure 34. The response is very similar to that reported in AFML-TR-65-17. The amplitudes are rather insensitive to stress, and a definite positive magnetostrictive characteristic is not observable except for stress values before fracture. The separation of the peak of absorption, as presumed in earlier efforts, do tend to coalesce for light loads. There is an indication that the phase response may be significant since the sum of the peak-to-peak amplitudes of the harmonics of the magnetoabsorption signal do not equal the peak-to-peak value of the magnetoabsorption signal itself.

The influence of stress on the magnetoabsorption signal and the amplitude of its harmonics for VascoMax 250W is shown in Figure 35. The large amplitudes are indicative of high permeability to be expected of a ferromagnetic specimen containing nickel, cobalt, and iron. It is interesting to note that the composition of this material is similar to that of permalloy and perminvar; particularly the latter. The material has a definite positive magnetostrictive characteristic up to a load of approximately 40 kpsi. That is, up to that load, the reversible permeability increases with tension. Thereafter, a decrease in permeability occurs with increasing stress as the

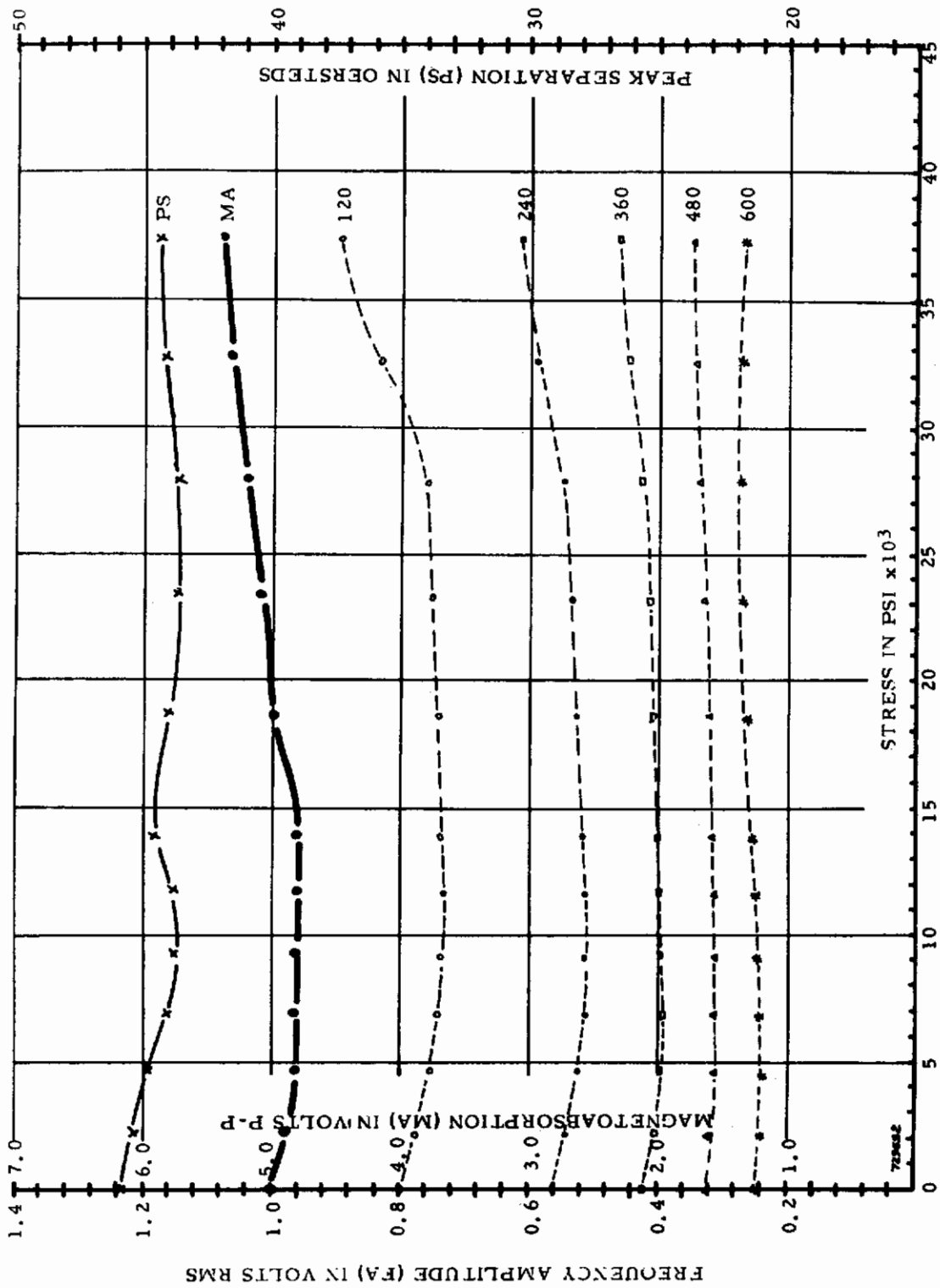


FIGURE 34. VARIATIONS OF MAGNETOABSORPTION AMPLITUDE, HARMONIC AMPLITUDE, AND PEAK SEPARATION WITH STRESS FOR ANNEALED IRON THERMOCOUPLE WIRE

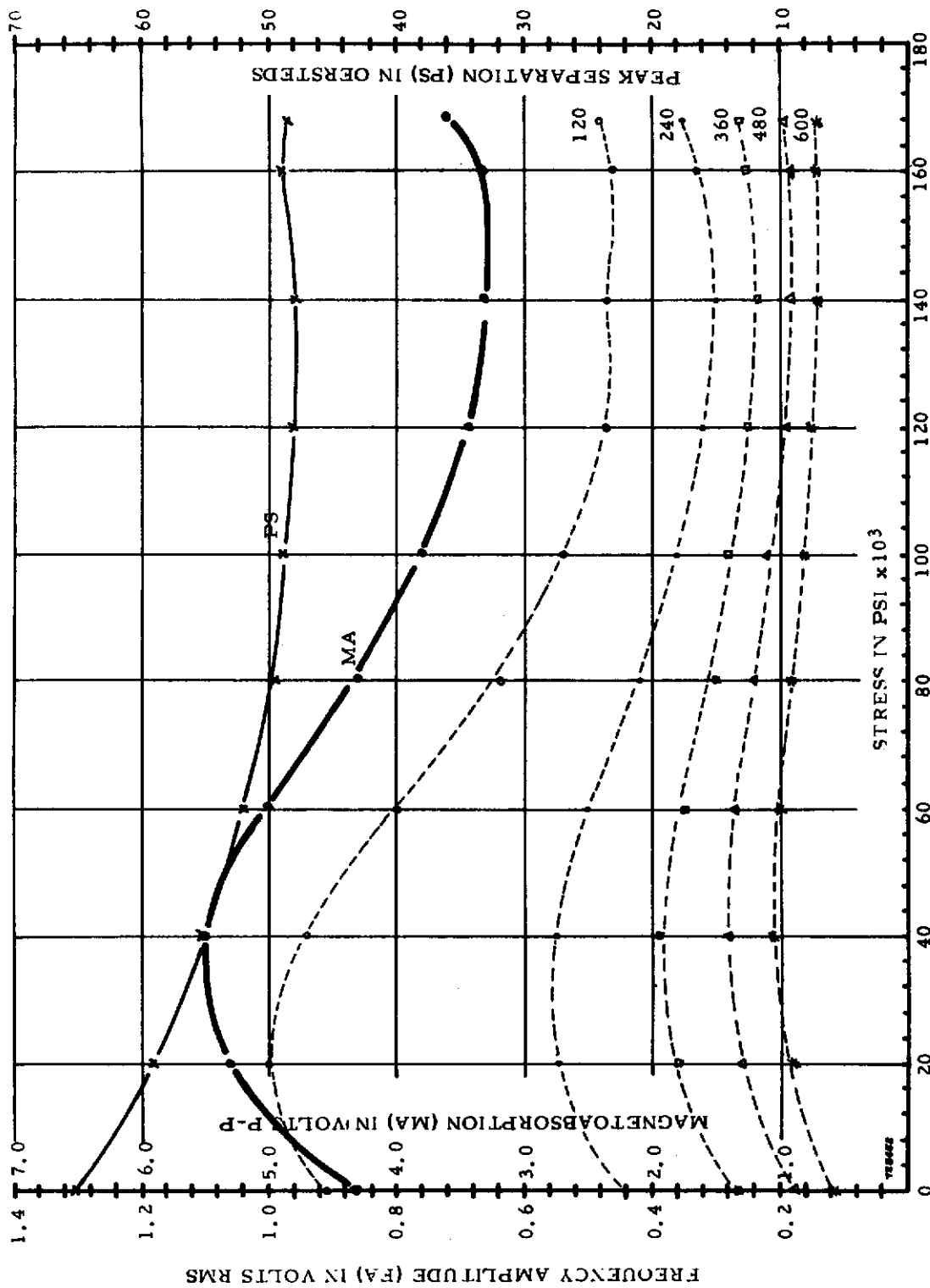


FIGURE 35. VARIATIONS OF MAGNETOABSORPTION AMPLITUDE, HARMONIC AMPLITUDE, AND PEAK SEPARATION WITH STRESS FOR SOLUTION ANNEALED 18% MARAGING STEEL WIRE

Contrails

material is hardened by plastic deformation. If this material has a typical positive magnetostrictive property, it is to be expected that yield point occurred near the point of maximum magnetoabsorption. Elongation measurements, not performed, would have given conclusive evidence to this assumption.

From Figure 35, it is further observed that the maximum in the amplitude of each of the harmonics does not coincide with the maximum in the peak-to-peak amplitude of the magnetoabsorption signal. The rise in the amplitude at the fracture point is unusual and may have occurred because most of the plastic deformation occurred within a very small percentage of the filling factor. Consequently, the remaining material, having the larger contribution to the magnetoabsorption signal and having returned to a point of less deformation, causes an increase in signal.

Lastly, the peak separation for this material has a definite exponential characteristic with increasing tensile stress. This indicates that the peak value of the magnetoabsorption occurs at smaller values of the bias magnetizing field as the load increases. This response could be used as a quantitative method of measuring stress in this solution-annealed maraging steel.

SECTION VI

RECOMMENDATIONS FOR ADDITIONAL EFFORT

On the basis of these efforts and those performed in earlier work, it is recommended that (1) magnetoabsorption techniques be extended to include instrumentation capable of measuring the amplitudes and phases of at least the first six harmonics of the magnetoabsorption, (2) through the use of such instrumentation, magnetoabsorption responses from ferromagnetic and ferromagnetic-clad material of interest to the sponsor be made as the material is subject to compression, tension, and fatigue testing, and (3) a magnetoabsorption detector be designed, constructed, and tested for measuring and/or telemetering magnetoabsorption signals.

REFERENCES

1. Rollwitz, W. L., and Whitney, A. W., "Special Techniques for Measuring Material Properties," AFML-TRD-64-123, 1964.
2. Rollwitz, W. L., and Claassen, J. P., "Special Techniques for Measuring Properties," AFML-TR-65-17, 1965.
3. Ramo, S., and Whinery, J. R., Fields and Waves in Modern Radio, John Wiley & Sons, New York, 1944.
4. Bozorth, R., Ferromagnetism, Van Nostrand Company, 1951.
5. Bunce, B. E., "Production Plating of Aluminum and Its Alloys," Electroplating, p. 317, September 1953.
6. Spooner, R. C., and Seraphim, D. P., "Phosphoric Acid Anodizing of Aluminum and Its Application to Electroplating," Transactions of the Institute of Metal Finishing, 31, pp. 29-45, 1954.
7. Green Letter Series, Aluminum Alloy X-7106, Alcoa, October 1963.
8. Holt, A. G., "Sensitivity of a Oscillator to Periodic Conductance Changes," The Radio and Electronic Engineer, February 1964.
9. Watkins, B. D., Ph.D. Thesis, Harvard University, 1952.

Contrails

APPENDIX I

SMALL PROBES AND THEIR COUPLING CIRCUITS

To measure magnetoabsorption from small volumes of ferromagnetic materials, small sample coils of several turns of wire were considered as probes. It is intended with these probes to observe the various material properties or defects at specific small areas on a ferromagnetic surface. As an example, by placing a hollow solenoidal probe over a slowly elongating ferromagnetic wire, the local changes in stress could easily be scanned as the probe traverses the entire wire specimen. Or, with another type probe, a ferromagnetic surface could be examined for locally fatigued areas. With such probes, it may be possible to observe: (1) stress magnitudes and directions, (2) stress gradients, (3) locally fatigued areas, (4) cracks, (5) variations in heat treatment, and (6) inclusions. Within the realm of feasibility, there are some optimum probe configurations for observing each property of a particular shaped specimen.

The following qualitative specifications are deemed appropriate for probes employing magnetoabsorption detection:

- (1) The RF field produced by the probe must couple well with the specimen under investigation.
- (2) The characteristic size of the coil-type probes should be comparable in size or smaller than the size of the defect to be observed. In other words, the defect must present a large filling factor to the probe.
- (3) The configuration of the probe should be dictated by the type of application.
- (4) Noise sources and pickup should be reduced by appropriate design of the probe, bias coils, and associated coupling circuit so that microphonics and stray inductions are avoided.

Figure 36 shows a number of common probe configurations, and, from these, a number of observations are made. An examination of the horizontal solenoid shows that very little of the RF field couples with the surface; consequently, further consideration of this configuration is excluded. The vertical solenoid exhibits an RF field that is symmetrical with respect to its axis of rotation. Thus, the vertical solenoid does not exhibit an inherent directional field when placed on a specimen except as may be caused by inhomogeneities in the specimen. The crescent-shaped and double-D probes, on the other hand, have an inherent directional property associated with their configuration. The crescent-shaped probe develops an RF field parallel to its axis. The

Contrails

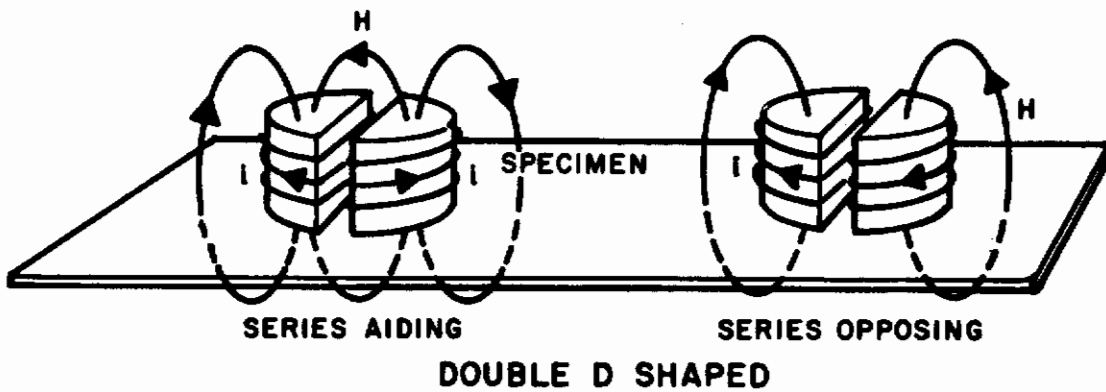
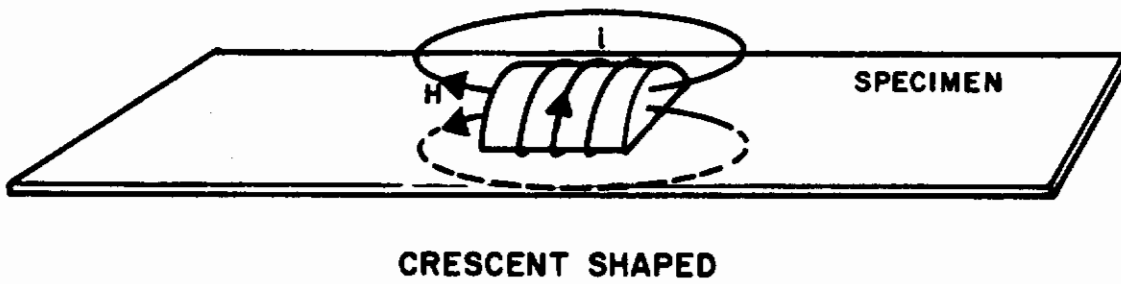
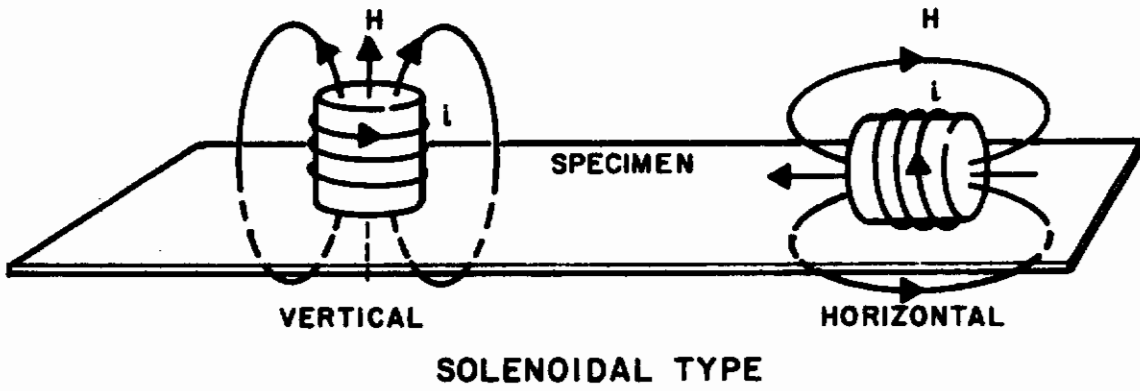


FIGURE 36. PROBE CONFIGURATIONS

double-D probe primarily develops fields normal to its symmetrical plane. The double-D probe of the series aiding type has the additional feature that it is capable of rejecting induction by a homogeneous external field whereas the other types shown in Figure 36 do not.

The bias coils can be similarly constructed to exhibit a directional property. It is this directional property of the fields that is so beneficial in achieving meaningful information from magnetoabsorption measurements.

In order to electrically connect a probe consisting of a few turns of wire to the marginal oscillator input, a coupling circuit must be employed. Without such a circuit, the marginal oscillator when connected directly to the probe cannot sustain oscillations. Consequently, the coupler must consist of a suitable value of inductance shunting the marginal oscillation input to sustain oscillations of a proper frequency. Furthermore, the remainder of coupling circuit must be capable of transferring very small impedance changes, $(\omega L_p \chi'' + j\omega L_p \chi') F^*$, from the probe to the inductance shunting the marginal oscillator. Two common coupling circuits are considered: the series resonant circuit of Figure 37 and the transformer circuit of Figure 38.

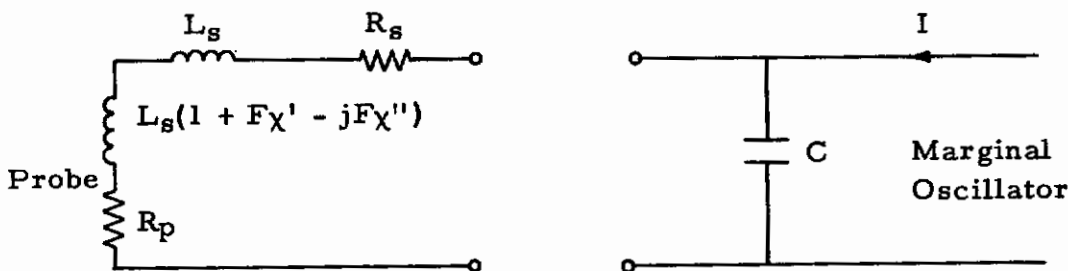


FIGURE 37. SERIES RESONANT CIRCUIT METHOD FOR COUPLING A SMALL COIL TO A MARGINAL OSCILLATOR

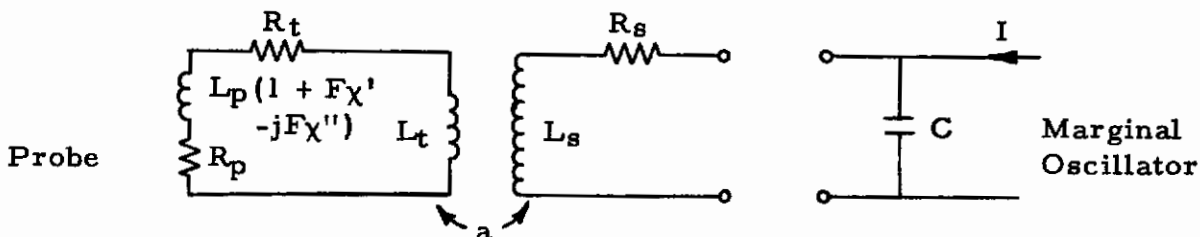


FIGURE 38. THE TUNED SECONDARY TRANSFORMER METHOD OF COUPLING A SMALL COIL TO A MARGINAL OSCILLATOR

*F is the effective filling factor for the probe, and χ' and χ'' are the real and imaginary parts of the susceptibility of the sample, respectively.

Contrails

With the assumption that the marginal oscillator feedback circuit functions to some degree as a constant current source I , the voltage across the series circuit is approximated by

$$E = I \frac{\omega^2 [L_s + L_p(1 + \chi'F)]^2}{R_p + R_s + \omega L_p \chi''} \quad (18)$$

where the symbols are defined in Figure 6, and where

$$\omega [L_s + L_p(1 + \chi'F)] \gg (R_p + R_s + \omega L_p \chi'')$$

has been assumed. Whereas for transformer coupling with an effective turns ratio of a , the resultant voltage across the marginal oscillator input is approximated by

$$E_s = \frac{I \left\{ \omega L_s + a^2 \omega [L_p(1 + \chi'F) + L_t] \right\}^2}{R_s + a^2 (R_p + R_t + \omega L_p \chi''F)} \quad (19)$$

where the symbols are defined in Figure 38, and where

$$\omega L_s + a^2 [L_p(1 + \chi'F) + L_t] \gg R_s + a^2 (R_p + R_t + \omega L_p \chi''F)$$

has been assumed.

A comparison of Equations (18) and (19) indicates that for small effective changes in $\omega L_p \chi'F$ or $\omega L_p \chi''F$ within the same probe that transformer coupling is more effective. This fact has also been shown to be true experimentally. Further, additional high pass filtering is achieved with the transformer coupled circuit so that external induction by the bias is effectively reduced by the low transformer inductance and small low frequency mutual inductance. Figure 39 shows the toroidal ferrite transformer actually employed to couple small probes to the marginal oscillator and one of the probes that couples to the input of the transformer. The transformer is mounted in a magnetic shielded chassis to prevent external fields from varying the permeability of the ferrite toroid. The transformer employs a high frequency ferrite core and has the following properties:

- (1) Primary turns = 150
- (2) Primary inductance = 600 μ h
- (3) Primary Q = 285 at 300 kcps
- (4) Secondary turns = 1, 3, 5, 7, 9, 11, 13, 15

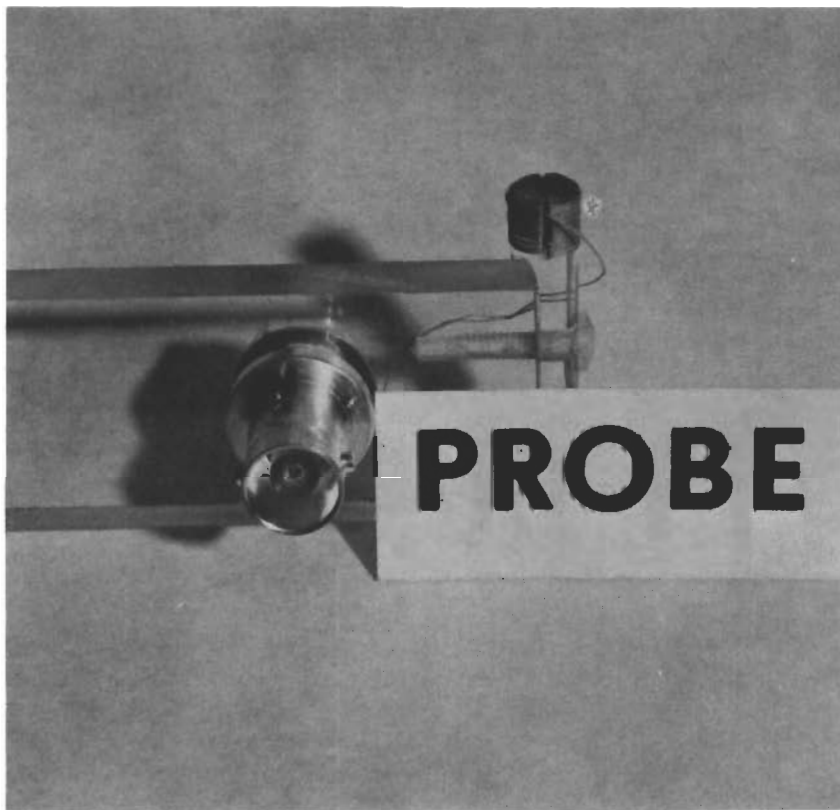
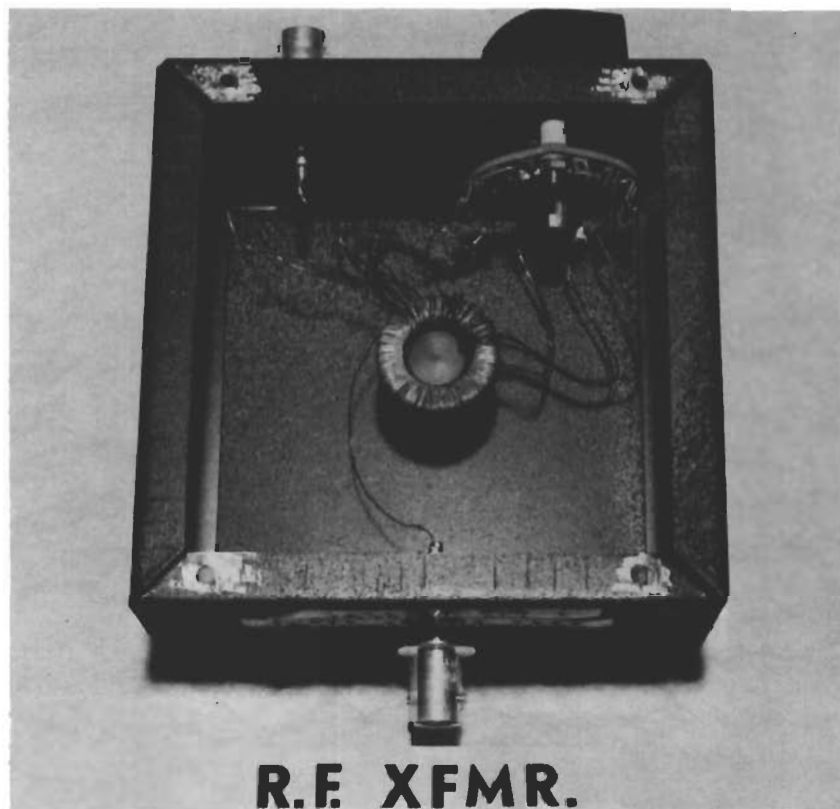


FIGURE 39. FERRITE TRANSFORMER AND A DOUBLE-D PROBE

Contrails

A number of double-D probes was constructed to investigate their capability and to perform a number of measurements. A sample of the probes constructed is shown in Figure 40a. Their diameters range from 1/4 inch to 1/16 inch as shown in Figure 40b.

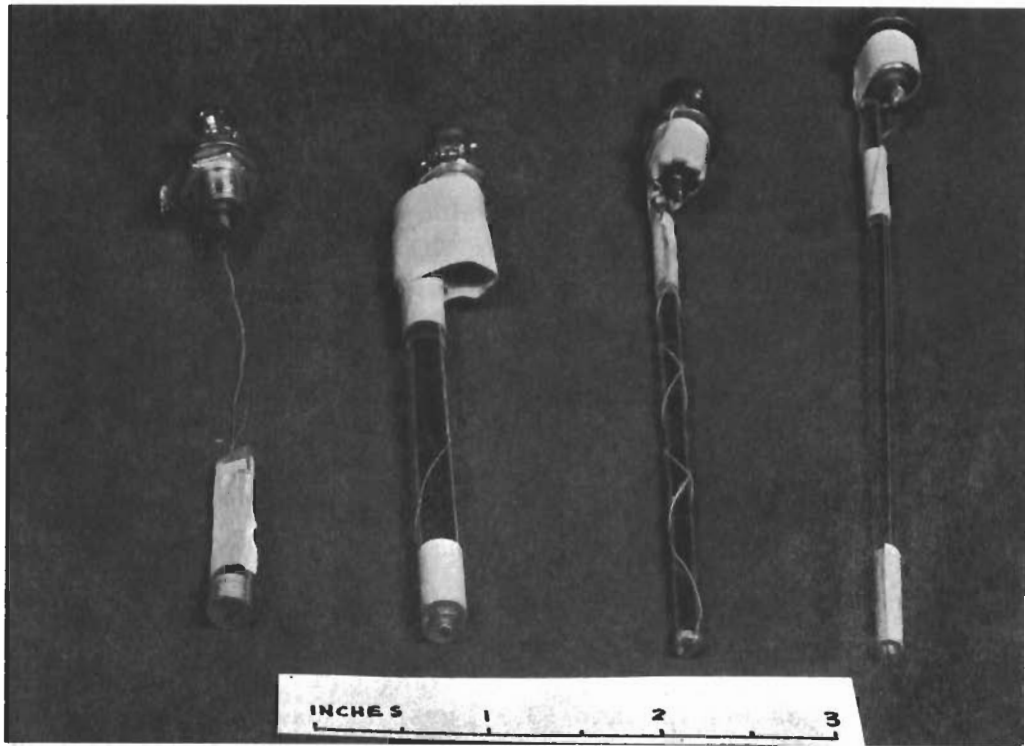


FIGURE 40a. A SELECTION OF DOUBLE-D PROBE

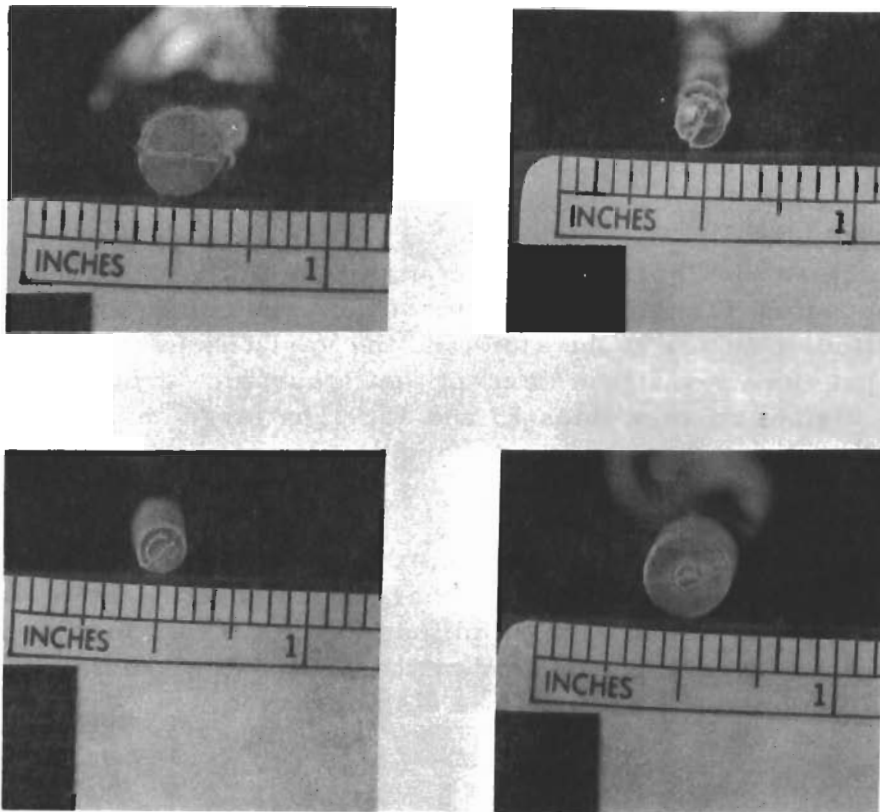


FIGURE 40b. THE TIPS FOR THE PROBES SHOWN IN FIGURE 9a

APPENDIX II

DETAILED RESULTS FROM A SLOTTED
MARAGING STEEL PLATE

The harmonic amplitude response along scan lines 3, 5, 8, 10, 13, and 15 for the maraging steel plate having nine EDW slots is presented in this appendix. The conclusion drawn from these results appears in Section II of the text.

The picture of the sample with six scans of the amplitude of the fundamental (120 cps) component superimposed is shown in Figure 41a. Scans along lines 3, 8, and 13 do not intersect an EDM slot. Scans along lines 5, 10, and 15 do intersect EDM slots. The influence of the various observable areas are clearly distinguished.

Figure 41b is the same type of picture for scans along the same line numbers for the amplitude of the second harmonic at 240 cps. Because of the variations along lines 8, 10, and 13 on the right-hand side, two other scans are included along lines 11, 12, and 13. These scans indicate a distinct change in the material at the extreme right along lines 11, 12, and 13. The cause of this change is not visible to the unaided eye, and the area was not inspected with a metal microscope. The material change, whatever its source, is rather large.

Figure 41c shows the scans along the same lines as Figure 41b but at the frequency of the third harmonic (360 cps). The large changes at the right along lines 11, 12, and 13 are not visible on this plot for the third harmonic. However, the variation in amplitude around each slot is more pronounced at 360 cps than at 240 cps.

The picture of Figure 41d is the amplitude of the fourth harmonic (480 cps) along the same scan lines as those of the previous figures. Here again are the amplitude changes at the slots, and the variations are essentially the same as the previous two figures except that a surface scratch, to the right of center, is visible on scan lines 13 and 15. The large changes on the extreme right on lines 11 and 13 are more similar to those of the 240-cycle scan than the 360-cycle scan.

The picture of Figure 41e is from the amplitude of the fifth harmonic (600 cps). Similar plots for the higher harmonics have not been made. Here again, there is the variation of the amplitude of the fifth harmonic around the slots and the very large variations of amplitude at the extreme right. The scratch variation on scans 13 and 15 is also observed.

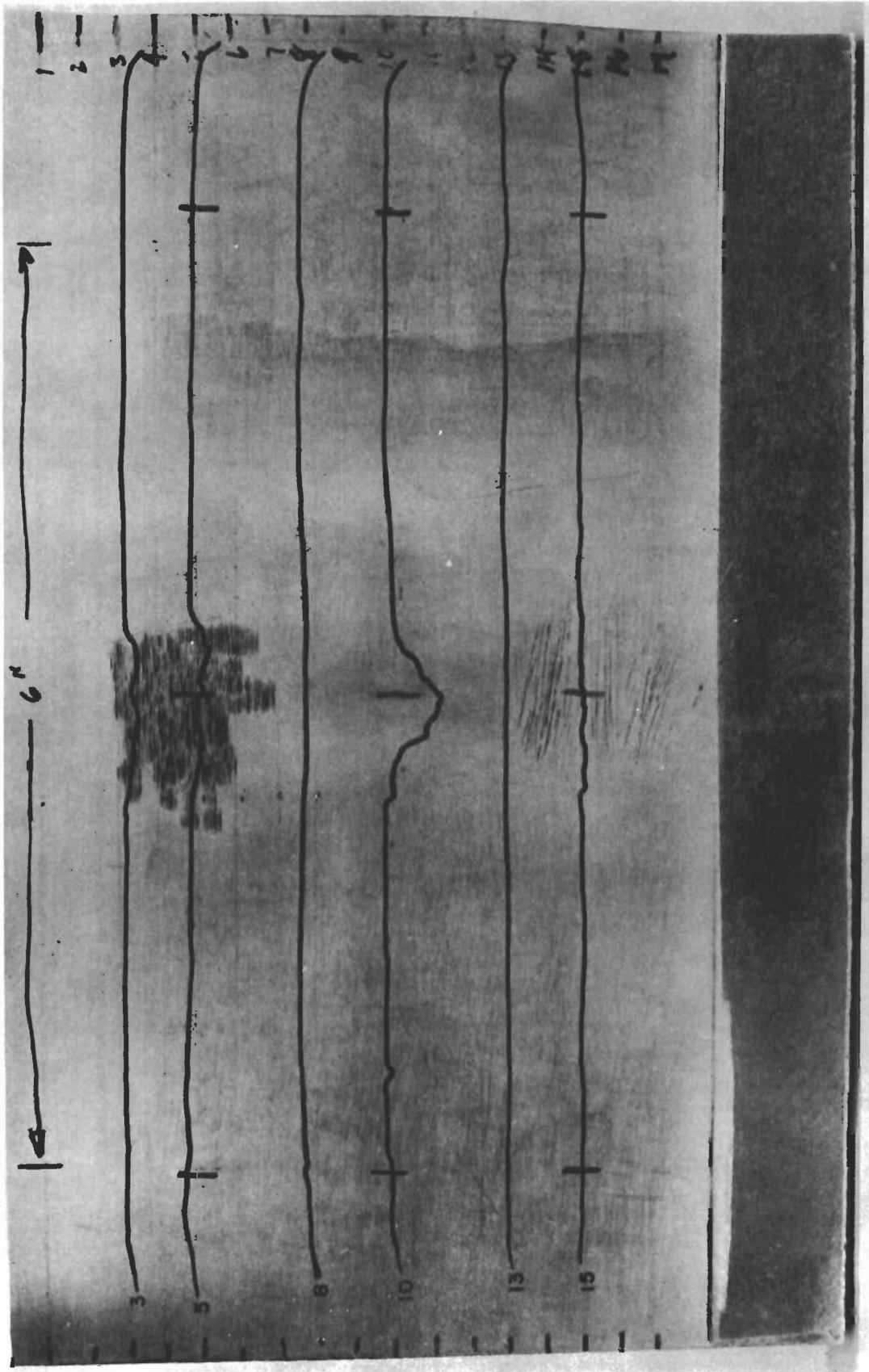


FIGURE 41a. VARIATIONS IN THE AMPLITUDE OF 120-CPS COMPONENT OF THE MAGNETOABSORPTION SIGNAL ALONG THE INDICATED SCANS FOR MARAGING STEEL SPECIMEN HAVING NINE EDM SLOTS

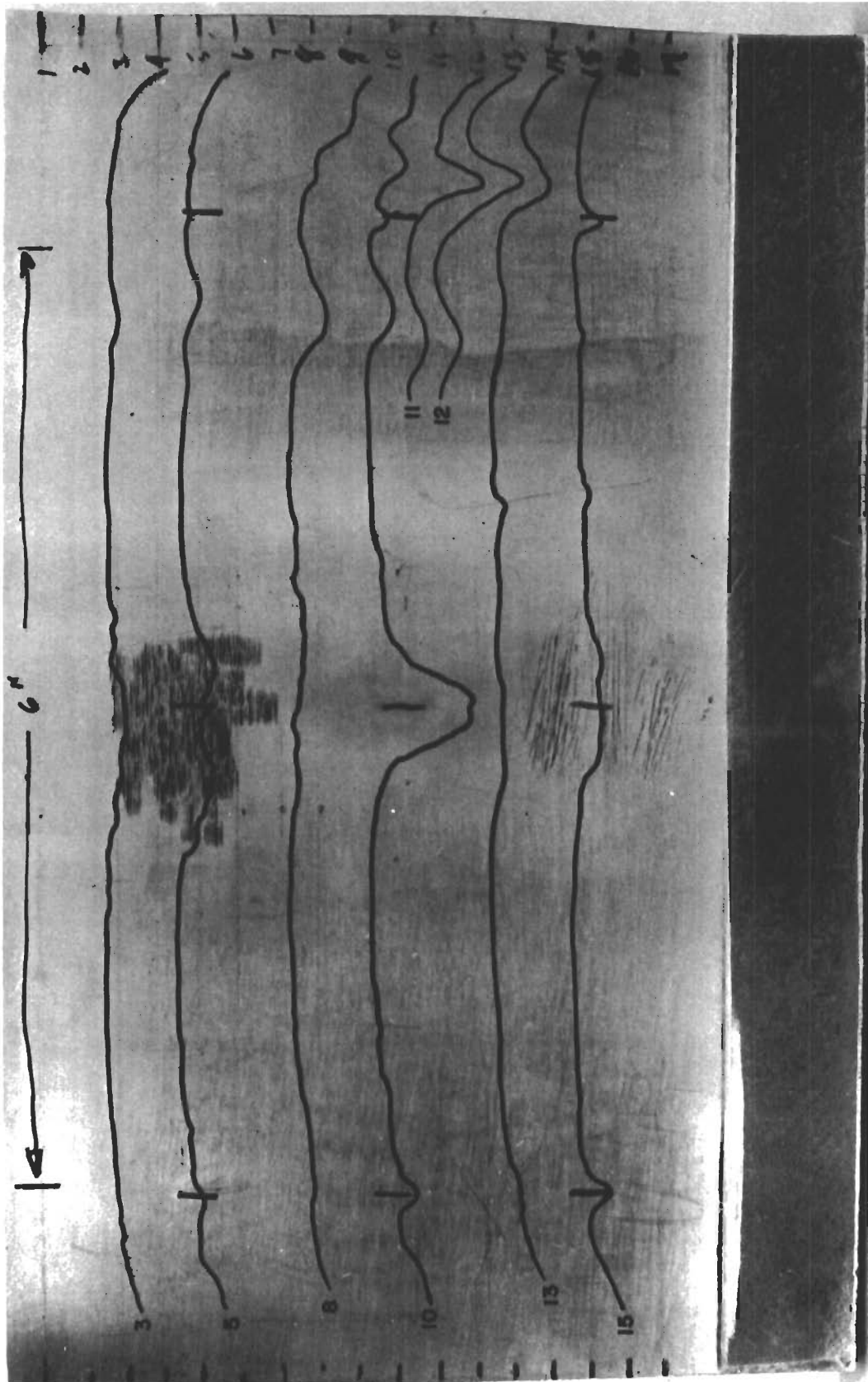


FIGURE 41b. VARIATIONS IN THE AMPLITUDE OF 240-CPS COMPONENT OF THE MAGNETOABSORPTION SIGNAL ALONG THE INDICATED SCANS FOR MARAGING STEEL SPECIMEN HAVING NINE EDM SLOTS

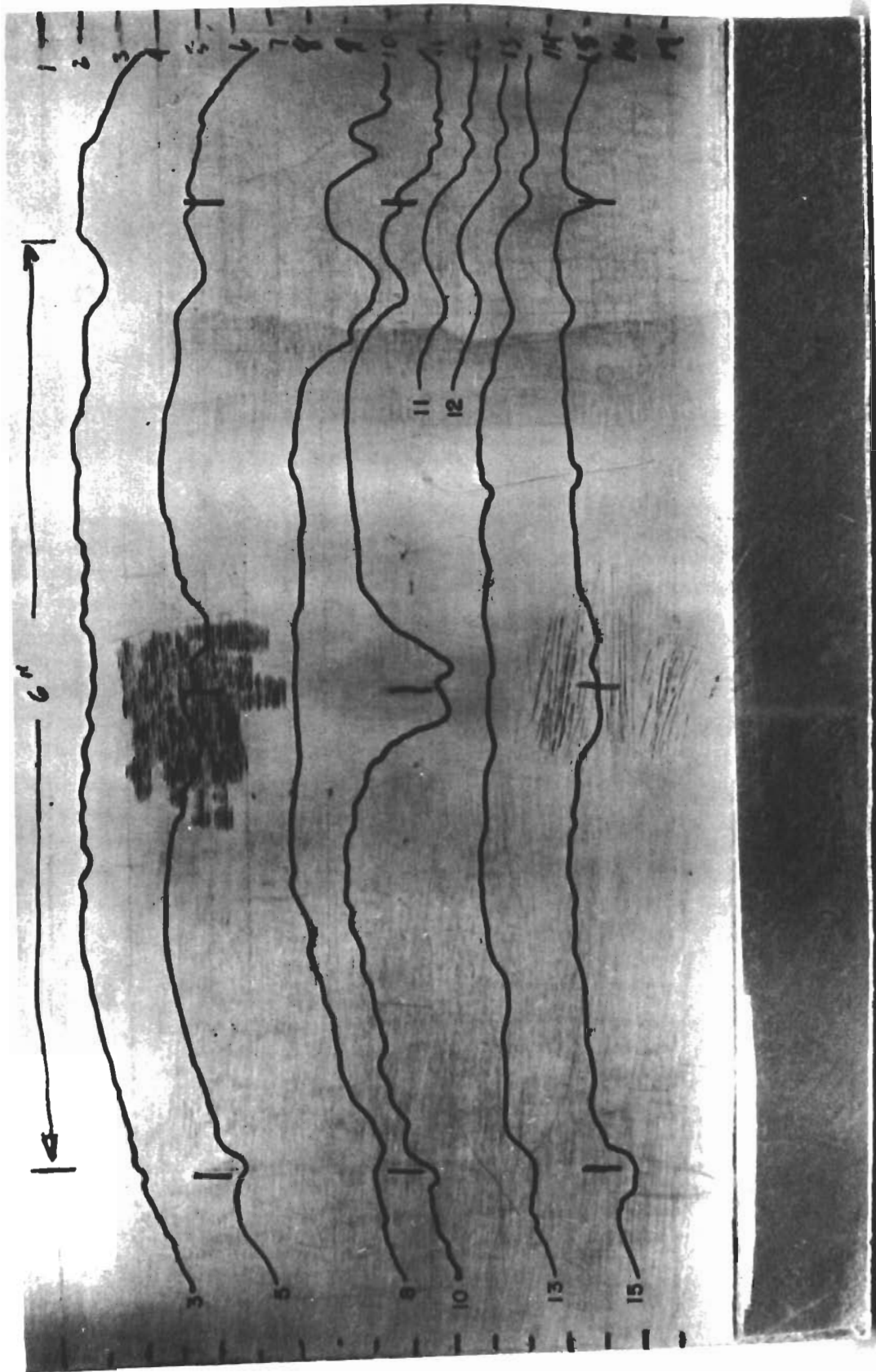


FIGURE 41c. VARIATIONS IN THE AMPLITUDE OF 360-CPS COMPONENT OF THE MAGNETOABSORPTION SIGNAL ALONG THE INDICATED SCANS FOR MARAGING STEEL SPECIMEN HAVING NINE EDM SLOTS

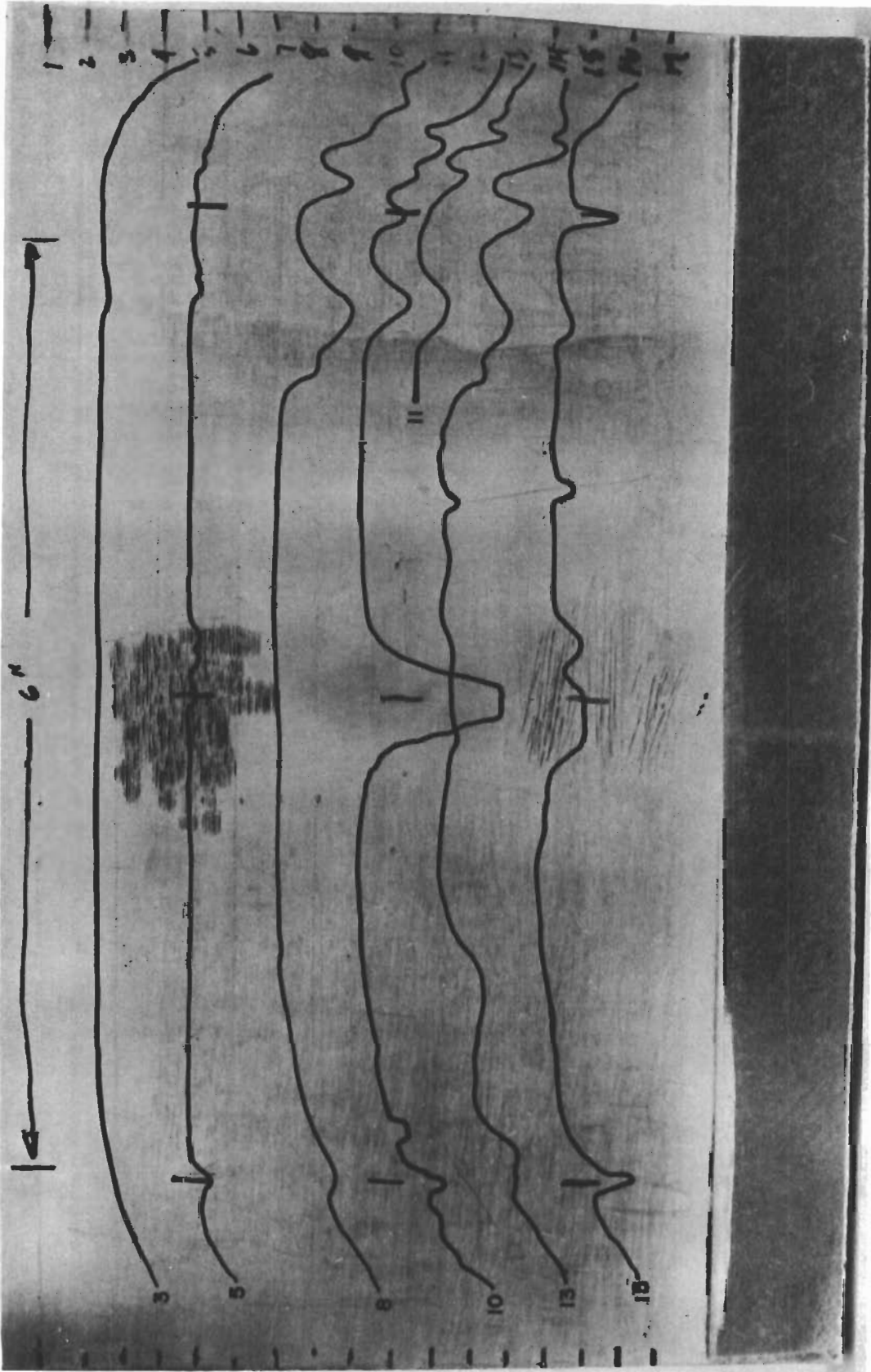


FIGURE 41d. VARIATIONS IN THE AMPLITUDE OF 480-CPS COMPONENT OF THE MAGNETOABSORPTION SIGNAL ALONG THE INDICATED SCANS FOR MARAGING STEEL SPECIMEN HAVING NINE EDM SLOTS

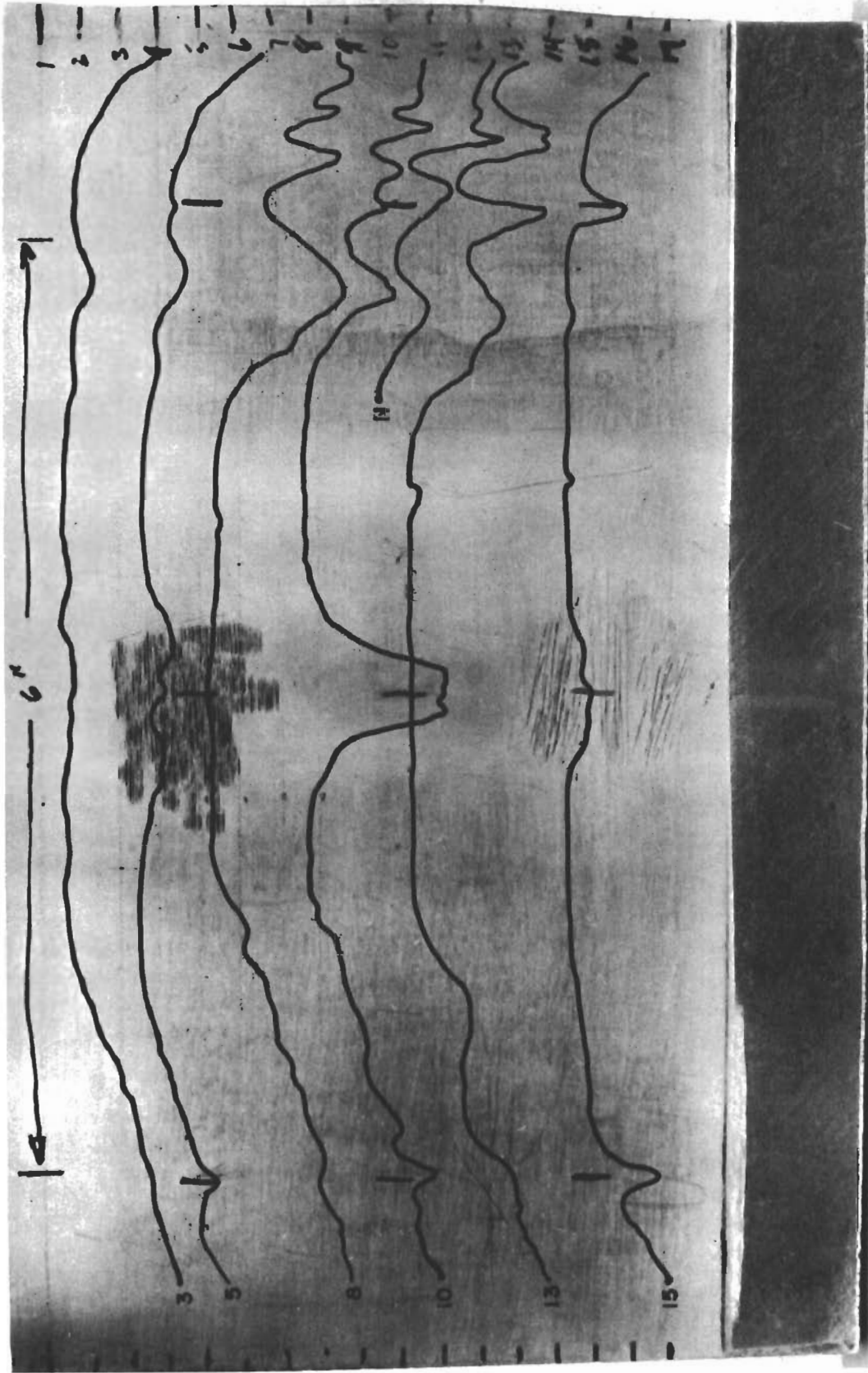


FIGURE 41e. VARIATIONS IN THE AMPLITUDE OF 600-CPS COMPONENT OF THE MAGNETOABSORPTION SIGNAL ALONG THE INDICATED SCANS FOR MARAGING STEEL SPECIMEN HAVING NINE EDM SLOTS

APPENDIX III

MAGNETOABSORPTION WAVEFORM DATA
FROM HY-80 STEEL

Figures 42, 43, and 44 show the waveforms taken at equal intervals along face "A" and "B" of specimens S-1, S-5, and S-6. The experimental condition and type of specimen are noted on each figure. A complete discussion of these responses is presented in Section III.

Contrails

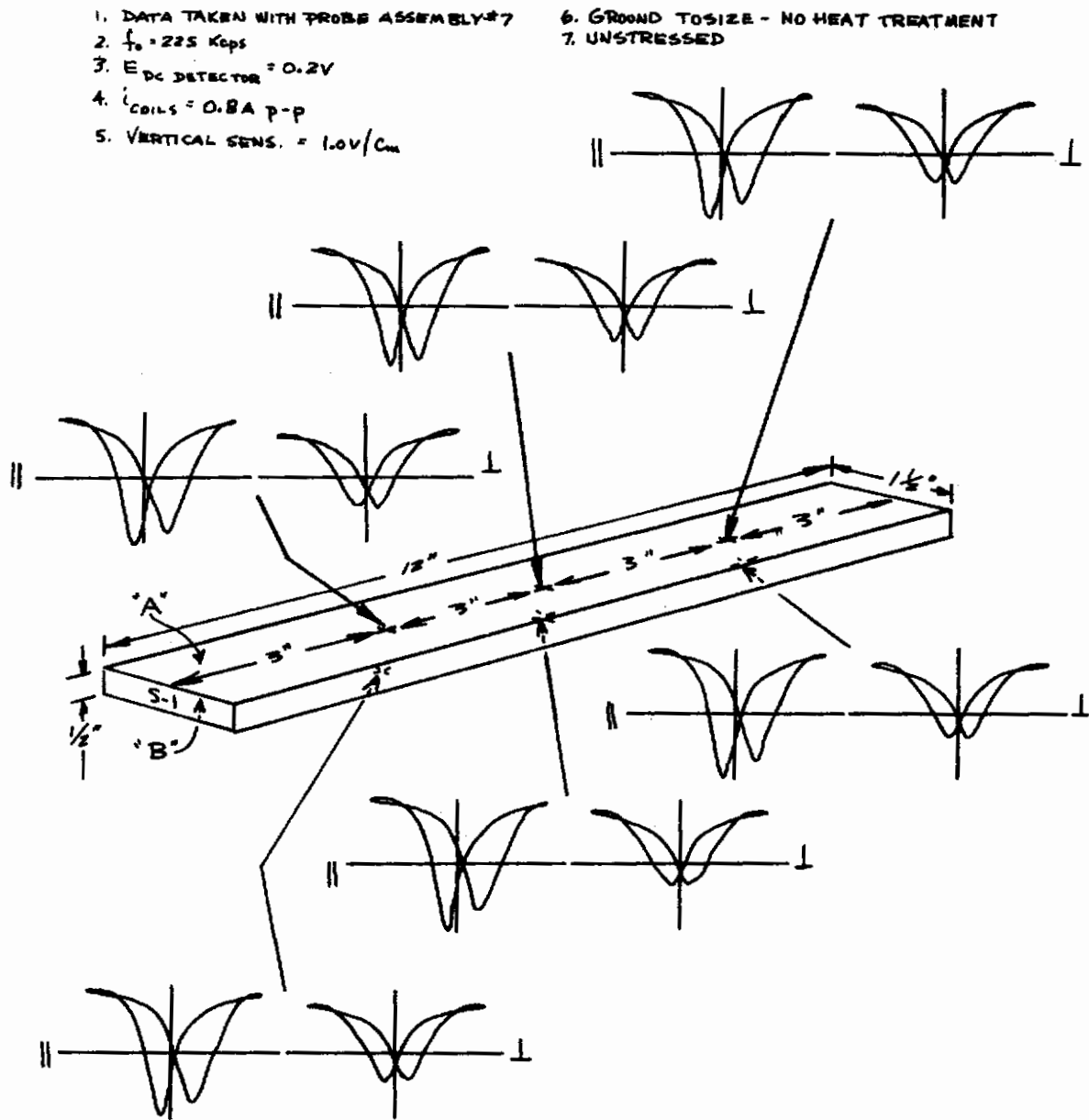


FIGURE 42. MAGNETOABSORPTION SIGNALS - SPECIMEN NO. S-1, HY-80 STEEL

Contrails

1. DATA TAKEN WITH PROBE ASSEMBLY #7

2. $f_0 = 225$ Kcps

3. $E_{DC DETECTOR} = 0.2V$

4. $i_{COILS} = 0.8A$ p-p

5. VERTICAL SENS. = $1.0V/cm$

6. GROUND TO SIZE - STRESS RELIEVED

7. 0.82% Residual Surface Deformation

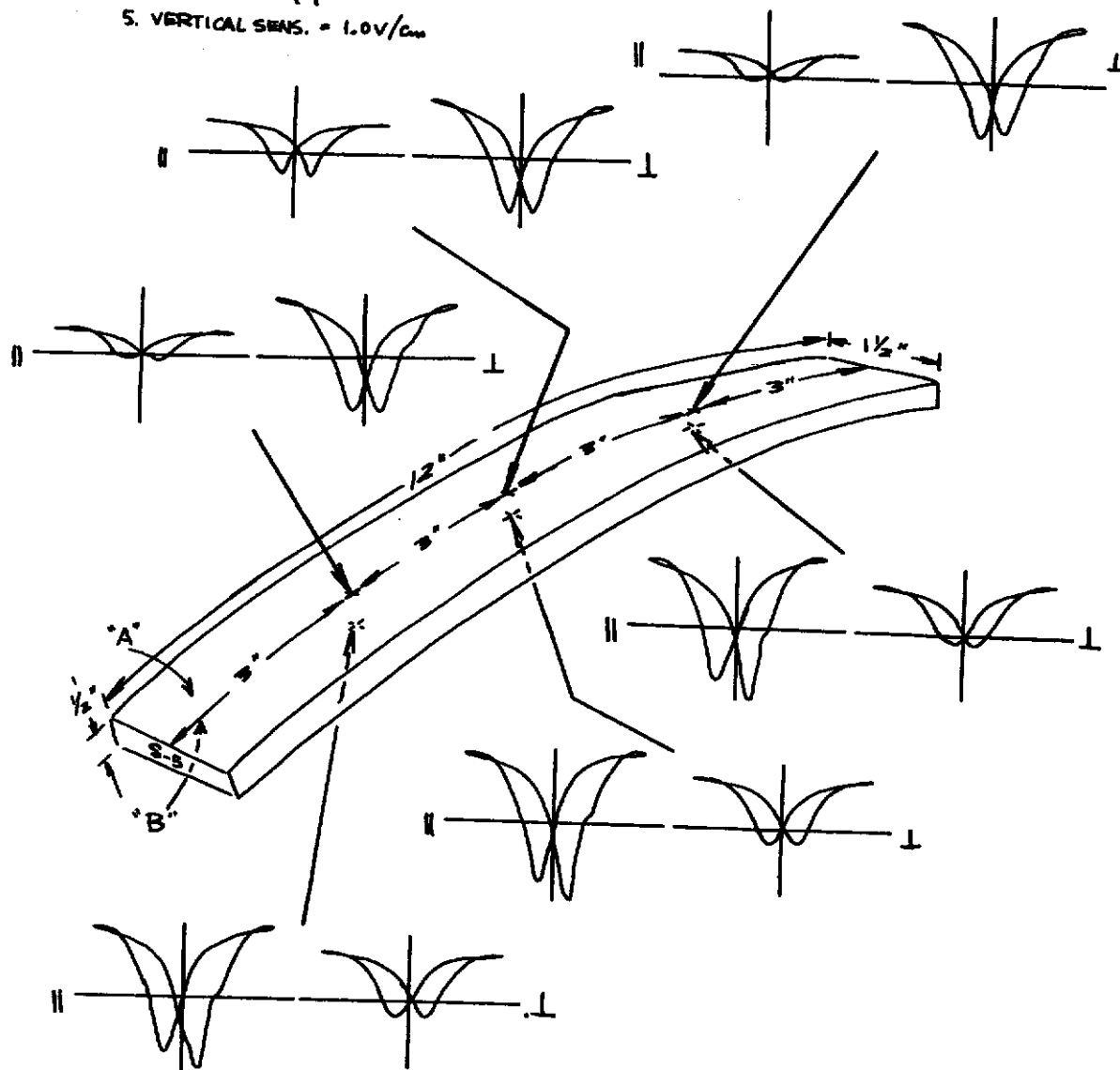


FIGURE 43. MAGNETOABSORPTION SIGNALS - SPECIMEN NO. S-5, HY-80 STEEL

Contrails

1. DATA TAKEN WITH PROBE ASSEMBLY #7
2. $f_0 = 225 \text{ kcps}$
3. $E_{\text{D.C. DETECTOR}} = 0.2 \text{ V}$
4. $i_{\text{COILS}} = 0.8 \text{ A p-p}$
5. VERTICAL SENS. = 1.0 V/cm
6. GROUND TO SIZE - STRESS RELIEVED
7. Approximately 1% residual surface deformation

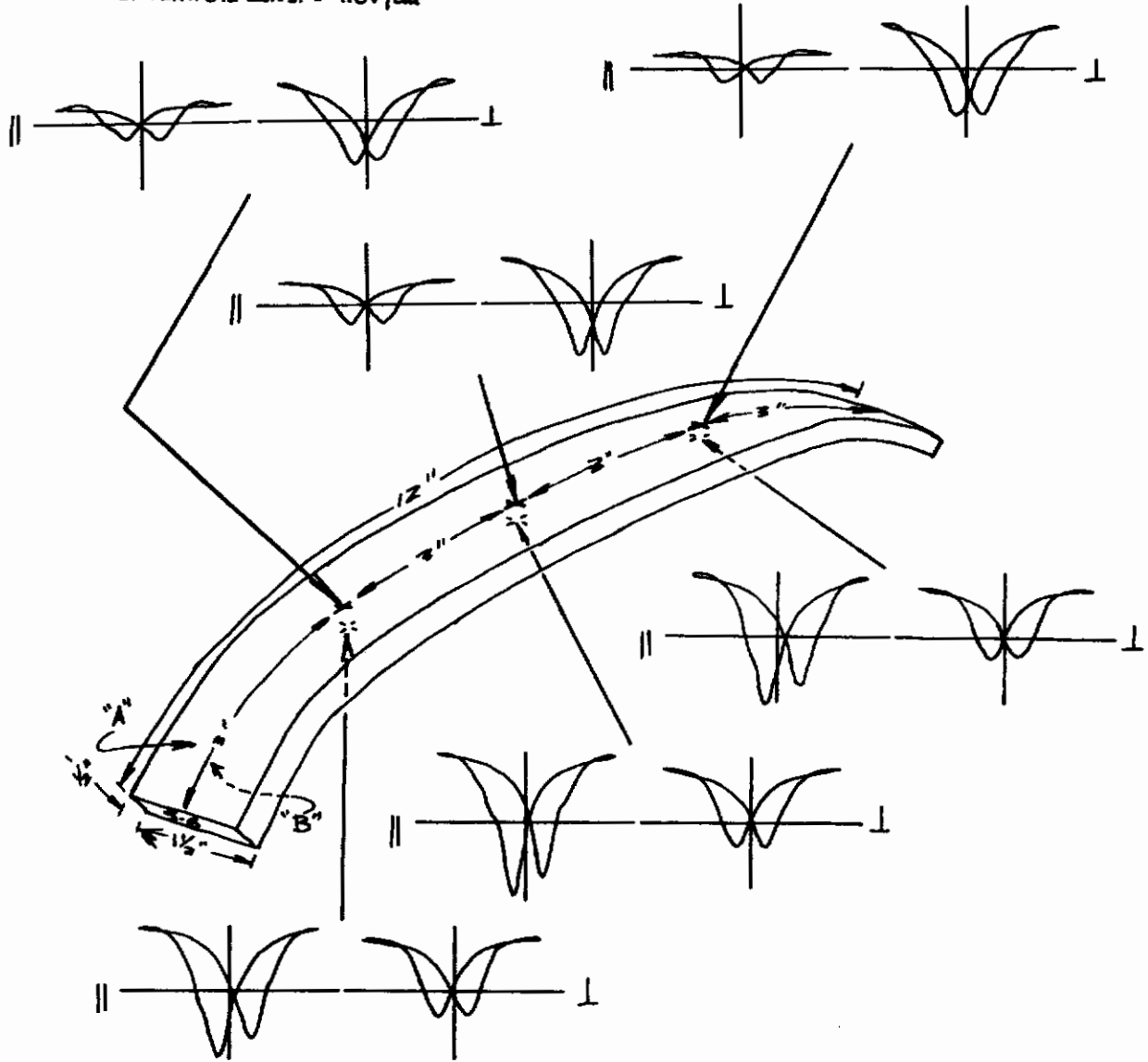


FIGURE 44. MAGNETOABSORPTION SIGNALS - SPECIMEN NO. S-6, HY-80 STEEL

APPENDIX IV

MAGNETOABSORPTION MEASUREMENTS FROM AN EXPLOSIVELY FORMED SHEET OF 1020 STEEL

The magnetoabsorption signals from a dome-shaped explosively formed piece of 1020 sheet steel are shown in Figure 45. These magnetoabsorption signals were measured with the probe shown in Figure 15. The radii of curvature for all of the measurement positions were sufficiently long to obtain a good measurement with a flat probe.

The magnetoabsorption curves of Figure 45 show that the convex face is relatively unstressed since there is little difference between the signals from the parallel and the perpendicular directions for the magnetic field. Parallel is defined as along a longitudinal line and perpendicular is along a latitudinal line. There are differences between the parallel and perpendicular signals at the edge position on the top face where the radius of curvature is small at the edge of the explosive forming. The curve from the outer edge of the plate was taken to attempt to obtain a curve for the undisturbed steel. Experience shows that the pictures shown at the outer edge indicate as nearly as possible the shape of the magnetoabsorption signals from undisturbed 1020 steel. Experience with mild steels has also shown that, with increasing applied stress, the magnetoabsorption signal at first increases in amplitude with little change in shape and then a rapid decrease with much change in shape.

When previous experience is applied to the data shown in Figure 45, it can be conjectured that the top and middle of the dome have a very mild stress along a longitudinal line; that the edge of the dome has a much greater stress along a longitudinal line; and that the outer edge is relatively undisturbed and unstressed.

On the concave side, the signal shape and amplitude at the top of the dome indicates that it is highly stressed but in a direction other than either a longitudinal or a latitudinal line. There appears to be less stress in the middle of the concave side of the dome, again in neither of the described directions. In contrast to the results on the convex face, the curve from the edge of the dome on the concave side seems to have a relatively lower stress than at the middle and top of the dome, again in a direction other than the two described.

The measurements on this explosive formed plate were brief, because it was available for a short time only. Since only one plate was available, nothing more can be concluded without a detailed study with many samples.

Contrails

MAGNETOABSORPTION DATA FROM EXPLOSIVE FORMED STEEL SHEET ONE INCH THICK -

Operating constants:

1. $f_0 = 225$ Kcps
2. detector coil assy. #7
3. E_{DC} detector = 0.2V
4. $i_{coil} = 0.8A$ p-p
5. H = magnetizing field applied radially
6. L = magnetizing field applied at right angles to radii

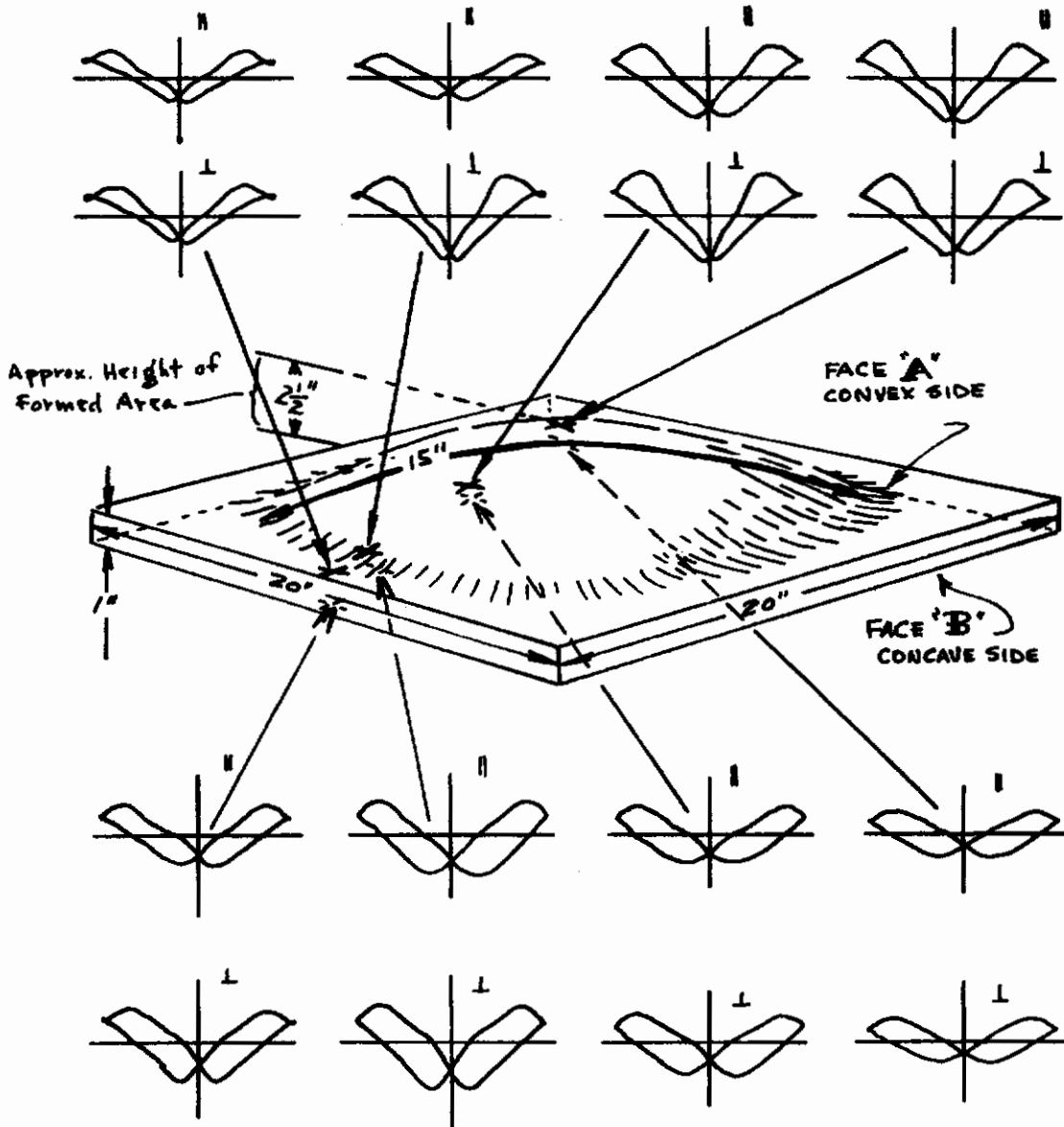


FIGURE 45. MAGNETOABSORPTION SIGNALS FROM AN EXPLOSIVELY-FORMED--DOME SHAPED PIECE OF 1020 STEEL

MAGNETOABSORPTION FROM NICKEL FILMS ON ALUMINUM

A. Description of Plating Technique

In order to obtain a useful plating of nickel onto an aluminum substrate, the following procedure has been found effective:

- (1) The material is cleaned in a 10% (by volume) hydrofluoric acid solution.
- (2) Anodization is accomplished for six minutes in a 25% (by volume) phosphoric acid solution at three amperes per square foot at room temperature.
- (3) The specimens are rinsed thoroughly in cold distilled water.
- (4) The plating is then accomplished in a conventional acid nickel-plating tank under power and constant agitation. The initial plating rate is 12 amperes per square foot for 1 minute and then 3 amperes per square foot for 5 minutes.

B. Loading and Elongation Methods

The specimen is grasped with a pair of drill chucks 4 to 6 inches apart. One drill chuck is mounted on the base while the other is mounted on the moment arm or moveable beam. The drill chuck is mounted 6 inches from the fulcrum. The fulcrum is composed of a pair of needle bearings about a stationary dowel pin. Loads can be applied on either side of the fulcrum at a distance of 18 inches from the fulcrum. Thus, a mechanical advantage of three results; i. e., for every one pound of weight applied 18 inches from the fulcrum, an effective load of 3 pounds is applied to the specimen. The beam and base of the loading device were reinforced to accept effective loads of 250 pounds at the specimen. A closeup photograph of the loading device with bias coils and sample coil is shown in Figure 46.

To measure strain, a light source was rigidly attached to the pivoted beam, and its image was focused across the laboratory on a meter stick. Thus, as the specimen elongated or contracted, the displacement could be measured on the meter stick with amplification. Since the specimen was 6 inches from the fulcrum and the meter stick was 14.3 feet away, the elongation or contraction could be measured with an amplification of 28.6. It is estimated that friction in the loading device and diffusion in the image contributed an error of $\pm 1/2$ mm at the meter stick. Referred to the specimen, this error is equivalent to an error of $\pm 7/10$ mils in the strain measurement.

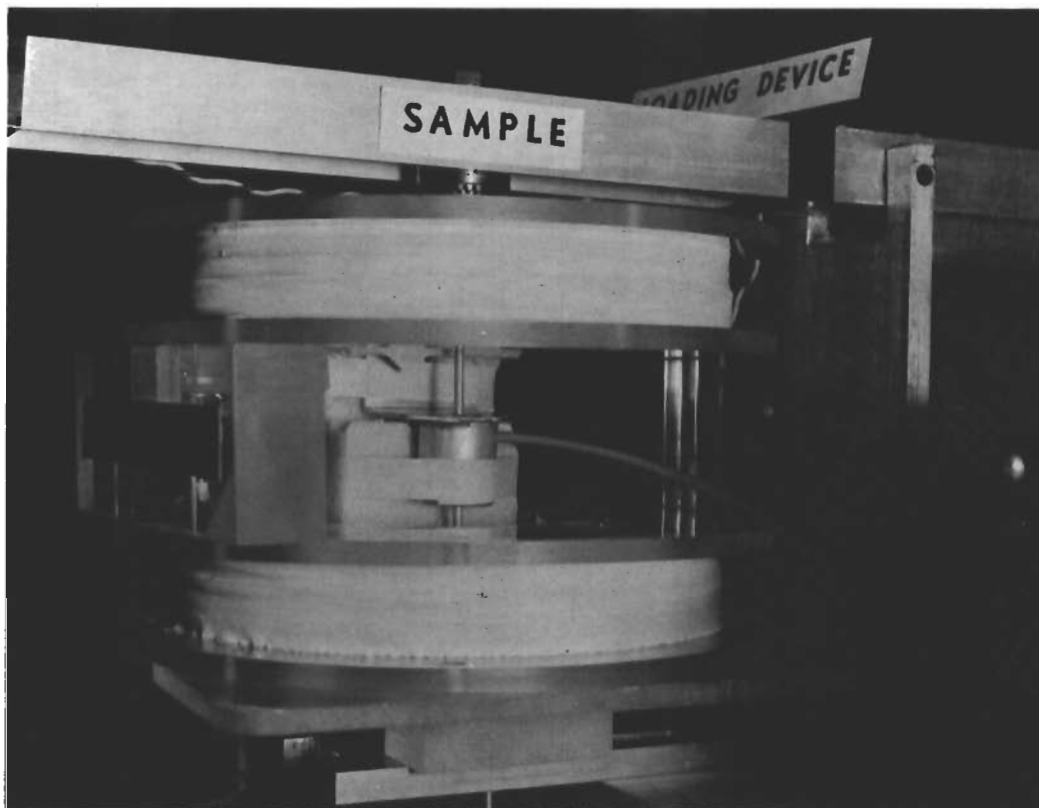
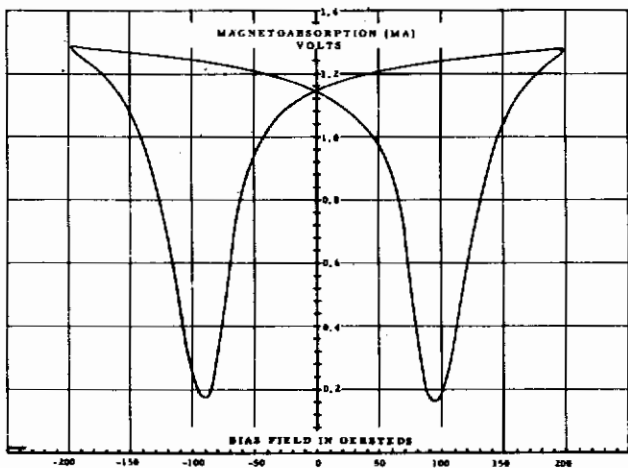


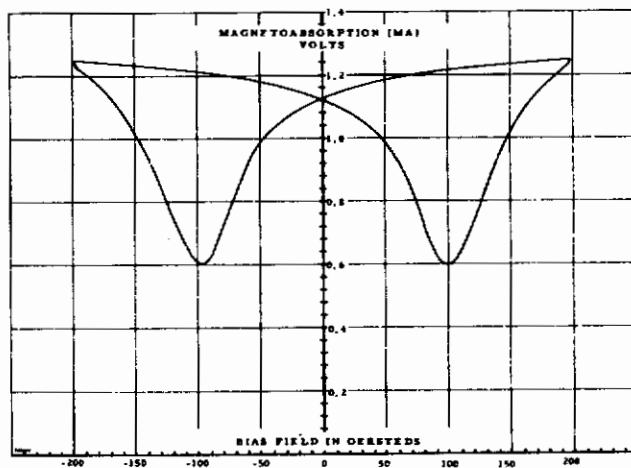
FIGURE 46. SAMPLE WITHIN CHUCKS,
SAMPLE COIL, AND BIAS COILS

C. Compilation of Magnetoabsorption Waveforms for Nickel-Plated
Aluminum Rods Having Various Diameters and Heat-Treatments

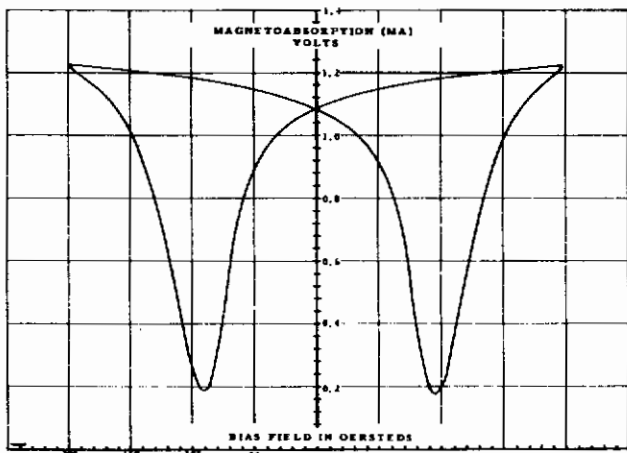
Figure 47 contains the magnetoabsorption signals obtained from an unannealed nickel-plated 1/8-inch aluminum rod at 10 and 5 pounds of compression, at no load, and at 20, 40, and 60 pounds of tension. Figure 48 shows magnetoabsorption curves taken at the same loads for an annealed specimen. The curves of Figures 49 and 50 were similarly taken from unannealed and annealed 1/16-inch nickel-plated aluminum rods at lower loads.



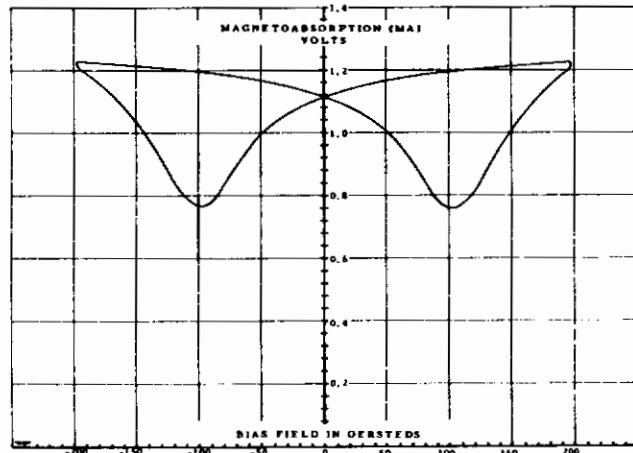
- 10 lb



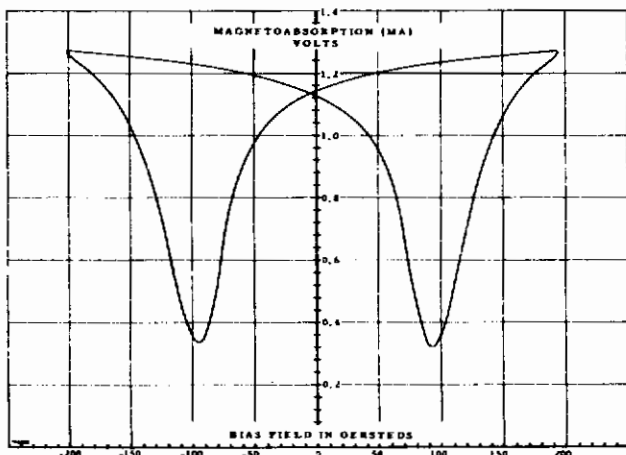
+ 20 lb



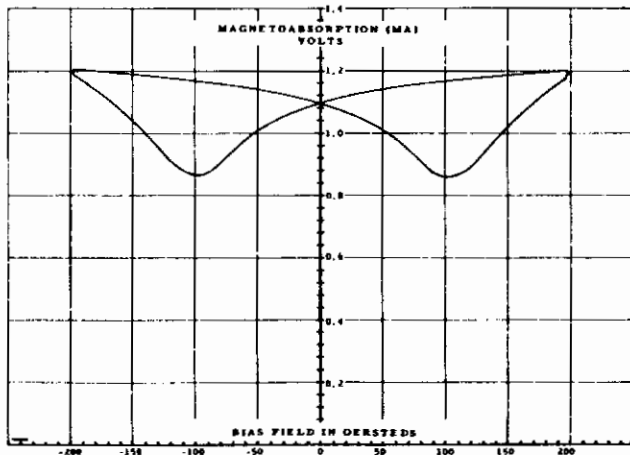
- 5 lb



+ 40 lb

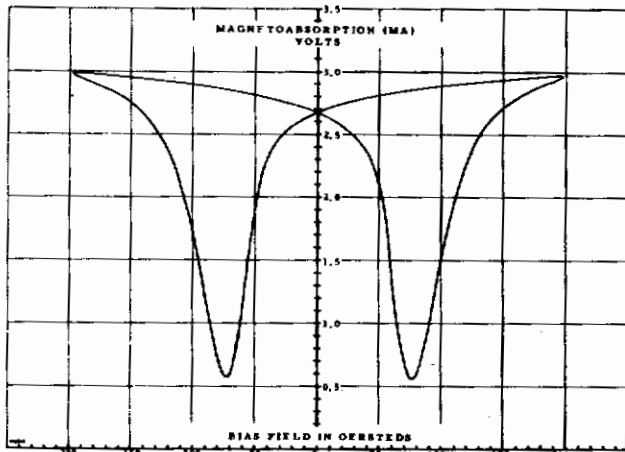


No Load

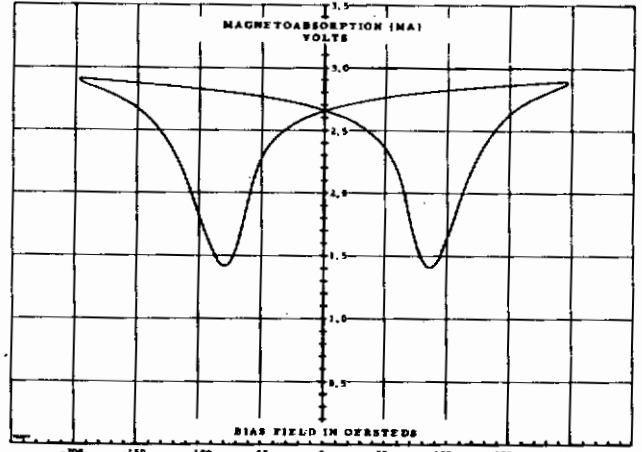


+ 60 lb

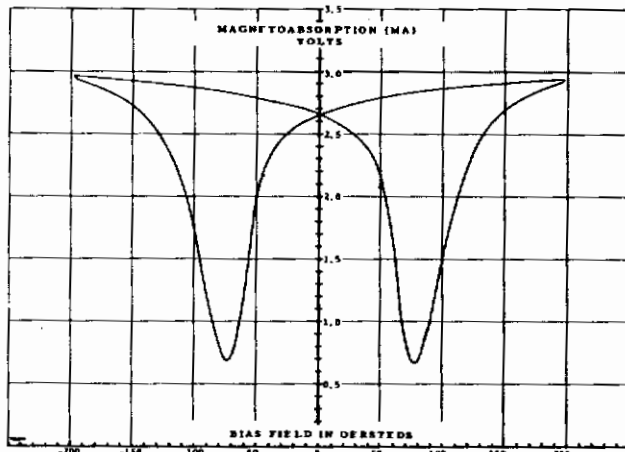
FIGURE 47. MAGNETOABSORPTION WAVEFORMS AS A FUNCTION OF LOAD FOR UNANNEALED NICKEL-PLATED ALUMINUM ROD OF 1/8-INCH DIAMETER



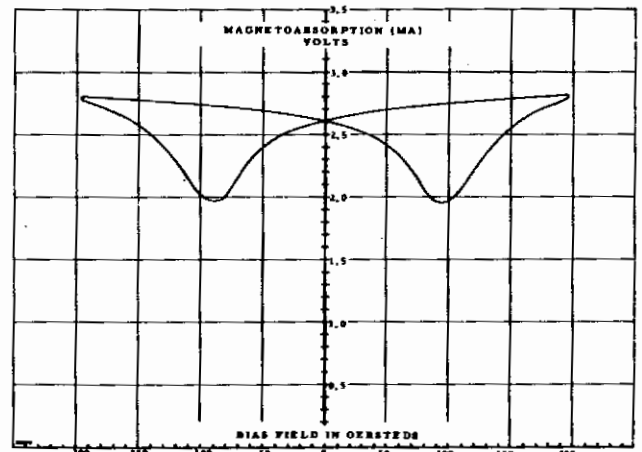
- 10 lb



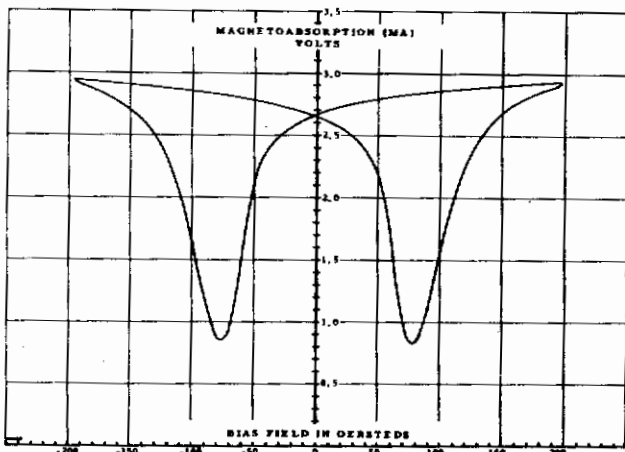
+ 20 lb



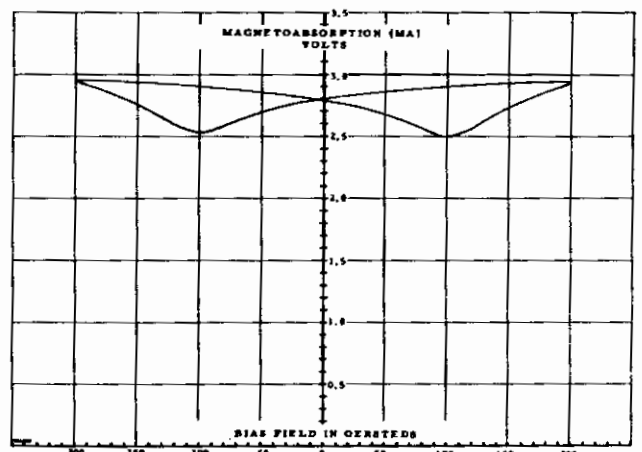
- 5 lb



+ 40 lb

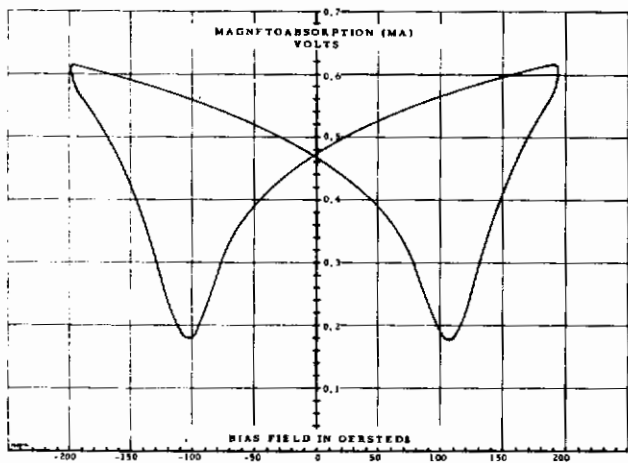


No Load

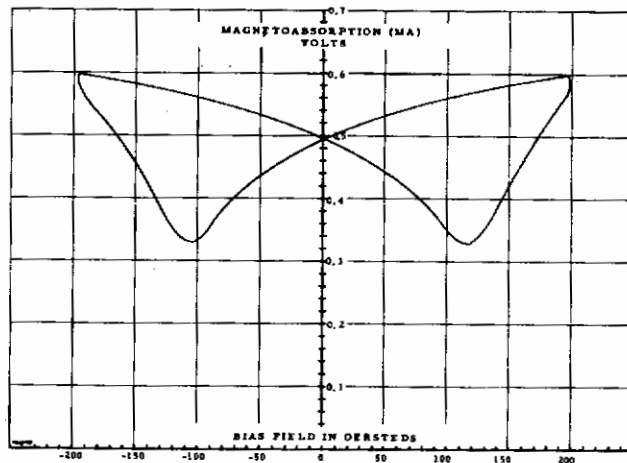


+ 60 lb

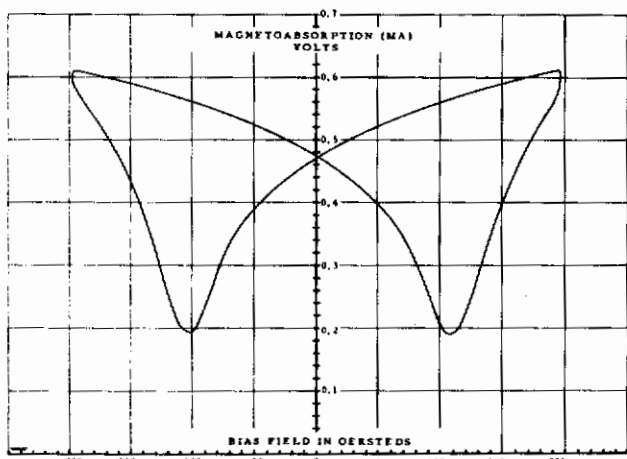
FIGURE 48. MAGNETOABSORPTION WAVEFORMS AS A FUNCTION OF LOAD FOR AN ANNEALED NICKEL-PLATED ALUMINUM ROD OF 1/8-INCH DIAMETER



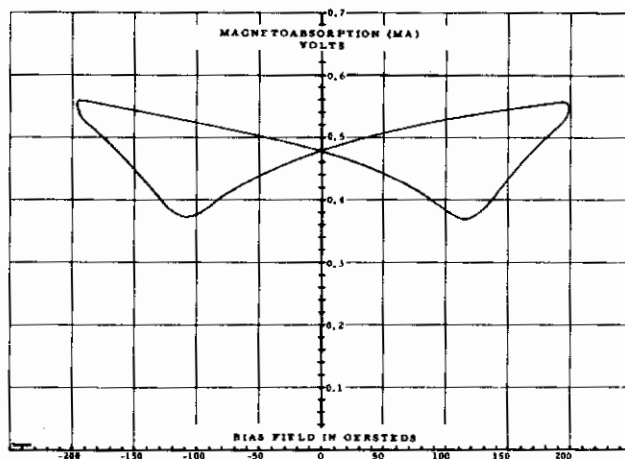
- 1 lb



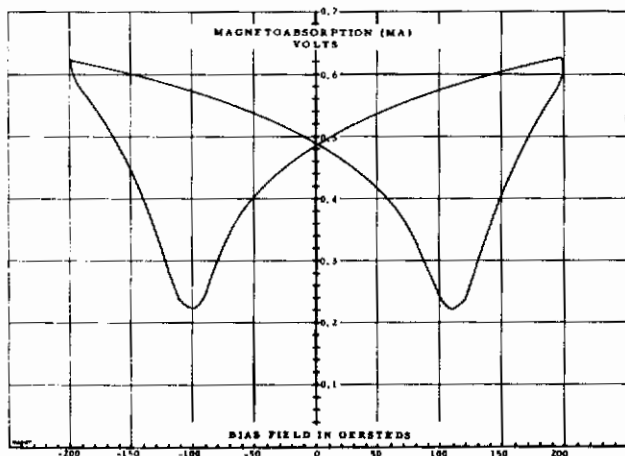
+ 5 lb



0.5 lb

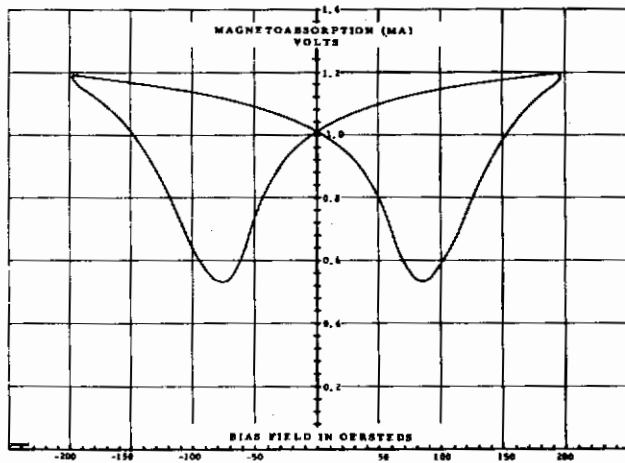


+ 10 lb

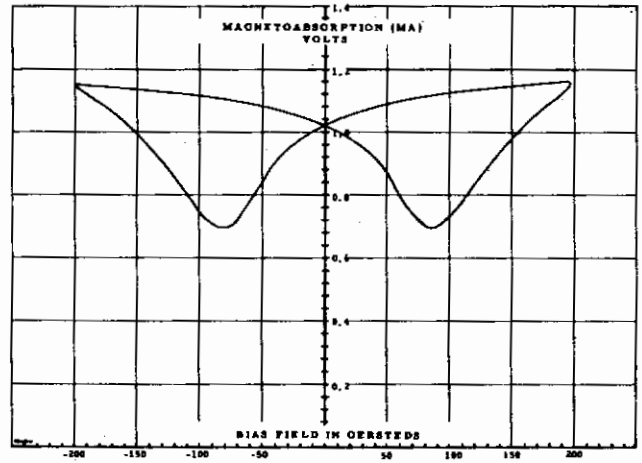


No Load

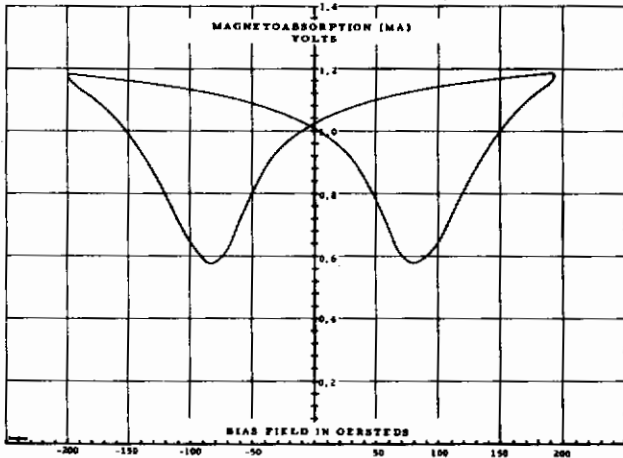
FIGURE 49. MAGNETOABSORPTION WAVEFORM CHANGES WITH LOAD FOR UNANNEALED NICKEL-PLATED ALUMINUM ROD OF 1/16-INCH DIAMETER



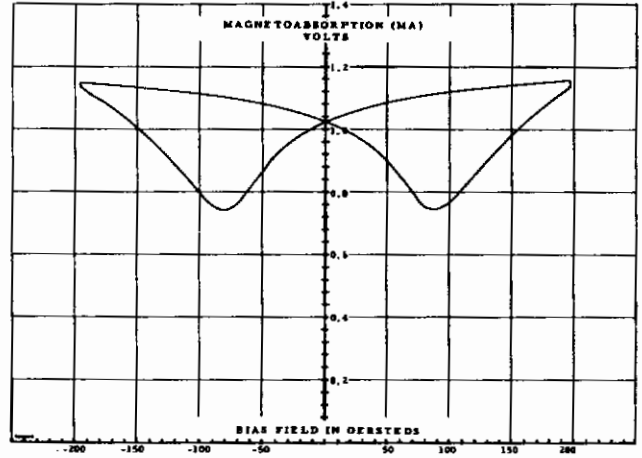
- 1 lb



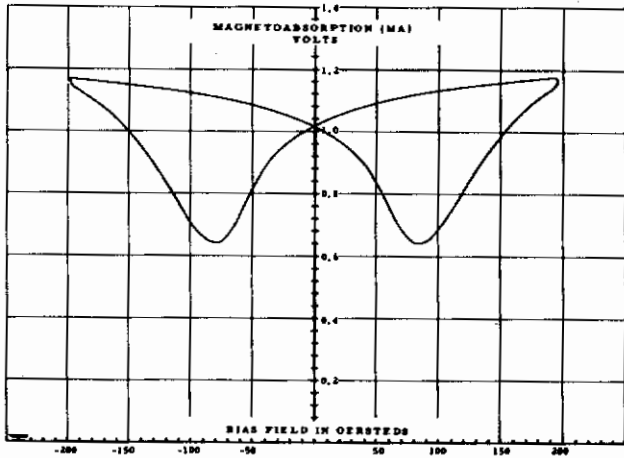
+ 4 lb



No Load



+ 6 lb



+ 2 lb

FIGURE 50. MAGNETOABSORPTION WAVEFORMS AS A FUNCTION OF LOAD FOR ANNEALED NICKEL-PLATED ALUMINUM ROD OF 1/16-INCH DIAMETER

MAGNETOABSORPTION HARMONIC AMPLITUDES
MEASUREMENTS FROM RODS

A. Experimental Technique

The system employed to perform these measurements is depicted in the block-diagram of Figure 51. The system as it appeared in the laboratory (except for the harmonic analyzer) is shown in Figure 52. A moment arm technique was employed to apply tensile loads on various wire specimens. The pivotal beam that forms the moment arm is shown in the left-hand portion of Figure 52. The Helmholtz bias coil and RF sample coil concentrically surround the specimen. An unassembled view of these coils with shield appears in Figure 53. The design specifications for the RF coil are shown in Table 1. It should be noted from the length of the RF coil that the magnetoabsorption signal will arise from a considerable length of the specimen (approximately 3 inches). If the RF magnetic field is small compared to the magnetic bias field, impedance changes with variations in magnetic bias field occurring within the sample coil are proportional to the square root of the reversible permeability. The marginal oscillator senses the impedance variations as frequency and amplitude modulations. The frequency modulation is identified as the dispersion signal, and the amplitude modulation is called the magnetoabsorption signal. As stress influences the reversible permeability, the marginal oscillator system detects the resultant changes in magnetoabsorption signal.

TABLE 1. SPECIFICATIONS FOR AN RF COIL

1. Dimensions 2-3/8-in. OD X 2-in. length
2. #28 AWG copper wire
3. N = 102 turns
4. Coil form plexiglass threaded to 52 threads/in.
5. Assembled with copper shield:

$$L = 400 \mu\text{h}$$
$$Q = 130 \text{ at } 500 \text{ KC}$$

B. Composition of the Samples

The compositions shown in Tables 2 and 3 have been obtained for the materials used.

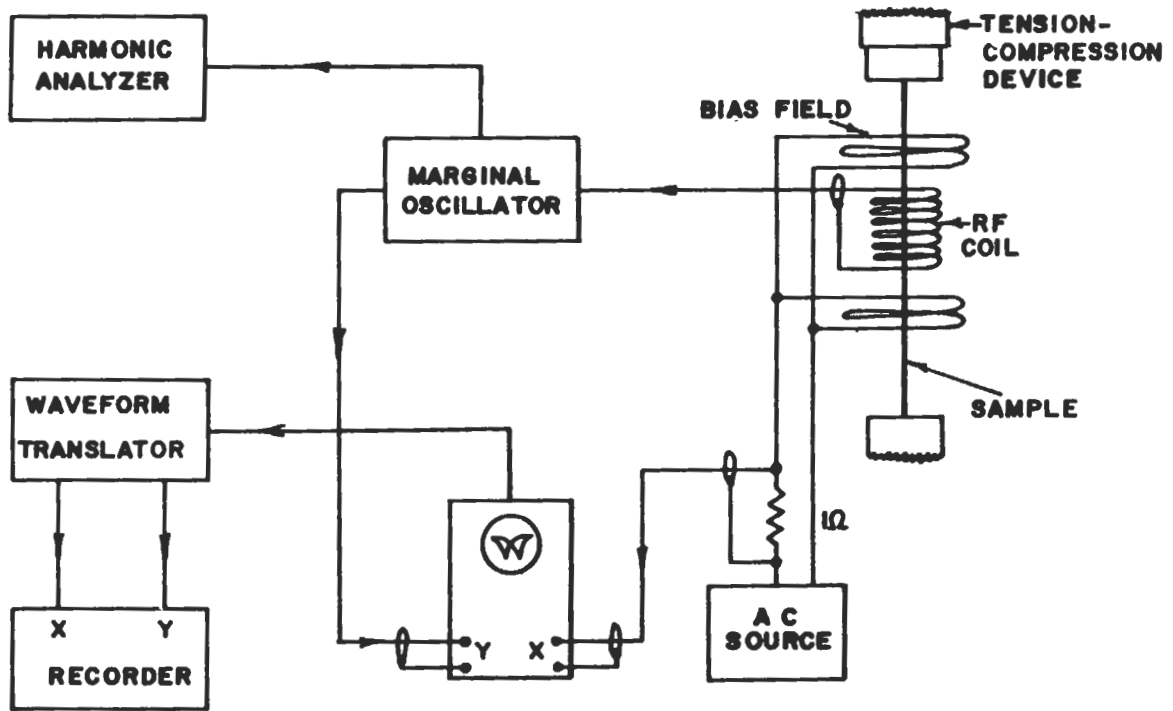


FIGURE 51. BLOCK DIAGRAM OF SYSTEM MEASURING THE HARMONIC CONTENT OF A MAGNETOABSORPTION SIGNAL FOR A SAMPLE UNDER STRESS

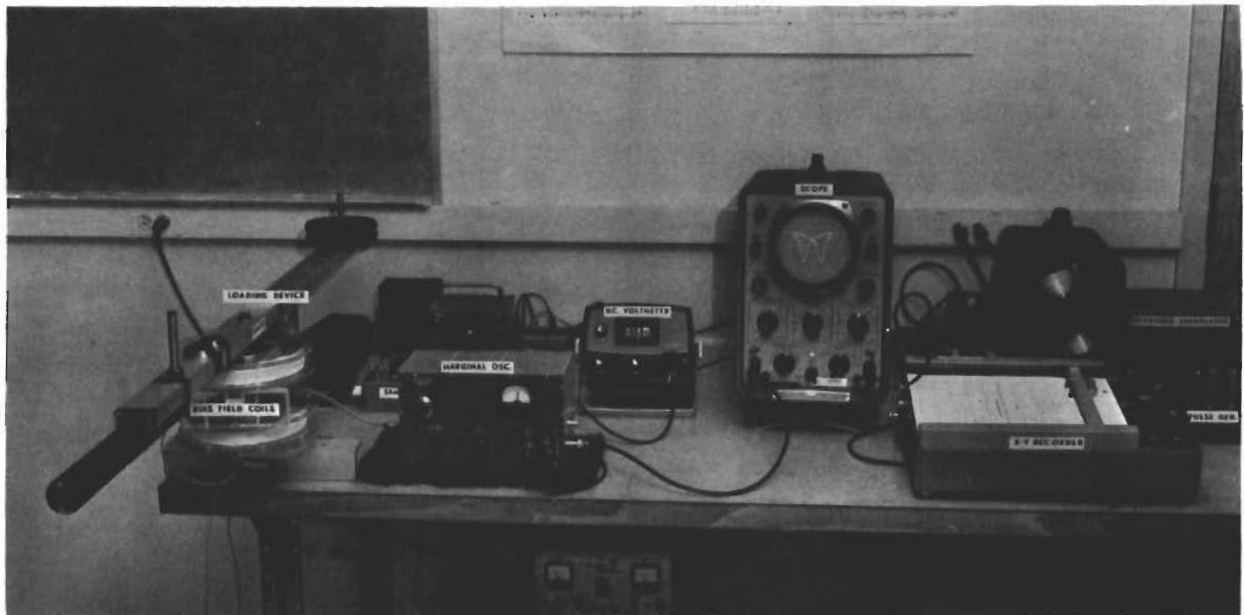


FIGURE 52. EQUIPMENT CONFIGURATION FOR MONITORING AND RECORDING MAGNETOABSORPTION AS A FUNCTION OF INCREMENTAL STRESS

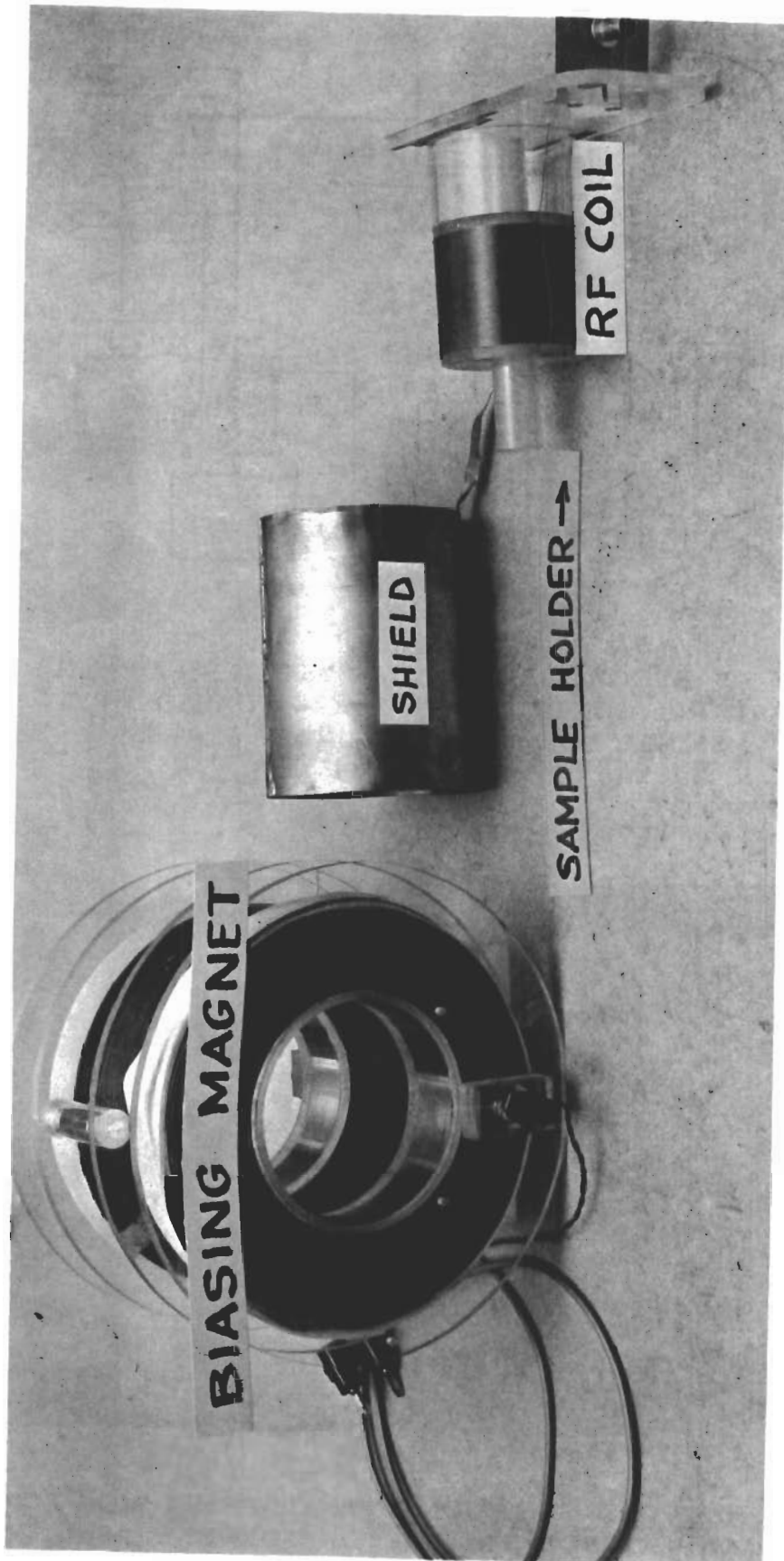


FIGURE 53. THE EXPLODED VIEW OF THE HELMHOLTZ BIASING MAGNET AND THE RADIO-FREQUENCY SAMPLE COIL PLUS ITS SHIELD

TABLE 2. COMPOSITION OF ANNEALED IRON THERMOCOUPLE WIRE

	<u>Narrow Specification Limits</u>	<u>Wide Specification Limits*</u>
Carbon	0.04/0.06	0.03/0.10
Manganese	0.23/0.28	0.20/0.30
Phosphorus	0.025 max	0.035 max
Sulphur	0.020/0.045	0.010/0.045
Silicon	0.005 max.	0.005 max.
Nickel	0.040/0.060	0.030/0.070
Chromium	0.010 max	0.030 max
Copper	0.100/0.125	0.080/0.135
Iron	Remaining	Remaining

TABLE 3. ANALYSES - 18% NICKEL MARAGING STEELS

	<u>Nominal VascoMax 250 AM** or CVM***</u>	<u>Certified Welding Filler Wire VascoMax 250 W CVM</u>
Carbon	0.03 max	0.02
Silicon	0.10 max	0.04
Manganese	0.10 max	0.01
Sulfur	0.010 max	0.007
Phosphorus	0.010 max	0.005
Nickel	18.50	18.19
Cobalt	7.50	7.94
Molybdenum	4.80	4.37
Aluminum	0.10	0.22
Titanium	0.40	0.52
Boron	0.003	0.001
Zirconium	0.02 added	0.005
Calcium	0.05 added	0.0005

*Leeds and Northrup cite: It is preferred that the analyses submitted conform to the limits of the "Narrow Specification," but, if a very limited selection of iron is available, analyses within the limits of the "Wire Specification" may be submitted for consideration.

**Air Melt

***Consumable Vacuum Melt

APPENDIX VII

GENERAL DESIGN CONSIDERATIONS FOR
MARGINAL OSCILLATORS

A. Circuitual Configuration of a Marginal Oscillator

Before the results of a number of papers on marginal oscillators are discussed, it is shown herein that significant accomplishments can be had with simple circuitual considerations. At the outset of this design problem, particular considerations are given to the choice of the marginal oscillator configuration shown in Figure 54.

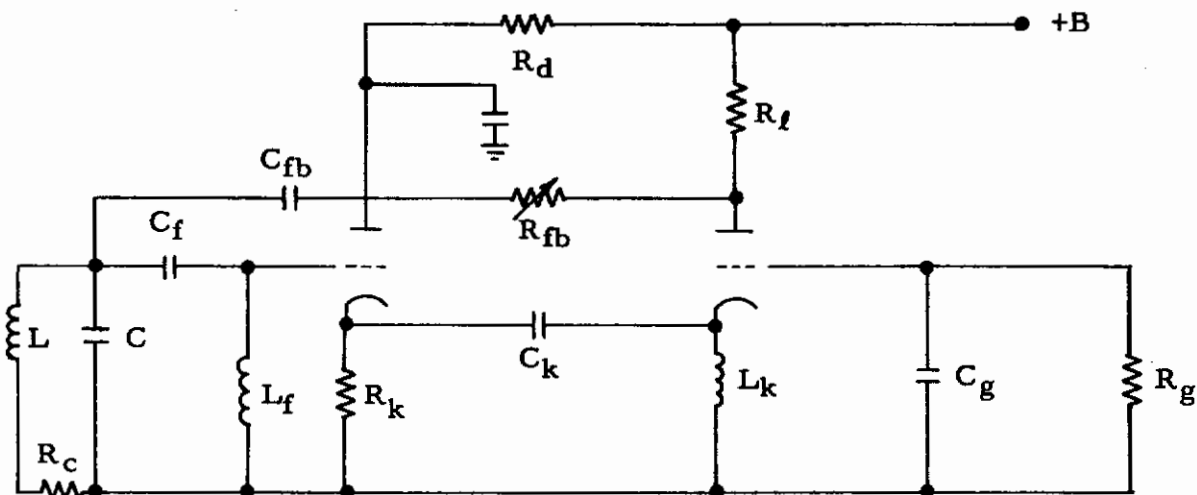


FIGURE 54. MARGINAL OSCILLATOR CONFIGURATION

The marginal oscillator consists of a cathode follower cascaded by a grounded grid amplifier. The output of the amplifier is fed back regeneratively through R_{fb} to the frequency selective grid circuit of the cathode follower. At the grid of the first stage appears the sample coil in which is placed a sample whose dissipative or dispersive characteristic (or both) is to be measured. The dissipative character occurs as an effective resistance change ΔR of the sample coil and the dispersive character occurs as an effective inductance change ΔL of the coil. The shunt capacitance, C , completes the resonant circuit of which the sample coil is the other member. A simple analysis of the resonance circuit which neglects the effects of other shunting impedances discloses that, at resonance, the equivalent shunt resistance R_s is given by

$$R_s = \frac{L}{C} \frac{1}{R_c} \tag{20}$$

Contrails

where $Q_L = \omega_0 L/R_C \gg 10$ has been assumed. Equation (20) relates R_s to R_C through a family of hyperbolas. To observe large changes in R_s due to small changes in R_C , the slope of R_s with respect to R_C [the derivative of Equation (20)] should be large. This is best accomplished by assuring that the sample coil is a high quality coil (that is, has a small R_C) and that the term L/C is large.

Normally, the change in resistance and inductance is brought about by a change in the magnetization of the sample through the use of a slowly varying external magnetic field. In order to avoid the induction of this variation into the grid circuit, it is necessary to insert a high pass filter consisting of L_f and C_f . The value of L_f is chosen in this application to be much larger than the inductance of the sample coil so that L_f presents a large impedance to signals of frequency near the frequency of oscillation, ω_0 , and a very small impedance to the frequency of the external magnetic field, ω_m . The value of C_f is selected so that the critical frequency of the filter is well below the frequency ω_0 . If it is assumed that the inductive reactance, X_{L_f} , is much smaller than the inductor's DC resistance, R_{dc} , and that the capacitive reactance, X_{C_f} , is much greater than the inductor's DC resistance, the transfer function, $G(\omega_m)$, of the unwanted frequency ω_m is

$$G(\omega_m) = -j\omega R_{dc}/X_{C_f} \quad (21)$$

where

$$X_{C_f} = 1/\omega_m C_f$$

and

R_{dc} = the inductor's (L_f) DC resistance

Since it is assumed that $X_{C_f} \gg R_{dc}$, then Equation (21) is a very small value and the unwanted frequency is highly attenuated. Therefore, the value of $G(\omega_m)$ is a measure of the ability of the circuit to reject externally induced voltages. From Equation (21), it is readily understood that the inductor should be of high quality. That is, R_{dc} , the resistance of the coil, should be very small for maximum rejection. As an example, if $\omega_m = 377$ (60 cycles), $R_{dc} = 13$, and $C = 0.001 \mu f$, then

$$G(377) = 4.9 \times 10^{-6}$$

Thus, if one volt is externally induced in the sample coil, then only 4.9 microvolts appears from grid to ground. It is highly advantageous that L_f be toroidally wound to avoid voltages at the grid from stray induction of L_f . The condition $\omega_m L_f \ll R_{dc}$ can be attained if a high frequency ferrite core is selected.

The cathode of the first stage is capacitively coupled to the cathode of the second. Whereas, commonly, the cathodes are connected directly, it is advantageous to prevent changes in bias of the second stage from influencing the bias of the first stage in order that high sensitivity may be retained. High sensitivity is preserved, as discussed in Holt [8], by reducing the nonlinearity that may occur with changes in bias. An inductor similar to L_f has been placed in the cathode of the second stage so that: (1) the bias may be entirely constructed through the use of an automatic level control, and (2) the first stage is not excessively loaded by the second. A by-product of such a cathode configuration of C_k and L_k is additional high pass filtering of the unwanted frequency ω_m .

B. The Automatic Level Control (ALC)

To assure stability in the level of oscillation, an ALC system is normally employed in conjunction with an oscillator. Since the signals are a function of oscillator levels, reliable measurements are possible only when the amplitude remains constant. The control is achieved by controlling the bias of the second stage which in turn varies the value of transconductance of the tube. Figure 55 is a graph of transconductance variations with grid bias for particular values of plate voltage for an Amperex 7308 Triode.

The gain expression of the second stage is given by

$$A_2 = \frac{g_m R_f}{1 + \frac{R_f}{R_p}} \quad (22)$$

where R_p is the plate resistance and g_m the transconductance. Since the gain is directly proportional to the g_m , and since the g_m is varied by the bias, then the bias can control the gain of the second stage. Note that the first stage is a cathode follower whose gain is very nearly one so that all of the gain in the oscillator is in the second stage.

The automatic action is accomplished by the system shown in the block diagram of Figure 56. In Figure 56, the cathode follower has been replaced by an amplifier of gain A_1 , and the grounded grid circuit by an amplifier with gain A_2 and an output impedance of R_o . For simplicity, the high pass filter has been left out since its effect at the radio frequency is nil. The loop to the right of Figure 56 represents the elements of the ALC. The operation of the ALC occurs in the following manner:

Under normal operating conditions, the voltage e_2 is amplified by A_3 , compared with V , the reference voltage, and detected by the diode. After filtering, the negative detected voltage E_c appears at the grid of A_2 . If the value of bias is sufficient to maintain the oscillation condition within the oscillator loop, the value of e_2 remains constant. If for some reason e_2 decreased by Δe_2 , this decrease is amplified by A_3

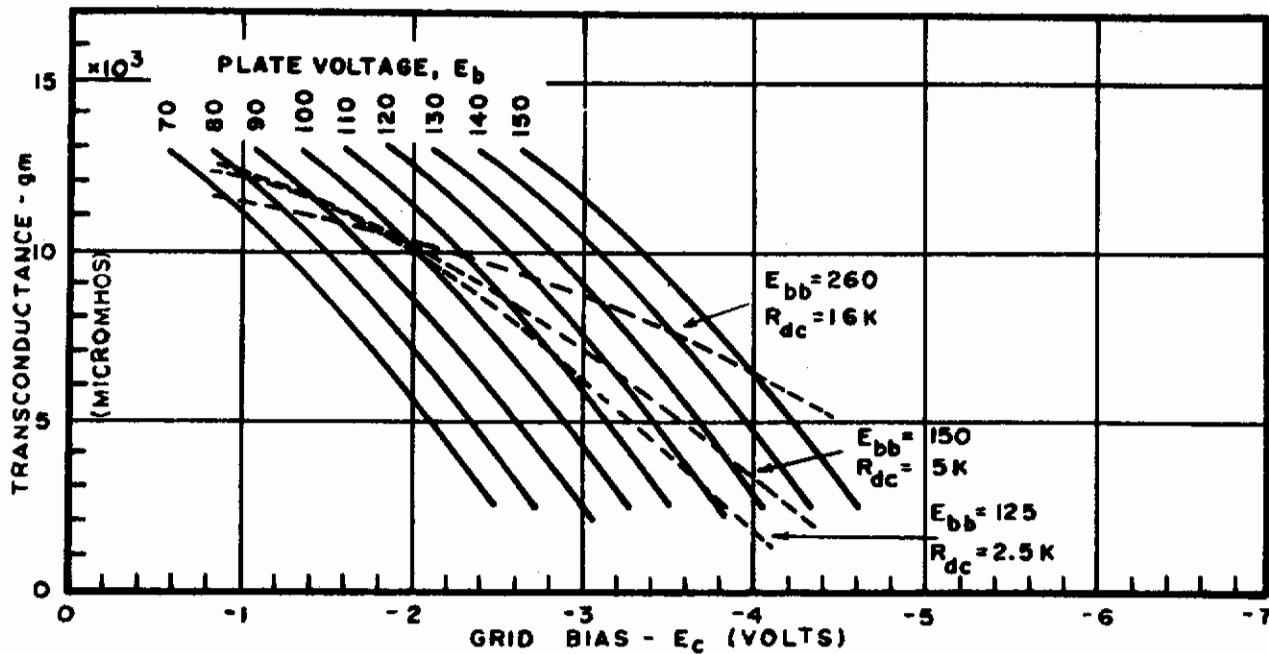


FIGURE 55. VARIATIONS OF TRANSCONDUCTANCE WITH GRID BIAS AND DC LOAD RESISTANCE

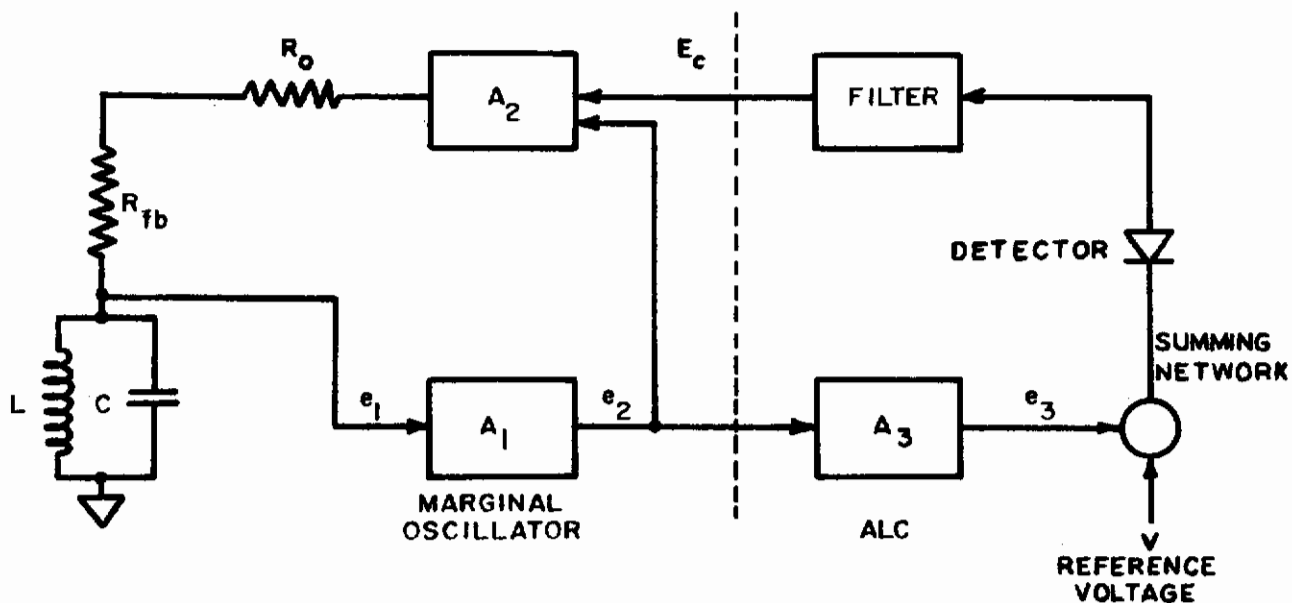


FIGURE 56. THE AUTOMATIC LEVEL CONTROL (ALC) SYSTEM USED WITH THE MARGINAL OSCILLATOR

compared with V and a less negative bias $E_c - \Delta E_c$ appears at A_2 . If the change of gain of A_2 is sufficient to maintain the oscillation condition, the value of e_2 is restored.

The ALC system may be reduced to a simple feedback network as shown in Figure 57. The elements of the marginal oscillator have been lumped into the block designated A of which e_2 is now the required output.

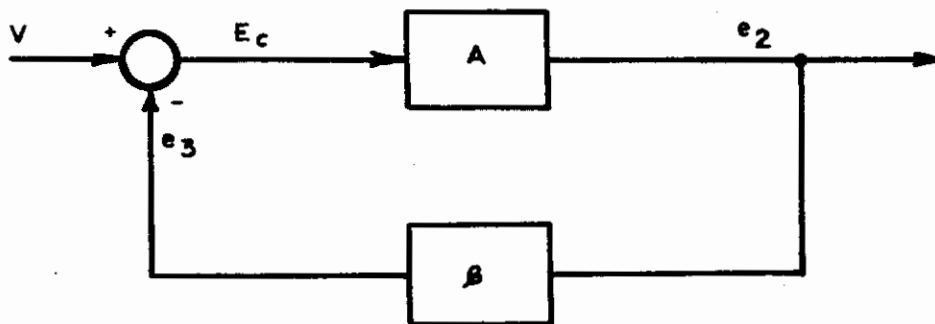


FIGURE 57. THE EQUIVALENT SERVO LOOP FOR THE ALC SYSTEM

In Figure 57, the block designated β includes A_3 , the detector and the filter of Figure 56. The transfer function, A , between the control voltage V and the output e_2 is given by

$$A' = \frac{A}{1 + \beta A} \quad (23)$$

Should a change in A occur, say dA , then the change A' is given by the differential of Equation (23), or

$$\frac{dA'}{A'} = \frac{1}{1 + \beta A} \frac{dA}{A} \quad (24)$$

From Equation (24), it is understood that a change in A' can be reduced by the factor $1 + \beta A$ if βA is large. Consequently, the output e_2 remains nearly constant for changes in A . There are within the system of Figure 56 two controllable elements to obtain a large value of βA . The most obvious is A_3 which in Figure 57 is equivalent to β . The remaining controllable element is A_2 . In the remaining portion of this section, it is shown that particular choices of circuit values for the ground grid amplifier, A_2 , yield a better ALC system action such that $\beta A \gg 1$.

In the circuit of Figure 58, the cathode follower and grounded grid are independently powered from a 260-V regulated plate supply through decoupling

resistors R_{d1} and R_{d2} , respectively. To retain sensitivity, each stage should be bias independently. Consequently, a common decoupling resistor has been avoided.

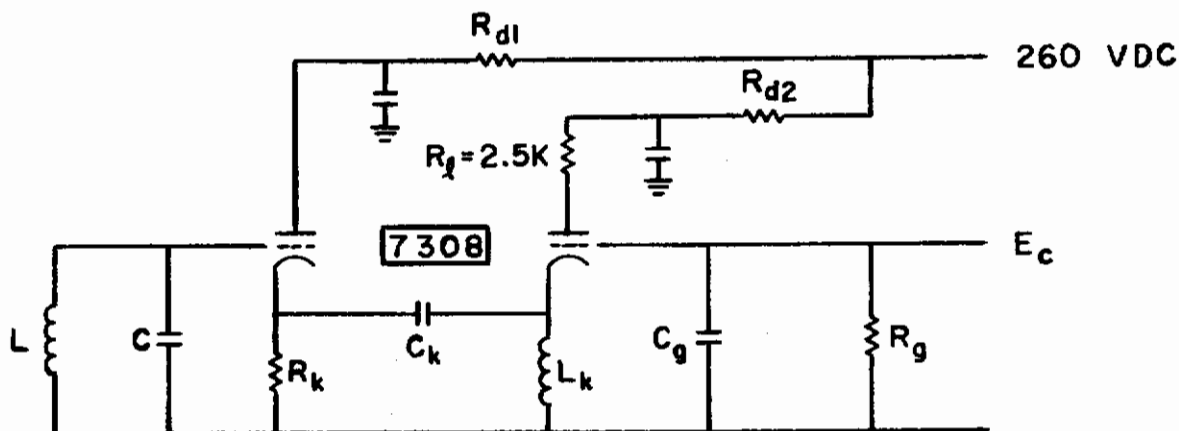


FIGURE 58. BIASING THROUGH DECOUPLING RESISTORS

The quiescent conditions for second stage are established at $E_c = -2$, $E_b = 100$, and $I_b = 10$ ma. Thus, R_{d2} must be $13.5 K\Omega$. The DC load resistance totals now $16 K\Omega$ where the resistance of the inductor L_k has been considered negligible. Now, through the use of the g_m characteristics of Figure 55 and the plate characteristics of Figure 59 for the 7308 tube, the variation of g_m with E_c is determined and plotted on Figure 55 for a plate supply voltage of 260 volts and DC load resistance of $16 K\Omega$. The resultant change in g_m with E_c is approximated by a straight line with slope

$$\frac{\partial g_m}{\partial e_c} = 1.650 \times 10^{-6}$$

for $-5 < E_c < -1$.

Now, however, if the same problem is reworked for the circuit shown in Figure 60, the change in g_m with E_c is approximated by

$$\frac{\partial g_m}{\partial e_c} = 3400 \times 10^{-6}$$

for $-4 < E_c < -1$. Thus, improvement by a factor greater than two results because of the use of the regulated supply with no decoupling resistors. In the prior case, the variations of the operating point along a flat load line ($R_{dc} = 16 K\Omega$) yielded smaller changes in g_m per unit change of grid bias.

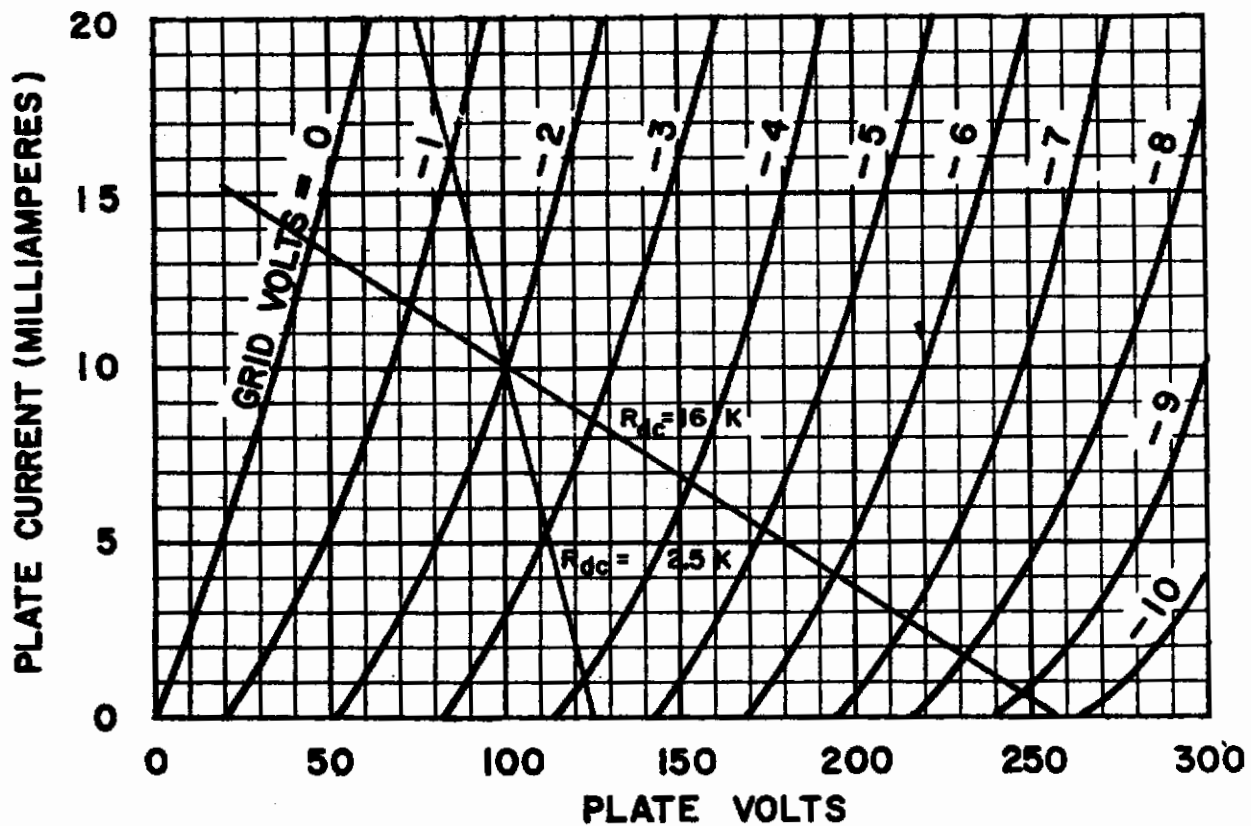


FIGURE 59. PLATE CHARACTERISTICS FOR 7308 TRIODE

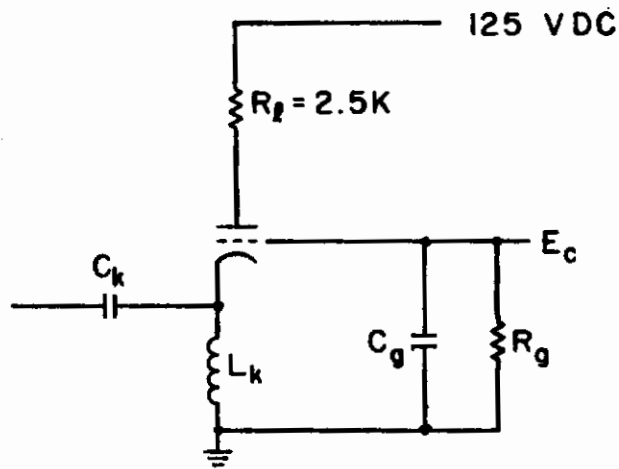


FIGURE 60. BIASING DIRECTLY FROM REGULATED SUPPLY

This problem initially arose from the fact that it was convenient to supply B+ through a decoupling resistor from an amplifier operating at 290 VDC. The above analysis shows that for improved ALC action this must be avoided. In the final design, a 150-V regulator tube was used with the marginal oscillator as shown in Figure 61 to drop the plate supply 315 VDC to 150 VDC. $\partial g_m / \partial e_c$ for the final design did not change appreciably from the latter example. The actual change in gain A_2 with change in E_c as shown in Figure 62 agrees very well with that predicted, since $\partial A_2 / \partial E_c = 3.4$.

C. Sensitivity, Bandwidth, and Noise Factor of Marginal Oscillators

Watkins [9] analyzes the marginal oscillator of Figure 63 on a nodal basis which begins with the differential equation

$$C \frac{dv}{dt} + G'v + \frac{1}{L} \int v dt - \frac{R_o}{R_F + R_o} f(v) = 0 \quad (25)$$

where all elements of the equation are defined in Figure 63, and where

$$f(v) = a_1 v + a_2 v^2 + a_3 v^3 + \dots \quad (26)$$

represents the nonlinear operation of the oscillator. From these expressions, Watkins arrives at the following sensitivity expression

$$\frac{\Delta E_g}{\Delta G(\omega_m)} = \frac{\frac{2}{3a_3} \left(\frac{R_F + R_o}{R_o E_g} \right)}{\left[1 + \left(\frac{2\omega_m}{\Delta\omega} \right)^2 \right]^{1/2}} \quad (27)$$

for periodic variations in marginal oscillator rf amplitude, ΔE_g , to periodic tuned circuit conductance changes ΔG_m which vary at radian frequency of ω_m . Associated with this amplitude change is a phase shift

$$\phi = \tan^{-1} (2\omega_m / \Delta\omega) \quad (28)$$

with respect to the conductance variations. Table 4 together with Figure 63 define each parameter in the above equations.

If Equations (27) and (28) are to be applied to a marginal oscillator measuring magnetoabsorption, it must be noted that the periodic conductance variation, resulting from magnetoabsorption in a test specimen, is composed of many significant harmonics. To faithfully reproduce these variations in the marginal oscillation, both the amplitude and phase of each resultant harmonic, the RF-amplitude variations caused by the magnetoabsorption, must also be preserved. The magnetoabsorption signal is then the sum of these harmonic

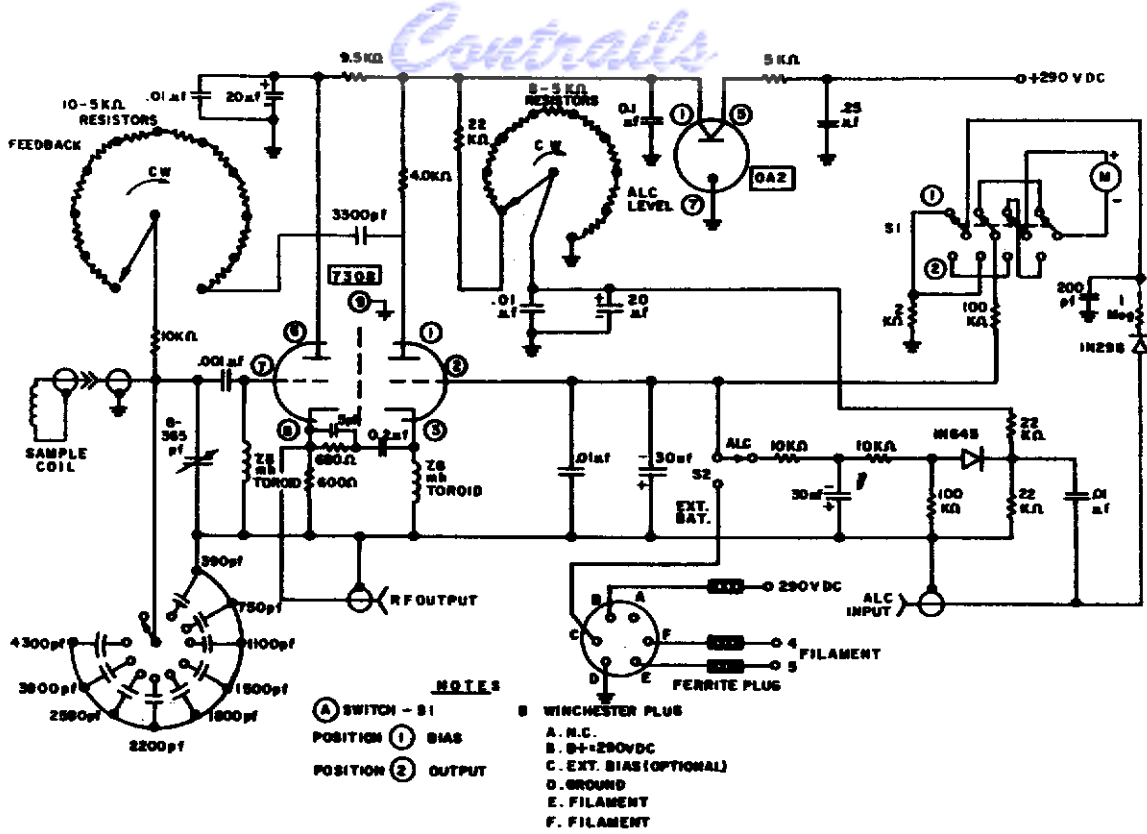


FIGURE 61. MARGINAL OSCILLATOR WITH REGULATED PLATE SUPPLY AND AUTOMATIC LEVEL CONTROL

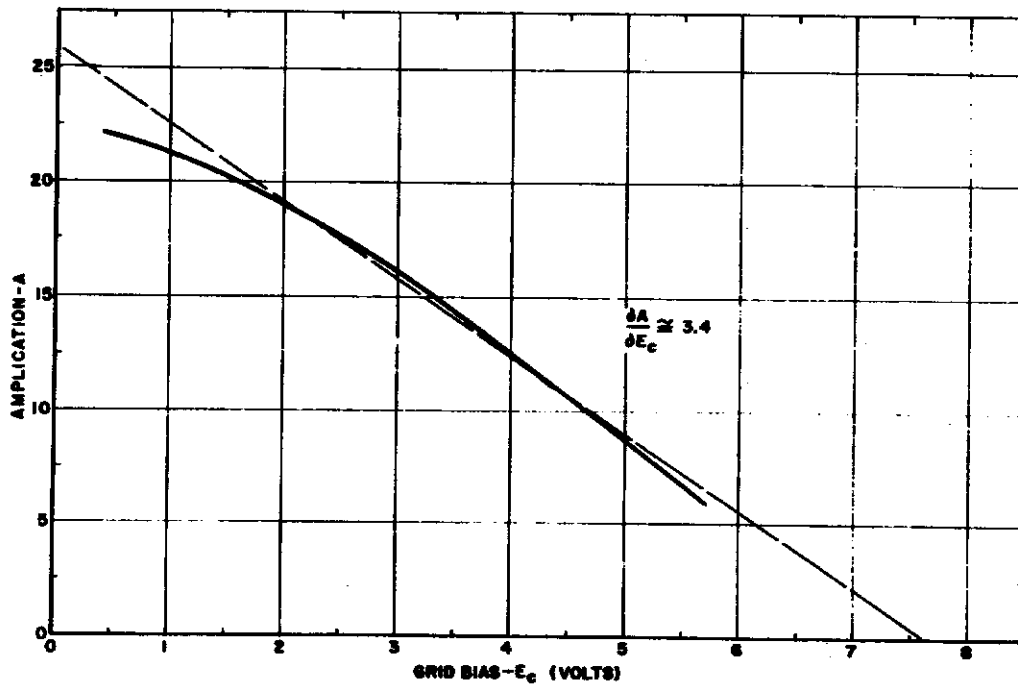
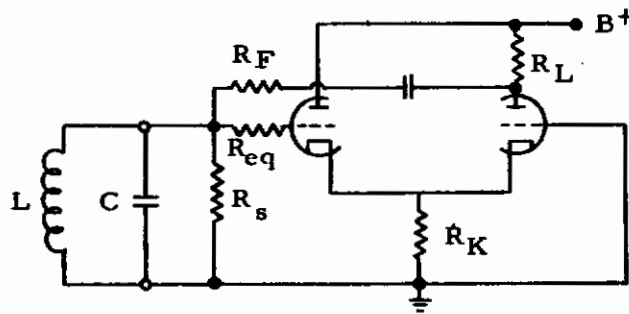


FIGURE 62. GAIN OF GROUNDED GRID AMPLIFIER WITH VARIATION IN GRID BIAS FOR 7308 TRIODE



(a) Basic Oscillator CKT

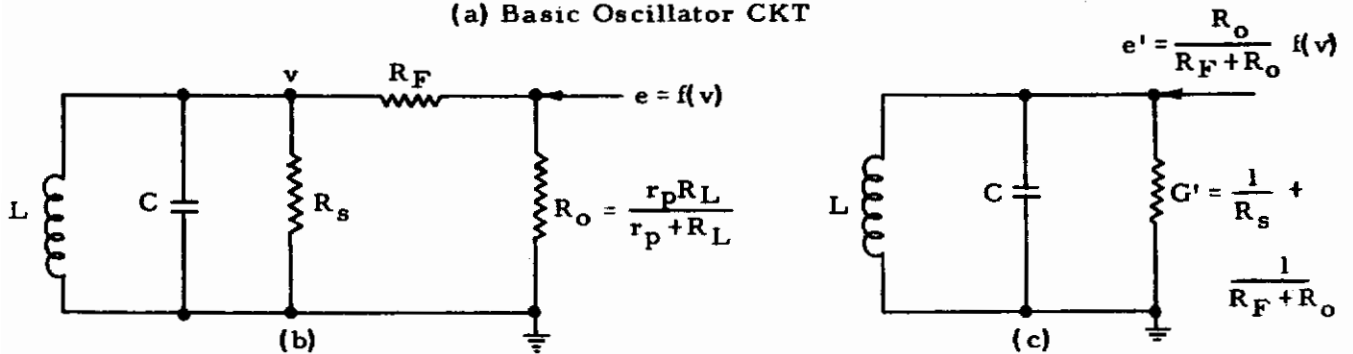


FIGURE 63. EQUIVALENT CIRCUITS OF THE OSCILLATOR

TABLE 4. DEFINITION OF PARAMETERS

Symbol	Meaning
a_3	- a measure of the third order nonlinearity of the oscillator
R_F	- the value of feedback resistor
R_O	- the output impedance of the second stage of the oscillator
E_g	- the RF amplitude across the tuned circuit
ω	- the frequency of oscillation
ω_m	- the frequency of conductance variations
$\Delta\omega = \frac{-3a_3}{2} \frac{R_O}{R_F + R_O} \frac{\omega R_s}{Q} \quad (29)$	
(the bandwidth of the tuned circuit)	
R_s	- the tuned circuit equivalent shunt resistance
Q	- the quality of the tuned circuit
R_L	- the plate resistor of the second stage

Contrails

RF-amplitude variations after demodulation. If the fifth harmonic, $5\omega_m$, is the highest significant harmonic above the fundamental conductance variation, ω_m , then to preserve the phase of this harmonic, it is required, by Equation (28), that the ratio of the frequency of the fifth harmonic to the frequency equivalent for half the bandwidth be less than 1/10 if the phase shift is to be less than 1/10 radian. This ratio is given by

$$\frac{5\omega_m}{\Delta\omega/2} = - \frac{20\omega_m}{3a_3} \left(\frac{R_F + R_O}{R_O} \right) \left(\frac{Q}{\omega R_s} \right) \frac{1}{E_g^2} \leq \frac{1}{10} \quad (30)$$

It follows that the corresponding fifth harmonic of the magnetoabsorption signal lags the conductance harmonic by only 5.7° if the equality of Equation (30) is assumed. All lower harmonics, of course, undergo smaller phase shifts. When the restriction of Equation (30) is applied to Equation (27), the following reduction of Equation (27) occurs

$$\frac{\delta E_g}{\delta G(5\omega_m)} = \frac{2}{3a_3} \frac{(R_F + R_O)}{R_O E_g} \left[1 - \frac{1}{2} \left(\frac{10\omega_m}{\Delta\omega} \right)^2 \right] \quad (31)$$

where it has been precluded that $\frac{5\omega_m}{\Delta\omega/2}$ has little influence on the sensitivity.

It is also understood from the inequality of Equation (30) that the bandwidth required of the oscillator to preserve the phase of the fifth harmonic becomes

$$\Delta\omega = 100\omega_m = - \frac{3a_3}{2} \frac{R_O}{R_F + R_O} \frac{\omega R_s}{Q} \times E_g^2 \quad (32)$$

Thus, increased sensitivity is attained by enlarging the term $\frac{R_F + R_O}{a_3 F_O E_g}$ provided the condition of Equation (30) is not violated. A rearrangement of the inequality in Equation (30) yields

$$\frac{20\omega_m Q}{3\omega R_s E_g} \left(\frac{R_F + R_O}{R_O a_3 E_g} \right) \leq \frac{1}{10} \quad (33)$$

which implies that, if $\frac{2(R_F + R_O)}{3R_O a_3 E_g}$ is to be large, then $\frac{10\omega_m Q}{\omega R_s E_g}$ must be very small so that their product is less than or equal to a tenth. Consequently, the problem becomes that of minimizing the expression

$$\frac{10\omega_m Q}{\omega R_s E_g} \ll 1 \quad (34)$$

When the substitutions of:

$$Q = \frac{\omega L}{R_c}$$

and

$$R_s = \frac{(\omega L)^2}{R_c}$$

are made in Equation (34), where

L = the tuned circuit inductance

and

R_c = the inductor's series resistance

then Equation (34) becomes

$$\frac{10\omega_m}{\omega^2 L E_g} \ll 1 \tag{35}$$

In an attempt to minimize the inequality Equation (35), it is preferable to accomplish this task by making $\frac{\omega_m}{\omega^2 L}$ very small since enlarging E_g reduces the sensitivity, $\frac{R_F + R_O}{a_3 R_O E_g}$. Qualitatively, to increase sensitivity, $\frac{R_F}{R_O}$ should be large and $a_3 E_g$ small. This requires a large value of feedback resistance, a small RF level, and extreme linearity of the oscillator. If this requirement for increased sensitivity is compared with the bandwidth, Equation (32), which may be rewritten as

$$\Delta\omega = 100\omega_m = -\frac{3a_3}{2} \frac{R_O}{R_F + R_O} E_g \omega^2 L E_g \tag{36}$$

It is noted that increased sensitivity can only be obtained at a sacrifice of bandwidth, if ω_m and $\omega^2 L E_g$ are held constant. In order that the RF field penetrate the ferromagnetic specimen, the rf frequency ω should be low consistent with the marginal oscillator technique. Consequently, sufficient bandwidth must be sought by reducing ω_m and increasing $L E_g$. Notice that increased bandwidth can be achieved faster by increasing E_g , since it occurs in Equation (36) as the square, rather than decreasing R_F with a resultant severe decrease in sensitivity.

The extension of Watkin's derivation is reasonable. If a sensitivity, $\left(\frac{\Delta E_g}{\Delta G}\right)^{-1}$, of -3.3×10^{-6} is desired, then

$$\frac{3a_3 R_o E_g}{2(R_o + R_F)} = -3.3 \times 10^{-6}$$

Substitution of this expression into Equation (33), for $\omega_m = 2\pi(120)$ and $\omega = 2\pi(5 \times 10^5)$, yields

$$L E_g = 2.3 \times 10^{-3}$$

If $E_g = 5$, then $L = 460 \mu\text{h}$. All the above values are in close agreement with the circuitual value actually employed. Further substitution into Equation (31) yields

$$R_F = -0.45 a_3 \times 10^{+10} - 2 \times 10^{+3}$$

If $a_3 = -5 \times 10^{-6}$ and $R_o = 2 \times 10^3$, then

$$R_F = 20.5 \text{ K}\Omega$$

The actual values of R_F employed are in the range 25 K Ω to 15 K Ω ; so agreement with theory is once again verified.

An examination of the noise figure of a marginal oscillator as derived by Watkins is also interesting. If the phase of the 5th harmonic is to be preserved, Watkin's noise figure expression becomes

$$F = F_o \left(1 + \frac{\Delta\omega}{10\omega_m} \right) \quad (37)$$

where

$$F_o = \frac{R_s}{R_F + R_o} + \frac{R_{eq}(R_s + R_F + R_o)}{R_s(R_F + R_o)^2} \quad (38)$$

$$R_{eq} = 2.5 \left\{ \frac{1}{g_{m1}} + \frac{1}{g_{m2}} \left[\frac{1 + g_{m1} R_K}{(g_{m1} R_s)^2} \right] \right\} \quad (39)$$

R_K = cathode resistor

$g_{m1,2}$ = transconductance of the triode sections

The factor F_o represents the inherent noises of the system, both shot noise (equivalent noise resistance R_{eq}) and thermal noises, R_s , R_F , and R_o . The factor $\Delta\omega/10\omega_m$ accounts for the additional noise arising from the intermodulation

noise products in the oscillator bandwidth $\Delta\omega$. Substituting the condition of Equation (30) into Equation (37) yields

$$F = 11F_0$$

Consequently, noise figure improvement must be sought by reducing F_0 . If the feedback resistor is larger than the output impedance of the oscillator, i. e., $R_F \gg R_0$, then F_0 reduces to

$$F_0 \cong 1 + \frac{R_s}{R_F} + \frac{R_{eq}}{R_F^2} + \frac{R_{eq}}{R_s R_F} \quad (40)$$

It is understood from Equations (39) and (40) that F_0 can approach a value of one if:

- (1) The value of the feedback resistor, R_F , is much larger than the shunt resistance, R_s , of the tuned circuit.
- (2) The equivalent tube noise, R_{eq} , is small. This is accomplished by using high transconductance triodes and a large value of cathode resistance, R_K .

D. The Broadband Amplifier

Several modifications were made to a broadband amplifier design previously employed. The amplifier functions as element A3 in Figure 56. These modifications were primarily necessary to allow increased input amplitudes to the amplifier without saturation occurring at the output. The results of these modifications assured that each stage of the amplifier was biased for maximum output capability consistent with minimum noise and distortion requirements. It was observed that at the increased inputs the amplifier oscillates at 5 megacycles with a one cycle per second modulation. Consequently, cathode bypass capacitors were removed to reduce open loop gain to prevent overloading and oscillation at large inputs. To preserve the closed loop gain, the feedback over the entire system was reduced. The schematic diagram of the amplifier incorporating these modifications is shown in Figure 64. The amplifier has the characteristics shown in Table 5.

TABLE 5. AMPLIFIER CHARACTERISTICS

Voltage gain	25
Bandwidth (3 dB)	20 cps to 5 mcs
Equivalent input noise level	20 μ v
Maximum output	80 volts, p-p

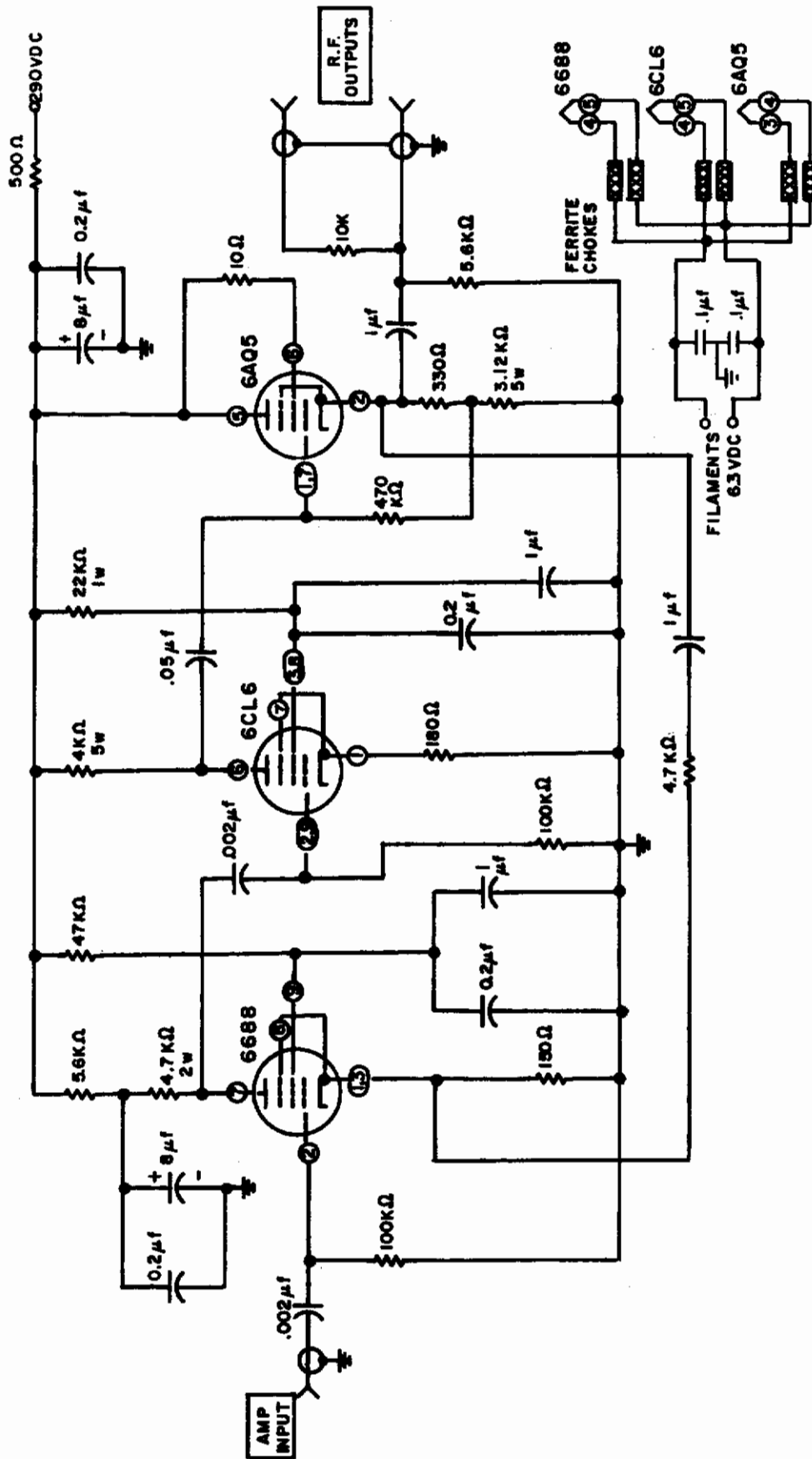


FIGURE 64. BROAD BAND AMPLIFIER

Unclassified
Security Classification

DOCUMENT CONTROL DATA - R&D		
<i>(Security classification of title, body of abstract and indexing annotation must be entered when the overall report is classified)</i>		
1. ORIGINATING ACTIVITY (Corporate author) Southwest Research Institute 8500 Culebra Road San Antonio, Texas 78206		2a. REPORT SECURITY CLASSIFICATION Unclassified
		2b. GROUP
3. REPORT TITLE Magnetoabsorption Techniques for Measuring Material Properties		
4. DESCRIPTIVE NOTES (Type of report and inclusive dates)		
5. AUTHOR(S) (Last name, first name, initial) Rollwitz, William L. Claassen, John P.		
6. REPORT DATE October 1966	7a. TOTAL NO. OF PAGES 104	7b. NO. OF REFS 9
8a. CONTRACT OR GRANT NO. AF 33(657)-10326	9a. ORIGINATOR'S REPORT NUMBER(S) AFML TR-66-76	
b. PROJECT NO. 7360		
c. Task No. 736002	9b. OTHER REPORT NO(S) (Any other numbers that may be assigned this report)	
d.		
10. AVAILABILITY/LIMITATION NOTICES This document is subject to special export controls & each transmittal to foreign governments or foreign nationals may be made only with prior approval of the Metals & Ceramics Div. (MAMD), AF Materials Lab., Wright-Patterson AFB, Ohio. Qualified requesters may obtain cys from DDC.		
11. SUPPLEMENTARY NOTES	12. SPONSORING MILITARY ACTIVITY Air Force Materials Laboratory (MAMD) Wright-Patterson AFB, Ohio	
13. ABSTRACT Research under Contract AF 33(657)-10326 was continued to determine the feasibility of using magnetoabsorption for the nondestructive evaluation of material properties. Previous efforts, reported in ML-TDR-64-123 and AFML TR-65-17, have shown that magnetoabsorption signals are derived from variations of the reversible permeability of ferromagnetic specimens with magnetic environment. Further, it had been shown that magnetoabsorption signals are readily affected by changes in reversible permeability as caused by stress, heat treatment, composition, impurity, and temperature. The effort of this period has been devoted to a refinement of the magnetoabsorption measuring equipment to detect low amplitude magnetoabsorption signals from specimens offering a small effective filling factor to a sample coil or probe. These refinements are primarily discussed in the Appendices. With this improved sensitivity, variations in harmonic content of magnetoabsorption signals arising from variations in the surface properties of a plate of maraging steel were related experimentally. Magnetoabsorption waveforms were also measured from and related to a weldment of maraging steel, stressed and stress-relieved specimens of HY-80 steel, and a bulge plate of 1020 steel. Magnetoabsorption signal changes and its harmonic amplitude variations from nickel-plated aluminum rods and other ferromagnetic wires were related experimentally to applied compressive and tensile loads.		

DD FORM 1 JAN 64 1473

Unclassified
Security Classification

14.	KEY WORDS	LINK A		LINK B		LINK C	
		ROLE	WT	ROLE	WT	ROLE	WT
	Magnetoabsorption Material Properties Ferromagnetism Permeability Stress Measurements Nondestructive Testing						

INSTRUCTIONS

1. ORIGINATING ACTIVITY: Enter the name and address of the contractor, subcontractor, grantee, Department of Defense activity or other organization (*corporate author*) issuing the report.

2a. REPORT SECURITY CLASSIFICATION: Enter the overall security classification of the report. Indicate whether "Restricted Data" is included. Marking is to be in accordance with appropriate security regulations.

2b. GROUP: Automatic downgrading is specified in DoD Directive 5200.10 and Armed Forces Industrial Manual. Enter the group number. Also, when applicable, show that optional markings have been used for Group 3 and Group 4 as authorized.

3. REPORT TITLE: Enter the complete report title in all capital letters. Titles in all cases should be unclassified. If a meaningful title cannot be selected without classification, show title classification in all capitals in parenthesis immediately following the title.

4. DESCRIPTIVE NOTES: If appropriate, enter the type of report, e.g., interim, progress, summary, annual, or final. Give the inclusive dates when a specific reporting period is covered.

5. AUTHOR(S): Enter the name(s) of author(s) as shown on or in the report. Enter last name, first name, middle initial. If military, show rank and branch of service. The name of the principal author is an absolute minimum requirement.

6. REPORT DATE: Enter the date of the report as day, month, year, or month, year. If more than one date appears on the report, use date of publication.

7a. TOTAL NUMBER OF PAGES: The total page count should follow normal pagination procedures, i.e., enter the number of pages containing information.

7b. NUMBER OF REFERENCES: Enter the total number of references cited in the report.

8a. CONTRACT OR GRANT NUMBER: If appropriate, enter the applicable number of the contract or grant under which the report was written.

8b, 8c, & 8d. PROJECT NUMBER: Enter the appropriate military department identification, such as project number, subproject number, system numbers, task number, etc.

9a. ORIGINATOR'S REPORT NUMBER(S): Enter the official report number by which the document will be identified and controlled by the originating activity. This number must be unique to this report.

9b. OTHER REPORT NUMBER(S): If the report has been assigned any other report numbers (*either by the originator or by the sponsor*), also enter this number(s).

10. AVAILABILITY/LIMITATION NOTICES: Enter any limitations on further dissemination of the report, other than those

imposed by security classification, using standard statements such as:

- (1) "Qualified requesters may obtain copies of this report from DDC."
- (2) "Foreign announcement and dissemination of this report by DDC is not authorized."
- (3) "U. S. Government agencies may obtain copies of this report directly from DDC. Other qualified DDC users shall request through _____."
- (4) "U. S. military agencies may obtain copies of this report directly from DDC. Other qualified users shall request through _____."
- (5) "All distribution of this report is controlled. Qualified DDC users shall request through _____."

If the report has been furnished to the Office of Technical Services, Department of Commerce, for sale to the public, indicate this fact and enter the price, if known.

- 11. SUPPLEMENTARY NOTES:** Use for additional explanatory notes.
- 12. SPONSORING MILITARY ACTIVITY:** Enter the name of the departmental project office or laboratory sponsoring (*paying for*) the research and development. Include address.
- 13. ABSTRACT:** Enter an abstract giving a brief and factual summary of the document indicative of the report, even though it may also appear elsewhere in the body of the technical report. If additional space is required, a continuation sheet shall be attached.

It is highly desirable that the abstract of classified reports be unclassified. Each paragraph of the abstract shall end with an indication of the military security classification of the information in the paragraph, represented as (TS), (S), (C), or (U).

There is no limitation on the length of the abstract. However, the suggested length is from 150 to 225 words.

14. KEY WORDS: Key words are technically meaningful terms or short phrases that characterize a report and may be used as index entries for cataloging the report. Key words must be selected so that no security classification is required. Identifiers, such as equipment model designation, trade name, military project code name, geographic location, may be used as key words but will be followed by an indication of technical context. The assignment of links, rules, and weights is optional.